

A SURFACE WATER $\delta^{18}\text{O}$ BASELINE FOR ARCHAEOLOGICAL STUDIES OF SEASONALITY AND
MOBILITY IN THE MAJES VALLEY AND PUCUNCHO BASIN OF SOUTHERN PERU

By

Emily Beatrice Peterson Milton

A THESIS

Submitted to
Michigan State University
in partial fulfillment of the requirements
for the degree of

Anthropology–Master of Arts

2020

ABSTRACT

A SURFACE WATER $\delta^{18}\text{O}$ BASELINE FOR ARCHAEOLOGICAL STUDIES OF SEASONALITY AND MOBILITY IN THE MAJES VALLEY AND PUCUNCHO BASIN OF SOUTHERN PERU

By

Emily Beatrice Peterson Milton

Oxygen isotopes in archaeological human and animal teeth provide a potential means to study past migration. In this thesis I evaluate oxygen isotopes as a way to measure highland site occupation seasonality and human movement between elevation zones in the Central Andes. I focus on two questions: 1) Do surface water $\delta^{18}\text{O}$ values vary predictably with altitude? and 2) Do surface water $\delta^{18}\text{O}$ values reliably record the wet and dry season? Using water samples collected from the Majes Valley and Pucuncho Basin of southern Peru, I establish the seasonal and spatial distribution of $\delta^{18}\text{O}$. The final dataset represents 98 water samples collected during wet and dry seasons between 2018-2019, from elevations 36 to 4938 meters above sea level.

Surface water $\delta^{18}\text{O}$ and δD values in the study area are consistent with regional and global meteoric waters. Individual water bodies demonstrate relatively higher $\delta^{18}\text{O}$ values during the dry season and lower $\delta^{18}\text{O}$ values in the wet season, matching predictions. Lowland and highland surface waters demonstrate overlapping ranges of $\delta^{18}\text{O}$, making it impossible to predict the values of surface waters based on elevation alone. Rather, local $\delta^{18}\text{O}$ appears to reflect evaporative processes influenced by stream order, catchment size, and the geographic position of a waterbody within the watershed. These data suggest oxygen isotopes are not independently suited to resolve questions of human mobility between elevation zones in the western Andes. Further testing is needed to understand the local seasonal and inter-zonal isotopic ecology.

Copyright by
EMILY BEATRICE PETERSON MILTON
2020

For Marley.

ACKNOWLEDGEMENTS

Many minds and hands contributed to the completion of this thesis. First, I thank my committee. To Dr. Katherine Moore, a most valued new mentor, for sharing her incredible reservoir of knowledge on South American anthropology and ecology; and for her unrelenting tenacity for responding to extensive, late-night inquiries. To Dr. Nathan Stansell for his steady hand in teaching South American climate and isotopic theory, the word “fractionation,” and his unsolicited interest in archaeological problems. To Doctor Hervé Bocherens for entertaining endless questions, instructing me in the careful art of biochemical analysis and interpretation, and encouraging creativity when faced with null results. To Dr. Gabe Wrobel, for his eager interest in an external project and for offering an open hand in a new department. Finally, to Dr. Jodie O’Gorman for her passionate enthusiasm to, “get it done!”

To Dr. Kurt Rademaker, an exceptional advisor and mentor. I owe this research and the studies that will follow it to his initial and ongoing support, as well as his enthusiastic encouragement of novel and bizarre questions. His belief that students can make important contributions to science is perhaps unparalleled. I have such gratitude to him and the approving committee for NSF grant 1659015 for funding part of my fieldwork, education, and research along the way.

To my fine comrades in research and adventure, Daniela Osorio and Sarah Meinekat, for helping to take notes while stuffing me full of laughter. To Brett Furlotte, an admirable field companion, union suit exemplar, and hilarious botanist.

I thank the Zuniga family, without whom this research would not have been possible. I thank Efraim for his careful work with Marley, and Ermitaño for his adventurous car rides,

fascinating narratives, and trustworthy dedication to helping a *Gringa* in need of water and tissue samples.

To the lab personnel at the University of Tübingen and Northern Illinois University, especially Dr. Dorothee Drucker and Josh Schwartz, for lending critical insights to my method-development and research design. To Dober Chala-Aldana for sharing and discussing his pilot data and samples. To Ruthann Yeaton for sticky notes containing key information.

I thank Dr. Bill Lovis for taking time from his retirement to review and support my research and Dr. Joe Hefner for his critiques of my R plots and lax stats.

To my early, but long-term mentors: Dr. Matt G. Hill for the intermittent reality checks; Dr. Larry Todd for commentary on glowing-teeth; Stephen Anderson for lessons in work-fun balance; and Matthew Neff for acting as a sounding board and editor. To all four for teaching me to think, question, and do archaeology as science and as anthropology.

I am so grateful for my cohorts at Northern Illinois University, the University of Tübingen, and Michigan State University. I thank Jordi for “wife chats”; Mike, Steph, and Taylor for keeping my downtime spirited and the karaoke mic hot; Autumn, Jeff, Mari, and Susan, for Friday tarot readings and welcoming me to MSU; Malcolm, Alex, Ashley, and Ernesto – for the good times and late nights in ESPP. To my 2019 cohort and fast friends, for spouting anarchy and activism in theory and praxis. To my people of the past, especially Kinsey, Jacquelyn, and Sophia for forcing extended breaks called ‘vacations’; to Rachel, a talented archaeologist and editor; and to the best house mates anyone could get quarantined with: Jack, Kevin, Peanut, TC, and Vic - I adore four of you.

Finally, I state my enormous gratitude for my family. Bradley, for the consistent reminder that laurels are not cushions; Peg, for biscuit-filled care packages, and unyielding writing support throughout these many years; and Evan, for letting me sleep on your couch, floor, and spare bed and supplying lab materials when I needed them most. To all three nuclears and to my extended family: thank you for patiently listening to rants about alpacas, mountains, and teeth. I love you all very, very much.

TABLE OF CONTENTS

LIST OF TABLES	xi
LIST OF FIGURES	xii
CHAPTER 1: INTRODUCTION	1
1.1 A Coast-Highland Connection.....	4
1.2 Summary of Research Problems	11
1.2.1 Baseline Data for a New Seasonality Proxy	12
1.2.2 An Elevation Transect for Provenance Research.....	12
1.3 Research Questions.....	13
1.4 Overview of Document Structure	14
CHAPTER 2: BACKGROUND	15
2.1 Archaeological Context	15
2.1.1 Coastal Sites	16
2.1.1.1 Quebrada Jaguay	16
2.1.1.2 Pampa Colorada 343	19
2.1.2 A High-Elevation Comparison.....	20
2.1.2.1 Cuncaicha	21
2.1.3 Outstanding Research at Cuncaicha.....	23
2.1.3.1 Site Seasonality	23
2.1.3.2 Human Provenance	25
2.1.4 Section Summary	26
2.2 Study Area	27
2.2.1 Local Geology	29
2.2.2 Hydrology	30
2.2.3 Highland Ecology	32
2.2.3.1 Fauna.....	33
2.2.3.2 Flora	34
2.2.4 Section Summary	35
2.3 Stable Isotopes	35
2.3.1 Stable Oxygen.....	36
2.3.2 Oxygen Isotopes for Archaeological Research	36
2.3.2.3 Analytical Interpretations.....	38
2.3.3 Section Summary	38
2.4 Stable Isotopic Inputs to the Study Area	39
2.4.1 Input Sources for the Pucuncho Basin and Western Slope	39
2.4.1.1 Pacific Inputs	41
2.4.1.2 The Atlantic Source	42
2.4.2 Stable Isotopic Controls	42
2.4.2.1 Fractionation	42

2.5 Climate Variability	43
2.5.1 Annual Variability, Seasonality	43
2.5.2 Inter-Annual Variability	45
2.6 Proposed Study and Predictions	46
2.6.1. Predictions.....	46
2.6.1.1 Andean Surface Water Seasonality	46
2.6.1.2 The Elevation Transect	49
CHAPTER 3: METHODS	50
3.1 Field Methods and Collection Procedure	50
3.1.1 Elevation Sampling	50
3.1.2 Temporal Sampling	52
3.1.2.1 Daily Tests	53
3.1.2.2 Seasonal Tests	53
3.1.2.3 Yearly Tests	53
3.1.3 Sampling Procedure	54
3.1.3.1 Labeling System.....	55
3.2 Laboratory Analysis of Oxygen and Hydrogen	55
3.3 Calculated Change for Temporal Tests.....	56
3.4 Software Analyses	57
3.4.1 Watershed and Stream Order Classifications.....	57
CHAPTER 4: RESULTS.....	59
4.1 General Results	59
4.1.1 Results of Sample Collection	59
4.1.2 Results of $\delta^{18}\text{O}$ and δD Analysis	63
4.1.3 Stable Isotopic Variation In Andean Surface Waters.....	71
4.2 Results of Seasonal Sampling	72
4.2.1 Local Variation in Andean Surface Waters Between Seasons	73
4.2.2 Results of Temporal Testing	76
4.2.2.1 Boxplot Assessment for All Temporal Tests	77
4.2.3 Daily Tests	78
4.2.3.1 Simultaneous Tests	78
4.2.4 Seasonal Tests	85
4.2.5 Yearly Tests	91
4.2.5.1 Annual Tests	94
4.2.5.2 Interannual Tests.....	94
4.2.6 Results of Temporal Comparisons.....	97
4.2.6.1 Change Over Multiple Time Scales, Controlled for Location	99
4.3 Spatial Variation in Stable Oxygen in Southern Peru	102
4.3.1 $\delta^{18}\text{O}$ Variation Across an Elevation Transect.....	103
4.3.2 Seasonal Variation in $\delta^{18}\text{O}$ by Elevation	106
4.3.2.1 Dry Season.....	106
4.3.2.2 Wet Season	107

4.3.3 $\delta^{18}\text{O}$ Variation Across Watersheds	109
4.3.3.1 Jaguay Drainage Basin	112
4.3.3.2 Majes Drainage Basin	114
4.3.3.3 Ocoña Drainage Basin	114
4.3.4 Variation in $\delta^{18}\text{O}$ by Stream Order	114
4.3.4.1 Jaguay Surface Waters	117
4.3.4.2 Majes Surface Waters	117
4.3.4.3 Ocoña Surface Waters.....	118
4.3.5 Range of $\delta^{18}\text{O}$ Across Elevations Throughout the Central Andes.....	120
4.4 $\delta^{18}\text{O}$ for Archaeological Human Provenance Research	124
4.4.1 Waters On and Off the Plateau	125
4.4.2 Abbreviated Vidal Ecozones	126
4.4.3 The Humans of Cuncaicha	129
CHAPTER 5: DISCUSSION AND CONCLUSIONS	132
5.1 General Comments	132
5.2 Seasonal $\delta^{18}\text{O}$ Variation in Regional Surface Waters	132
5.2.1 Prospectus for a Seasonal Proxy	134
5.3 Spatial $\delta^{18}\text{O}$ Variation in the Central Andes	135
5.3.1 Reconciling the Watershed Effect and Archaeological Aims.....	137
5.4 Isotopic Methods	139
5.4.1 The Baseline: Isotopes Through Time, Across Space.....	139
5.4.2 Consider the Dentist: Microdrills and Teeth	141
5.5 Next Steps	141
5.5.1 Seasonality Research.....	141
5.5.2 Mobility Research.....	143
5.6 For Posterity.....	144
5.7 Summary of Conclusions	145
5.8 A Case for Interdisciplinary Science	146
REFERENCES	148

LIST OF TABLES

Table 1: Summary of Results. In order of increasing elevation. Water Sample (WS) number indicates the year the sample was collected.	65
Table 2: Summary of Sampling for Each Field Season.....	73
Table 3: Results of Daily Tests.	80
Table 4: Statistical Results for Simultaneous Tests.	84
Table 5: Results of Seasonal Sampling.	86
Table 6: Statistical Results of Seasonal Sampling.....	88
Table 7: Results of Annual Sampling.	91
Table 8: Results of Annual Statistical Tests.	94
Table 9: Results of Interannual Tests.	95
Table 10: Results of Interannual Statistical Tests.....	95
Table 11: Results of Elevation Subsets.	103
Table 12: Results Divided by Watershed.....	109
Table 13: Summary of $\delta^{18}\text{O}$ Variation Among Stream Orders.....	115
Table 14: Summary of Data from Bershaw et al. 2016.	120
Table 15: $\delta^{18}\text{O}_{\text{DW}}$, $^{87}\text{Sr}/^{86}\text{Sr}$, and $\delta^{13}\text{C}_{\text{VPDB}}$ values from the humans of Cuncaicha.....	129

LIST OF FIGURES

Figure 1: Map of the Central Andean study region. Light blue circle shows study area.	3
Figure 2: Map of the study area. Sites include Pampa Colorada 343 and Quebrada Jaguay 280 at the coast, Cuncaicha in the highlands, and three Alca obsidian sources.	5
Figure 3: Aerial view of the three sites and Alca obsidian sources. Imagery from Google Earth Pro.	16
Figure 4: Overview of Quebrada Jaguay 280. View to the north during the dry season.	19
Figure 5: View of the shell middens at Pampa-Colorada 343. View to the northeast during the dry season. Photo courtesy of Kurt Rademaker.	20
Figure 6: Cuncaicha rockshelter archaeological site on the Andean Plateau. View to the south during the dry season. Nevado Coropuna is visible to the east behind the shelter.	22
Figure 7: Cross-section of an adult vicuña incisor showing parallel enamel growth lines characteristic of an ever-growing tooth.	25
Figure 8: Map of Cuncaicha rock shelter, Pucuncho Basin, and Alca-1, 4, and 5 sources.	28
Figure 9: Map of Ocoña, Jaguay, and Majes watersheds.	31
Figure 10: The prominent water bodies of the study area. These include high-altitude springs (upper right, dry season) and wetlands (upper left, wet season); as well as canals (lower left, dry season) and rivers and streams (lower right, dry season) found at all elevations.	32
Figure 11: A herd of vicuña on the Andean Plateau, posed in front of Nevado Coropuna. Image shows llareta cushion plants and bunch grasses during the dry season.	34
Figure 12: Predicted seasonal variation in $\delta^{18}\text{O}$ in precipitation for the Pucuncho Basin based on OIPC modeled values for water sampling locations of Chala-Aldana et al., 2018.	44
Figure 13: SENAMHI stream gauge data for 2018-2019 in the Majes (top) and Ocoña (bottom) watersheds. Each graph shows volume of stream discharge (left axis) over time (bottom axis). Together these images show the complete onset, peak, and decline of the 2018-2019 wet and dry seasons in the study area.	48
Figure 14: Map of the Survey Area. The survey route (light pink line) extends from Pampa Colorada 343 and Quebrada Jaguay 280 to Cuncaicha. Sampling crossed three watersheds, the Ocoña, Jaguay, and Majes Drainages.	51

Figure 15: Map of key sampling locations below the plateau. The confluence of Río Capiza (dashed yellow line) and the Río Colca (dashed blue line) mark the beginning of the Río Majes (blue area). The Río Blanco (dashed pink line) discharges over the plateau rim (dotted white line) around ~3500 masl.	52
Figure 16: Map provides an example of stream orders in the study area.	58
Figure 17: Map of all sample locations within the survey area. Yellow triangles show dry season testing and blue circles indicate wet season sampling.	60
Figure 18: Density of samples collected for wet (blue line) and dry (yellow line) seasons. The dry season shows a bimodal distribution of samples; most were collected below 1000 masl or above 3500 masl. The wet season shows a unimodal distribution with most samples collected from above 3500 masl.	63
Figure 19: Plot of $\delta^{18}\text{O}$ and δD for all samples. The black line is the Global Meteoric Water Line (GMWL) $\delta\text{D} = 8(\delta^{18}\text{O}) + 10\text{‰}$. The dashed black line reflects the local surface water line (LSWL) $\delta\text{D} = 7.86(\delta^{18}\text{O}) + 7.08\text{‰}$. Class 1-5 indicates stream order, where first order streams are the smallest volume. The enriched samples below the line are discussed in Figure 21.	72
Figure 20: Seasonal datasets plotted with the respective wet and dry season Local Surface Water Lines (LSWL). Dry season samples (yellow dots) and LMWL ($\delta\text{D} = 7.75 * \delta^{18}\text{O} + 5.52\text{‰}$) are presented on the left and wet season samples (blue dots) and LMWL ($\delta\text{D} = 8.15 * \delta^{18}\text{O} + 11.22\text{‰}$) presented on the right. Values that plot below the GMWL and LSWLs reflect enriched waters.	74
Figure 21: $\delta^{18}\text{O}$ plotted against δD for sample locations replicated as part of the seasonality study. Dashed black line indicates the global meteoric waterline $\delta\text{D} = 8.0 * \delta^{18}\text{O} + 10.00\text{‰}$. Blue solid line $\delta\text{D} = 8.10 * \delta^{18}\text{O} + 10.83\text{‰}$. indicates the local meteoric water line during the wet season. Yellow dashed line represents the local meteoric water line during the dry season $\delta\text{D} = 7.36 * \delta^{18}\text{O} + 3.14\text{‰}$. More samples appear to plot below the line during the dry season.	76
Figure 22: Box plot assessment for the per mil $\delta^{18}\text{O}$ difference between paired temporal samples. Mean instrumental precision (0.03‰) shown by the dashed black line. Maximum instrumental precision (0.22‰) indicated by the dotted grey line.	78
Figure 23: Map of daily sampling locations. Replicate tests are dark blue: the Río Majes, SIM-01 (383 masl); The Río Colca, SIM-02 (896 masl); the Río Grande, SIM-03 (2980 masl), SIM-04 (3396 masl), and SIM-05 (3727 masl); Quebrada Pariaviri, SIM-06 (3967 masl); and the Río Arma, SIM-07 (4085 masl). The diurnal sample (lighter blue), DIUR-01 (3936 masl) derives from the Quebrada de Rata.	81
Figure 24: Observed $\delta^{18}\text{O}$ for simultaneous (dark blue triangles) and diurnal (light blue circles) pairs. Samples include the Río Majes, SIM-01 (383 masl); The Río Colca, SIM-02 (896 masl); the	

Río Grande, SIM-03 (2980 masl), SIM-04 (3396 masl), and SIM-05 (3727 masl); Quebrada Pariaviri, SIM-06 (3967 masl); and the Río Arma, SIM-07 (4085 masl). The diurnal sample, DIUR-01 (3936 masl) derives from the Quebrada de Rata. 82

Figure 25: Change in $\delta^{18}\text{O}$ between pairs collected for daily tests. Replicate tests (dark blue triangles) include the Río Majes, SIM-01 (383 masl); The Río Colca, SIM-02 (896 masl); the Río Grande, SIM-03 (2980 masl), SIM-04 (3396 masl), and SIM-05 (3727 masl); Quebrada Pariaviri, SIM-06 (3967 masl); and the Río Arma, SIM-07 (4085 masl). The diurnal sample (light blue circle), DIUR-01 (3936 masl) derives from the Quebrada de Rata. All demonstrate less change than the maximum machine error (0.22‰)..... 83

Figure 26: Map of the seasonal sample locations: the Río Majes, SEAS-01 (383 masl); The Río Grande, SEAS-02 (1379 masl); the Canal de Pacaychara, SEAS-03 (1811 masl); Huacllay Canal, SEAS-04 (1960 masl); Iray Canal, SEAS-05 (2521 masl); Quebrada de Rata, SEAS-06 (3936 masl); the Río Arma, SEAS-07 (4310 masl); Río Colunga, SEAS-08 (4333 masl); Río Cuncaicha, SEAS-09 (4347 masl); Quebrada Japuchaca, SEAS-10 (4435 masl); Quebrada Pucunchitoyocc, SEAS-11 (4717 masl); and Bofedal Pucunchitoyocc, SEAS-12 (4720 masl). 87

Figure 27: Plot showing $\delta^{18}\text{O}$ values for each sample in the seasonal pairs. Data are coded by wet (blue triangles) and dry (yellow circles) seasons. The Majes (purple), Jaguay (blue), and Ocoña (coral) drainages are indicated. Location codes reflect: the Río Majes, SEAS-01; The Río Grande, SEAS-02; the Canal de Pacaychara, SEAS-03; Huacllay Canal, SEAS-04; Iray Canal, SEAS-05; Quebrada de Rata, SEAS-06; the Río Arma, SEAS-07; Río Colunga, SEAS-08; Río Cuncaicha, SEAS-09; Quebrada Japuchaca, SEAS-10; Quebrada Pucunchitoyocc, SEAS-11; and Bofedal Pucunchitoyocc, SEAS-12. 89

Figure 28: Plot showing the difference in $\delta^{18}\text{O}$ (‰) between seasonal sample pairs. Location codes in order of increasing elevation: the Río Majes, SEAS-01; The Río Grande, SEAS-02; the Canal de Pacaychara, SEAS-03; Huacllay Canal, SEAS-04; Iray Canal, SEAS-05; Quebrada de Rata, SEAS-06; the Río Arma, SEAS-07; Río Colunga, SEAS-08; Río Cuncaicha, SEAS-09; Quebrada Japuchaca, SEAS-10; Quebrada Pucunchitoyocc, SEAS-11; and Bofedal Pucunchitoyocc, SEAS-12. All samples demonstrate more change than maximum machine error (0.22‰) and maximum daily change (0.16‰). 90

Figure 29: The $\delta^{18}\text{O}$ of surface waters sampled during the dry season in multiple years. Annual samples (<1 year; yellow circles) include: Quebrada Pariaviri, YR1-01 (3966 masl); Río Arma, YR1-02 (4300 masl); and Quebrada Cuncaicha, YR1-03 (4457 masl). Multiyear samples (>3 years; orange triangles) include the Río Majes, MYR-01 (383 masl); The Río Grande, MYR-02 (1379 masl); Río Grande, MYR-03 (2980 masl); Río León Huactana MYR-04 (4384 masl); Quebrada Cuncaicha (3-year) MYR-05 (4457 masl); and Quebrada Cuncaicha (4-year) MYR-06 (4474 masl). 92

Figure 30: Map of the yearly sample locations. Annual samples (<1 year) include: Quebrada Pariaviri YR1-01 (3966 masl); Río Arma, YR1-02 (4300 masl); and Quebrada Cuncaicha, YR1-03

(4457 masl). Multiyear samples (>3 years) include the Río Majes, MYR-01 (383 masl); The Río Grande, MYR-02 (1379 masl); Río Grande, MYR-03 (2980 masl); Río León Huactana MYR-04 (4384 masl); Quebrada Cuncaicha (3-year) MYR-05 (4457 masl); and Quebrada Cuncaicha (4-year) MYR-06 (4474 masl)..... 93

Figure 31: Per mil difference in $\delta^{18}\text{O}$ between surface waters sampled during the dry season in multiple years. Annual samples (<1 year; yellow circles) include: Quebrada Pariaviri, YR1-01 (3966 masl); Río Arma, YR1-02 (4300 masl); and Quebrada Cuncaicha, YR1-03 (4457 masl). Multiyear samples (>3 years; orange triangles) include the Río Majes, MYR-01 (383 masl); The Río Grande, MYR-02 (1379 masl); Río Grande, MYR-03 (2980 masl); Río León Huactana MYR-04 (4384 masl); Quebrada Cuncaicha (3-year) MYR-05 (4457 masl); and Quebrada Cuncaicha (4-year) MYR-06 (4474 masl)..... 96

Figure 32: Per mil $\delta^{18}\text{O}$ change for simultaneous (dark blue), diurnal (light blue), seasonal (green), one-year (yellow) and multi-year (orange) tests. Numbers correspond to sampling locations for each test in order of elevation. Maximum observed machine error indicated by the black dashed line (0.22‰). Maximum daily change (0.16‰) indicated by the blue dashed line. Maximum yearly change (0.58‰) indicated by the orange dotted line. 98

Figure 33: Measured per mil difference in $\delta^{18}\text{O}$ at the daily (yellow) and seasonal (red) scales for the Quebrada de Rata, Río Arma, and Río Majes..... 100

Figure 34: Per mil change in the $\delta^{18}\text{O}$ of surface waters at the daily (yellow), seasonal (red), and annual (blue) scales for the Río Arma, Río Grande, and Río Majes. Pairings from the Quebrada Cuncaicha reflect yearly change at a one- and four-year scale..... 102

Figure 35: Map of all sampling locations illustrating the $\delta^{18}\text{O}$ values of the collected surface waters. 104

Figure 36: Distribution of $\delta^{18}\text{O}$ across elevation. The plot incorporates all samples. Four outliers include WS1962 (pink) in the Ocoña drainage basin, WS1815 (blue) in the Majes drainage basin, and the paired samples WS1945 and WS1965 (orange) from the Jaguay drainage basin..... 105

Figure 37: Distribution of $\delta^{18}\text{O}$ of Andean surface waters by elevation. Data are divided by season. Yellow dots (left) reflect the 2018 and 2019 dry season samples and blue triangles (right) the 2019 wet season samples. 108

Figure 38: Dot plot of $\delta^{18}\text{O}$ range for the three sampled drainage basins. The Ocoña expresses the most depleted surface water values overall, and the Jaguay the most enriched values. ... 110

Figure 39: $\delta^{18}\text{O}$ variation by elevation divided by individual watersheds. Jaguay drainage is on the left, Majes center, and Ocoña right. Data are coded by wet (blue triangles) and dry (yellow circles) seasons..... 111

Figure 40: Map of the Jaguay drainage basin and the Quebrada de Rata samples.	113
Figure 41: Map showing stream order for sampling locations.	116
Figure 42: Stream order $\delta^{18}\text{O}$ values for the Jaguay, Majes and Ocoña watersheds.....	119
Figure 43: Map of Bershaw et al. 2016 (circles) and Milton 2018-2019 (triangles) water sample locations. $\delta^{18}\text{O}$ values scaled to be consistent across both datasets.....	121
Figure 44: Bershaw et al. 2016 (dark grey circles) and Milton's 2018-2019 (light grey triangles) surface water samples plotted in a regression of $\delta^{18}\text{O}$ and δD . The solid black line is the Global Meteoric Water Line ($\text{GMWL } \delta\text{D} = 8(\delta^{18}\text{O}) + 10\text{‰}$).	122
Figure 45: The elevation distribution of $\delta^{18}\text{O}$ in surface waters for both Bershaw et al. 2016 (dark grey circles) and Milton 2018-2019 (light grey triangles) data.	124
Figure 46: Plot comparing the spread of possible $\delta^{18}\text{O}$ values off (light grey circles) and on (dark grey triangles) the Andean Plateau.....	126
Figure 47: Dot plot of the spread of $\delta^{18}\text{O}$ values observed in the surface waters across three Central Andean ecozones. Coastal (<500 masl), Yungas (500-2500 masl), and Highland (>2500 masl).....	128
Figure 48: $\delta^{18}\text{O}_{\text{DW}}$ values for the five humans of Cuncaicha plotted against surface water values from the study area.	130
Figure 49: The $\delta^{18}\text{O}_{\text{DW}}$ for the humans of Cuncaicha plotted against the $\delta^{18}\text{O}$ values in surface waters from the Central Andes.	131

CHAPTER 1: INTRODUCTION

Our species experiences physiological stress at high-altitude because of environmental factors such as hypoxia, increased ultra-violet (UV) radiation, cold temperatures, and low humidity (Moore 1979, 2017). The Andes mountains of South America, which average 4000 meters above sea level, constitute the second highest elevation landscape in the world. Evidence from multiple archaeological sites indicates humans began using the Andes at the end of the Last Ice Age (Capriles et al. 2016; Latorre et al. 2013; Rademaker et al. 2014; Yacobaccio 2017). The broader behavioral and mobility strategies of the first Andeans, and the eventual processes of permanent occupation and animal domestication in the high Andes remain uncertain.

Decades of archaeological excavations in South America have led some archaeologists to postulate that high-altitude adaptations developed over multiple millennia (Aldenderfer 2006, 2011; Aldenderfer 1998). Research following this model proposes that phenotypical adaptations to altitude emerged through restricted short-term forays into the highlands from lower elevations (Capriles et al. 2018; Capriles et al. 2016; Haas et al. 2017). Others have proposed that humans may have entered the Andean system at the northern margins, developing adaptations as they migrated south, gradually travelling upward. In the latter model, the Andes would have functioned as a migration corridor for initial groups colonizing the continent (Osorio et al. 2017). A third potential suggests no adaptations are necessary for humans to stay at altitude long-term; rather, resource structure underlies the tenability of montane landscapes. A detailed study of regional settlement systems could provide a viable

approach to unraveling the processes of high-altitude adaptation, initial land use practices, and the eventual domestication of llamas and alpacas in the Central Andes.

In this thesis I present three linked archaeological sites that support a detailed study of settlement systems and adaptation in the Central Andes (Figure 1). I evaluate the potential of using oxygen isotopes to elucidate the connection between these sites. Oxygen isotopes preserved in the enamel apatite of human and animal teeth may be applied as tracers of both human mobility and climate seasonality. As the first phase of study, I have developed a localized oxygen isotope baseline to assess whether stable oxygen would provide a viable means to resolve anthropological questions in the region. In this introduction I present a brief history of the archaeological sites and review previous research to identify outstanding problems and questions requiring further investigation. I discuss my selection of oxygen isotopes to contribute to these issues and conclude with the proposed study and an outline for the document.

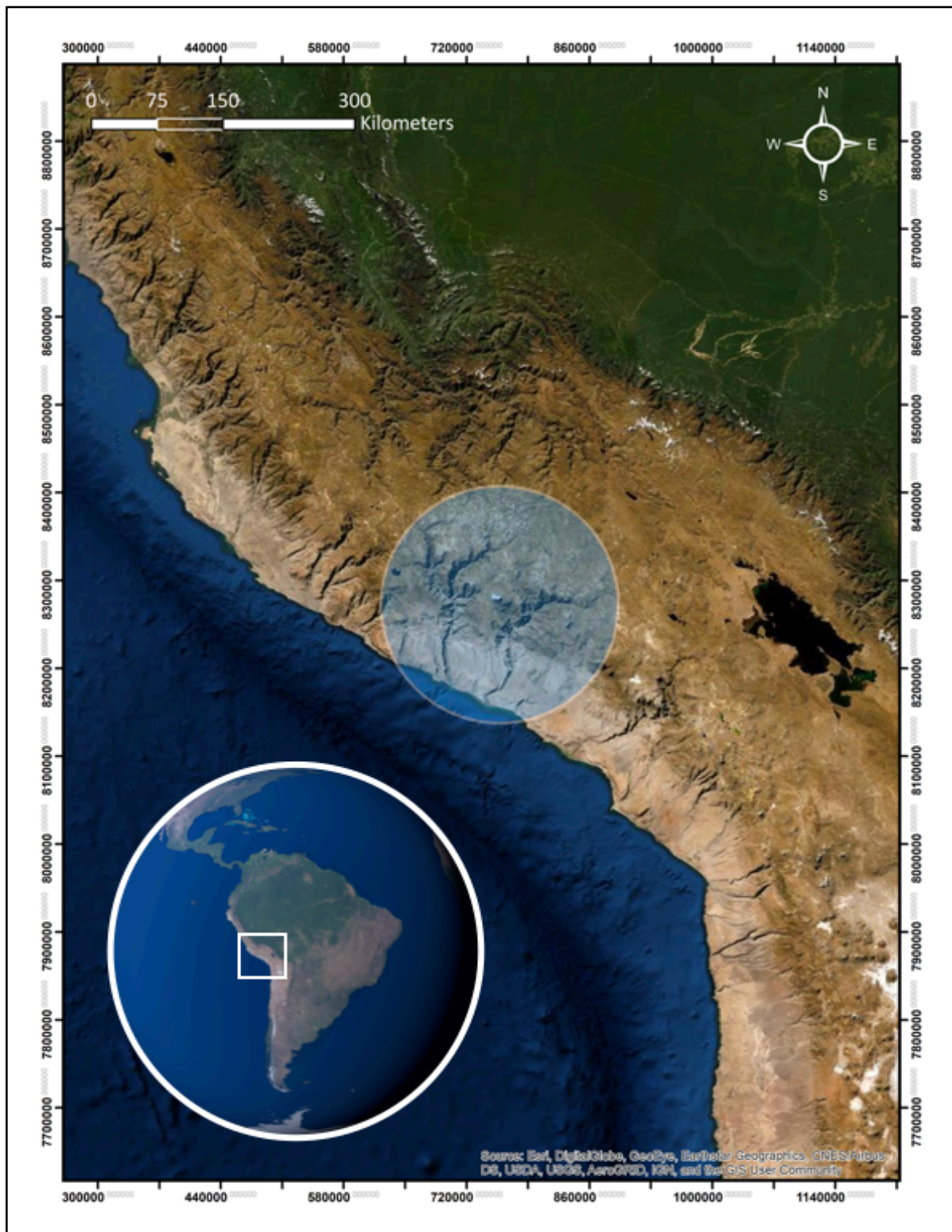


Figure 1: Map of the Central Andean study region. Light blue circle shows study area.

1.1 A Coast-Highland Connection

Near the end of the Terminal Pleistocene (TP), after 14,000 years ago, the first people to colonize South America encountered a complicated backdrop of diverse ecosystems. The mountainous spine that bisects the continent separates the arid Pacific Coast from the lush tropics of the Amazon. On the western border, the steep orography of the Andes Mountains results in vertically stacked ecological zones, each characterized by unique resource structures (Vidal 1981). Studying the first peoples of South America requires the examination of these varied landscapes and associated adaptive strategies.

In southern Peru, material evidence substantiates a connection among various ecological zones that began in the Terminal Pleistocene (TP) and continued well into the Holocene. Some of the earliest archaeological indicators of highland use are found along the Pacific Coast (Figure 2). In 1996, excavations at the maritime site, Quebrada Jaguay 280 (QJ-280), revealed Alca obsidian flakes and a single tool in TP deposits (Sandweiss et al. 1998). The volcanic glass, Alca, outcrops at multiple locations to the north in the high Andes (Rademaker 2006; Rademaker, Glascock, et al. 2013). As no natural processes can transport the tool stone to the coast, the presence of obsidian at QJ-280 points to an early use of the highlands by the first peoples of South America. The material connection extends through both time and space. Northwest of QJ-280, at the coastal site Pampa Colorada 343 (PC-343), Alca obsidian is also found in association with Early Holocene shell middens and human burials (McInnis 2006).

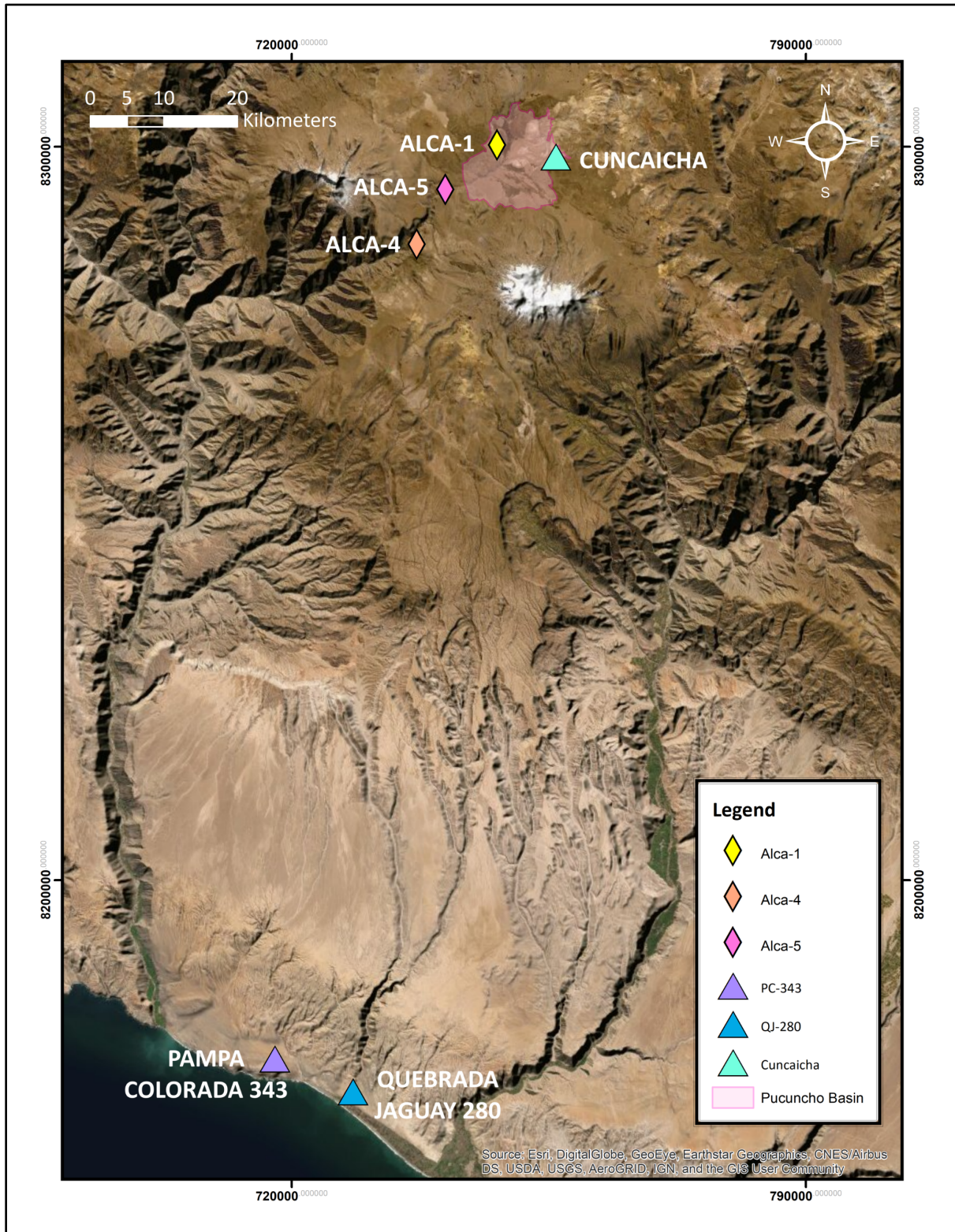


Figure 2: Map of the study area. Sites include Pampa Colorada 343 and Quebrada Jaguay 280 at the coast, Cuncaicha in the highlands, and three Alca obsidian sources.

In 2007, a key site for understanding the coastal obsidian was discovered approximately 150 kilometers to the north. At 4480 meters above sea level, the Cuncaicha rockshelter in the Pucuncho Basin is the highest elevation Ice Age archaeological site in the western hemisphere (Rademaker et al. 2014; Rademaker 2012). The oldest levels date to the Terminal Pleistocene, between 12,600-11,200 years ago, a date range that overlaps the TP sequence at QJ-280 (Rademaker and Hodgins 2018). Cuncaicha is contemporaneous with many of the oldest known sites in South America, and older than most in the Central Andean region (Rademaker, Bromley, et al. 2013). Artifacts from the TP deposits include a rich faunal assemblage of local ungulates and small mammals, and evidence for bone tool and bead production. The dense and diverse lithic assemblage consists of stone tools and debitage manufactured from highland raw materials, such as Alca obsidian. Charred botanicals and ash demonstrate that plants were incorporated into the diet and used for fuel, while unique crafting items such as quartz crystals and ochre suggest symbolic or creative activities were performed on site. In the Early Holocene, ~ 11,800 to 8,200 years ago, non-local low-elevation raw materials and shell appear indicating an increased reliance on inter-zonal movement or trade; and three EH burials post-dating the occupation sequences suggest a change in site use and significance over time.

Alca obsidian at the coast hints at an intriguing connection between low and highland ecosystems; a link manifested through either trade or direct transport. Today, the Pacific coast of southern Peru is extremely arid, and in some areas fresh-water, edible plants, and fauna are only seasonally available. In the local highlands, water and game are perennial resources, but the extreme elevation and cold inflicts an exacting toll on the human body. The physiological challenges at high elevation may have necessitated specific biocultural responses, including

cold-adapted technology or mobility strategies that used lower elevation zones. The obsidian link provides an archaeological mechanism to assess regional settlement systems and potentially, high-altitude occupation and adaptation. If obsidian arrived at the coast via a trade network it may reflect groups exercising residential movement within interior zones. Alternatively, direct transport would require logistical travel to the highlands but not necessitate an extended stay in the Andes.

The obsidian data from the tree linked sites provide convincing evidence of high-altitude use from the time of human arrival in the area. Resolving the connection between the regional low and high elevation landscapes, and nature of Cuncaicha's changing deposits, requires secure evidence to reveal patterns of annual landscape use, migration strategies, and trade networks between the coast and high Andes. Suitable archaeological proxies for mobility may include (A) direct provenance data from human remains or, in the absence of biological tissues; or (B) more indirect measures, such as seasonality data from multiple sites across a region.

Provenance research seeks to identify the origin of an individual or item by tying their chemical signatures to source locations in the environment. Such analyses are commonly applied to raw materials or human remains to trace how far humans have transported items, or themselves, across a landscape. In the Central Andean region, the application of provenance analyses to the human remains at Cuncaicha and PC-343 could reveal whether groups resided predominantly at low, middle, or high elevations.

Data revealing season of site use will help determine the time of year high-elevation living took place, and whether that was restricted to a single season (wet or dry). Further, comparing seasonality data from the coast and the highlands could reveal whether groups

occupied the landscapes at the same or different times of the year. While the former might imply a trade connection, the latter would more likely reflect inter-zonal movement by a single group.

Macro botanical and tooth eruption data from Cuncaicha's juvenile fauna suggest a wet-season occupation between March-April (Moore 2016b). However, neither analytical technique is equipped to identify a dry season occupation. For this reason, Moore (2016) suggested a stable isotopic study of the preserved adult camelid (vicuña or guanaco) teeth, as a potential method of resolving the full season of site use at Cuncaicha.

Stable isotopes could provide a viable method of analysis for both seasonality and provenance research. Isotopes occur in semi-predictable ratios throughout the environment and do not decay over time, thus they provide a useful mechanism for identifying past and present environmental parameters (Michener and Lajtha 2007). Humans and animals incorporate the isotopic composition of their local environment via eating, breathing, and drinking (Schoeninger 1995; Schoeninger and Moore 1992; Schwarcz and Schoeninger 1991). Recent advances in archaeological research have demonstrated the reliable potential of using isotopic markers in tooth and bone as proxies for variations in climate (Green et al. 2018; Sharp and Cerling 1998), ecological change, (Cerling et al. 2015), diet (Knudson et al. 2007; Knudson et al. 2015; Tung and Knudson 2018), and geographic movement (Knudson et al. 2009; Tung and Knudson 2018).

Oxygen isotopes, presented in delta-notation (δ), are commonly applied to seasonality research. $\delta^{18}\text{O}$ values measured from meteoric waters reflect the amount, source, and season of precipitation (Craig 1961a; Dansgaard 1964; Gat 1996, 2000). In the study area, the austral

wet season extends from late December to mid-April, corresponding with incoming Atlantic Ocean moisture carried across the continent by the easterlies (Garreaud et al. 2009). Therefore, it is likely that highland seasonality is predominately reflected in local surface waters as they record annual pulses of precipitation. Surface water seasonality must be tested directly to be sure regional aquifers do not attenuate the incoming signal from precipitation.

In addition to seasonal fluctuations, $\delta^{18}\text{O}$ in surface waters and vegetation varies across a landscape and often reflects atmospheric processes such as latitude and altitude (Craig 1961a). Oxygen isotopes have been proposed and applied elsewhere as a promising biomarker for identifying movement between the distinctive ecological zones of the Andes (Dufour et al. 2014; Haas et al. 2017; Knudson 2009). The hypothesized justification states that waters available in cold, wet highland locations will demonstrate lower ($\delta^{18}\text{O}$) values than those found in the warmer, drier lowlands. The elevation trend has been based on interpolated values provided by the Oxygen Isotopes in Precipitation Calculator (OIPC) (Bowen 2017; Bowen and Revenaugh 2003; Bowen et al. 2005). The calculator is an online tool that predicts the stable isotopic composition of precipitation based on location. The actual patterning of $\delta^{18}\text{O}$ in the surface waters of the west Central Andes, and how those data pertain to archaeological research questions, is only tentatively known, as extensive and intensive field sampling of surface waters is limited (Knudson 2009).

In 2017, Chala-Aldana conducted a stable isotopic study of provenance for the humans of Cuncaicha to investigate whether they developed at or travelled to the high-altitude Pucuncho Basin. The study utilized radiogenic strontium ($^{87}\text{Sr}/^{86}\text{Sr}$) and biogenic oxygen ($\delta^{18}\text{O}$) data sampled from the enamel carbonates of the five individuals' teeth. To construct a baseline

for interpretation Chala-Aldana collected plant and water samples along an elevation transect from the Pacific Coast near QJ-280, to the Pucuncho Basin near Cuncaicha. Plants incorporate local strontium bedrock values, and those plants in turn are ingested by surrounding fauna and humans (Knudson et al. 2010; Scaffidi and Knudson 2020; Scaffidi et al. 2020). Fresh surface waters constitute a primary drinking water source for humans and animals. Chala-Aldana's samples represents the first attempt to map differences in environmental isotopic compositions between low and high elevations in the Central Andes.

Unfortunately, a local strontium isotope baseline was not possible because there was insufficient plant material collected for analysis. Therefore, oxygen isotope data from water samples provided a critical secondary line of evidence to the interpretation that the humans of Cuncaicha developed at altitude. Yet the preliminary environmental data for oxygen isotopes provided conflicting results. Three of the six low elevation (<3500 masl) samples published by Chala-Aldana et al. (2018) provided lower stable oxygen values that would be expected at high altitude . Simultaneously, 3 of the 14 highland samples presented the reverse trend, reporting lower values than expected. At the time of publication, Chala-Aldana (2017) explained the anomalous samples as follows:

In the case of the samples Pu-wa-021, Out-wa-004 and Out-wa-002, which came from standing waters above 3500 masl (Table 8), it is likely that high evaporation rates for the winter 2015 led to an increase of the $\delta^{18}\text{O}$, likely explaining the values obtained. Standing waters are more affected by evaporation than flowing waters. In the case of the samples outside the basin [at low elevation], rapid flow from high elevation waters (Knudson, 2009) likely caused the anomalies in the samples Out-wa-012, Out-wa-013 and Out-wa- 014. $\delta^{18}\text{O}_{\text{MW}}$ [sic] values of the rest of the samples –after excluding the values with anomalies- fit within the expected OIPC trend. (33)

Due to the challenges involved in setting a baseline from plants, the final interpretation considered regional strontium values that had been published elsewhere (Chala-Aldana 2017). However, a recent regional dataset published by Scaffidi et al. (2020) suggests strontium may not account for movement between elevations. The regional bedrock in some areas of the Central Andes presents as a series of uniform geologic layers that bisect multiple elevation zones. The bedrock geology renders strontium a poor candidate to independently distinguish migration of humans or animals between low and high elevation. Considering the incredible utility of a biochemical proxy to differentiate between low and highland living, it is crucial to resolve whether stable oxygen is demonstrably suited to archaeological provenance research in the Andes or whether another isotope will need to be considered.

1.2 Summary of Research Problems

Based on the density and diversity of the earliest site deposits, Rademaker et al. (2014), have postulated that the Cuncaicha rock shelter may have been used as base camp as early as the Terminal Pleistocene. Such an interpretation would suggest a more rapid biogeographic expansion into high-altitude landscapes than previously proposed (Aldenderfer 2006, 2011; Aldenderfer 1998). Capriles et al. (2016) contest Rademaker et al.'s conclusion directly and argue instead that the Pleistocene occupations likely correspond to “circuits of seasonal logistical mobility” (p. 99).

Determining the seasonality for the Cuncaicha occupation sequences will not resolve the debate regarding site function. However, in combination with other archaeological measures including sediment micromorphology, faunal and lithic analyses, and paleobotanical studies, seasonality would provide critical insights into how humans first began to colonize

high-elevation landscapes (Rademaker et al. 2016). Provenance data from human remains promise the greatest potential for identifying the emergence of extended highland use.

1.2.1 Baseline Data for a New Seasonality Proxy

The faunal and botanical indicators at Cuncaicha reveal wet season occupations during both the Terminal Pleistocene and Early Holocene. Whether the site was also used during the dry season remains untested. Establishing whether there was a dry season occupation will require a new seasonality proxy. Moore (2016) recommended an incremental stable isotope analysis of the archaeological adult faunal teeth at Cuncaicha. As the first phase of this research, I sample the surface waters of the high elevation landscape surrounding Cuncaicha to investigate the seasonal isotopic ecology of the area.

1.2.2 An Elevation Transect for Provenance Research

$\delta^{18}\text{O}$ measured on human and animal tooth enamel have been proposed as a meaningful way to study migration between western Andean ecological zones (Knudson 2009). The principles proposed by Knudson (2009) have since been deployed as assumptions to underly arguments for permanent high-elevation land use by 9,000 to 7,000 years ago (Chala-Aldana et al. 2018; Haas et al. 2017; Haas et al. 2020). All three studies suggest that the $\delta^{18}\text{O}$ values measured from enamel carbonate (Chala-Aldana et al. 2018) or bone bioapatite (Haas et al. 2020; Haas et al. 2017) are consistent with reported values for highland waters. However, with the exception of the 20 water samples collected by Chala-Aldana (2017), the actual stable oxygen patterning of available drinking waters in the local study areas has yet to be explicitly

established. An environmental baseline for the west Central Andes will provide the needed data to confirm or reinterpret such studies.

1.3 Research Questions

The goal of this interdisciplinary thesis is to develop a reliable $\delta^{18}\text{O}$ baseline for the surface waters of the Majes Valley and nearby highlands of southern Peru. I defined the study area based on the location of the three interlinked archaeological sites, Quebrada Jaguay 280, Pampa Colorada 343, and Cuncaicha. To develop the baseline, I collected 98 samples from flowing waters between 36 and 4938 meters in elevation over three austral seasons: July 2018 (dry), February and March 2019 (wet), and June 2019 (dry).

The intended outcome is twofold: first, an environmental dataset is necessary to justify developing a new, exacting method of seasonality for Andean sites; second, an elevation transect will reveal whether stable oxygen is a suitable isotope for provenance research, including studies that assess movement or residence among different altitudinal zones (Chala-Aldana et al. 2018; Haas et al. 2017; Knudson 2009). The research conducted for this thesis does not include the stable isotopic study of the archaeological materials from Cuncaicha. Rather, it initiates the development of an environmental baseline to justify and review archaeological research. I address the following research questions:

- 1. Does $\delta^{18}\text{O}$ measured from the surface waters in the Pucuncho Basin record seasonal change?**

I investigate seasonal and annual oxygen variation in the surface waters in the study area surrounding Cuncaicha as the first phase in developing an isotopic proxy of seasonality.

2. Do the surface waters between the Pacific coast and Andes demonstrate distinct $\delta^{18}\text{O}$ values at different elevations?

I conducted a targeted elevation-transect from the coast to the highlands to identify the specific elevation patterning and primary controls for surface water $\delta^{18}\text{O}$ in the study area.

I develop a baseline for surface water $\delta^{18}\text{O}$ using samples collected from the low elevation Majes Valley and highland Pucuncho Basin during austral wet and dry seasons.

1.4 Overview of Document Structure

To begin, the background in Chapter 2 provides a justification for the intended research in terms of both the archaeological questions asked and the environmental sampling approach applied. It begins by expanding on the archaeological coast-highland connection in southern Peru and describing the research area. The history of investigations and outstanding research questions for the three sites are synthesized. This is followed by a review of stable isotopic analysis in archaeological and environmental research and sets specific predictions for the project based on the regional geography of the research area. Chapter 3 presents the field and analytical methods used to construct elevation and seasonal surface water baselines. Chapter 4 presents the results of three seasons of data collection. Part 1 summarizes general results. Part 2 presents the results of seasonal sampling and Part 3 covers the results of the elevation transect. Chapter 5 discusses the implications of the stable oxygen isotope data for seasonality and mobility studies in the south-Central Andes. In conclusion, Chapter 6 reveals the composite limitations and implications of this work to suggest future directions for stable oxygen analyses in Andean archaeology.

CHAPTER 2: BACKGROUND

Chapter 2 presents a regional literature review to justify the proposed isotopic study. I first review in depth the archaeological evidence for a Terminal Pleistocene and Early Holocene connection between the coast and highlands of southern Peru. I then provide a geological and ecological summary of the study area. Next I review the principles of stable isotopic research, the applications in archaeology, and specific regional controls as they pertain to the study. I conclude by proposing two predictions for expected seasonal and elevation $\delta^{18}\text{O}$ baselines in the project area.

2.1 Archaeological Context

Recent excavations and collections work at the highland site Cuncaicha and the coastal sites Quebrada Jaguay 280 (QJ-280) and Pampa Colorada 343 (PC-343) provide the materials necessary to investigate inter-zonal connections more closely (Figure 3). The next phase of investigation requires determining whether the presence of non-local raw materials, at the coast by the Terminal Pleistocene and in the highlands by the Early Holocene, are the product of direct or indirect (trade) procurement (Rademaker 2017).

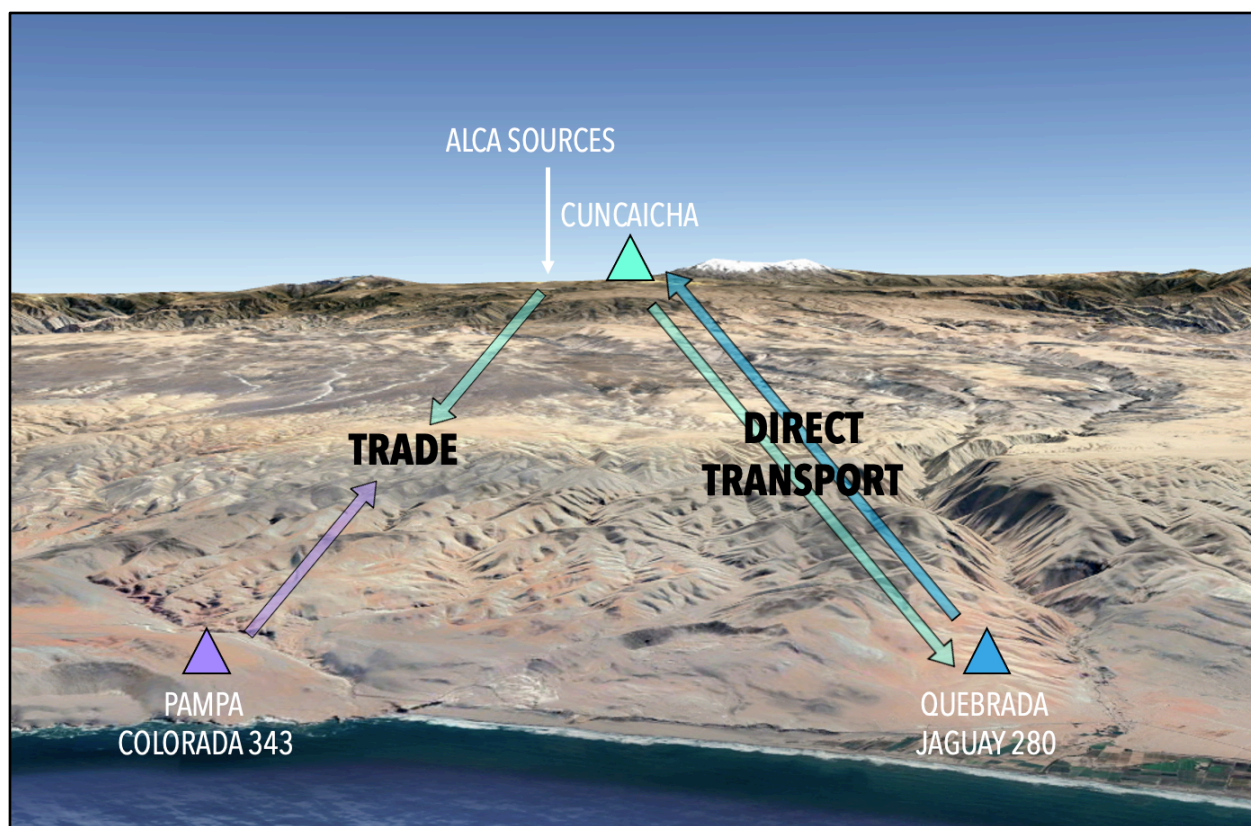


Figure 3: Aerial view of the three sites and Alca obsidian sources. Imagery from Google Earth Pro.

2.1.1 Coastal Sites

2.1.1.1 Quebrada Jaguay

Robust evidence for a Terminal Pleistocene (TP) coast-highland connection first emerged at Quebrada Jaguay 280 (QJ-280), a maritime site seven kilometers inland from a paleo-shoreline in southern Peru (Figure 4) (Sandweiss et al. 1998). TP and Early Holocene (EH) levels at QJ-280 date between 13,000 to 8,300 calibrated years BP (Jones et al. 2017; Sandweiss et al. 1998). Both TP and EH strata contain subtypes of Alca obsidian sourced ~140 kilometers north to the high-altitude core of the Andes Mountains (Sandweiss et al. 1998; Rademaker et al. 2013) (

Figure 4). Other non-local artifacts at the site include petrified wood from the Upper Moquegua formation ~30 kilometers to the north and *Opuntia ficus-indica* (prickly pear cactus) seeds, which derive from a mid-altitude zone in the Peruvian Pampas (Rademaker 2017; Rademaker 2012; Tanner 2001). The faunal assemblage at QJ-280, which includes marine shells, fish vertebrae, and crab, supports the notion that the people who used the site effectively exploited marine resources.

To assess the time of year QJ-280 was occupied, the time of harvest was determined for a sub sample of the shells comprising the site middens. $\delta^{18}\text{O}$ and $\delta^{13}\text{C}$ were measured incrementally from the growth bands of 36 marine shells to reconstruct seasonal sea surface temperatures. The analysis provided a means to determine what time of year the shells were harvested. The data suggest occupations may have been restricted to the austral spring and summer months between February to April (Gruver 2018). These seasonality data are consistent with the summer occupations proposed by Sandweiss (1998). Sandweiss hypothesized that site use would depend on the availability of freshwater in the area. In the present day, water is only observed in the quebrada bed in austral summer. The seasonal flow emerges and dissipates with the wet season in the high Andes. If the timing of modern water flow reflects the annual availability in the past, it is possible that freshwater resources may have limited tenure at QJ-280.

Where groups resided outside of this period remains unknown. It is possible that the inhabitants of QJ-280 networked along the coast in a year-round occupation of a littoral resource patch. Alternatively, coastal groups may have moved inward to exploit the resources of interior zones (Gruver 2018; Rademaker 2017; Sandweiss et al. 1998). In the latter scenario,

the non-local material at QJ-280 points to either mid- or high-altitude zones as potential supplemental habitats.

In 1998 Sandweiss argued convincingly that the Terminal Pleistocene dates, seasonal nature of water flow, and presence of Alca obsidian at QJ-280 supported inter-zonal mobility model of settlement where people moved between the highlands and the coast. While others have incorporated the site in discussions of the coastal migration theory, their statements are generally tentative, given the paucity of South American coastal sites dated to the Pleistocene (Braje et al. 2019; Dillehay et al. 2008; Erlandson 2001; Erlandson et al. 2011).

A revised chronology from QJ-280 reveals that regionally, coastal occupations may have been contemporaneous with or younger than those established for the highlands (Rademaker, personal communication). The new data place the Terminal Pleistocene occupations between 12,400 to 11,500 calibrated years BP and the Early Holocene deposits between 9,700 to 8,200 calibrated years BP (Rademaker and Gruver 2018). These dates support a reconsideration Sandweiss' original model. It is possible that transhumance between elevation zones followed an established migration in the interior. Understanding the settlement systems of the first Andeans will require comparing seasonal evidence from contemporary sites in other locations.



Figure 4: Overview of Quebrada Jaguay 280. View to the north during the dry season.

2.1.1.2 *Pampa Colorada 343*

Fifteen kilometers west of the Quebrada Jaguay drainage, Pampa Colorada 343 (PC-343) is another early maritime site with raw materials from the interior (Figure 5). Two radiocarbon dates on shell reveal an EH age between ~8,920-8,265 calibrated years BP (McInnis 2006). PC-343 contains expansive shell middens and intermittent human burials. Materials at the site include diverse fauna such as surf clams, fish, chiton, and bird; and an assortment of lithic materials including scrapers, awls, projectile points, and debitage. Like Quebrada Jaguay 280, stone tools of petrified wood and Alca obsidian suggest the occupants at PC-343 were familiar with groups or landscapes beyond the coast. For this site, an isotopic study of the human remains would provide the most accurate estimate of human movement

among zones. Contextual evidence dates the human remains to the Early Holocene. If accurate these individuals represent some of the oldest human burials on the Peruvian coast.

Comparably ancient highland and lowland burials would provide the most direct means of studying the difference in lifeways between the Andes and Pacific coast. As of yet, no stable isotopic analyses have been conducted to determine the provenance of the PC-343 human remains.



Figure 5: View of the shell middens at Pampa-Colorada 343. View to the northeast during the dry season. Photo courtesy of Kurt Rademaker.

2.1.2 A High-Elevation Comparison

The Alca obsidian recovered at Quebrada Jaguay 280 and Pampa Colorada 343 led Rademaker (2006) to search the surrounding highlands for outcrops of obsidian and potential

early sites. Subsequent survey resulted in the characterization of five Alca sub-sources and nine highland hunter-gather sites (Rademaker 2012, Rademaker et al. 2013). One site, Cuncaicha, revealed intact strata, rich archaeological deposits, and Terminal Pleistocene (TP) and Early Holocene (EH) dates comparable to the earliest occupations at QJ-280. Analyses at Cuncaicha are ongoing, as discussed below.

2.1.2.1 Cuncaicha

The Cuncaicha rockshelter (4480 masl) is located ~150 from the coast in the Pucuncho Basin, Peru (Rademaker, Bromley, et al. 2013; Rademaker et al. 2014) (Figure 6). A robust chronology from 38 accelerator mass spectrometry (AMS) bone collagen dates brackets the TP and EH occupations with 23 dates spanning between 12,600-11,200 and seven dates between 9500-9000 calibrated years BP (Rademaker and Hodgins 2018). The composite assemblage includes rich deposits, spanning over ten thousand years, of assorted stone tools and animal bones, and rare objects such as crystals, seashell, and ochre. Such persistence of place at Cuncaicha suggests ongoing importance of the Pucuncho Basin for Andean peoples, from initial exploration to contemporary populations (Francken et al. 2018; Rademaker and Moore 2018). For the TP assemblage alone, 100 formal tools, nearly 15,000 pieces of debitage, 6.5 kilograms of faunal material, and ochre show that diverse activities took place at the site from the earliest occupations (Rademaker and Moore 2018; Rademaker et al. 2021 In Prep).



Figure 6: Cuncaicha rockshelter archaeological site on the Andean Plateau. View to the south during the dry season. Nevado Coropuna is visible to the east behind the shelter.

The composition of Cuncaicha's assemblage changes through time. In stark contrast to the deposits at the coast, the Terminal Pleistocene levels of Cuncaicha contain no readily identifiable non-local materials from a different ecological zone. Most of the TP artifacts are local to the surrounding area or sourced to a nearby highland location (Rademaker et al. 2021, In Prep). Further, the presence of bone needles and lithic scrapers and awls suggest technological adaptations suited to the cold environment. The local origin and design of the artifacts suggests the humans occupying the site either had expansive knowledge of the regional ecology upon arrival or were quick to learn the surrounding resource structure.

The Early Holocene assemblage expands to include non-local raw materials from lower elevations, such as marine shells and petrified wood from the Upper Moquegua formation (Rademaker pers comm). The local EH artifacts indicate the sustained use of the highlands in the Terminal Pleistocene continued through the Early Holocene. These materials may reflect emerging trade networks or expanding resource forays.

In 2015, during the fourth and final season of excavations at Cuncaicha, five human burials were recovered. Three EH burials, dating between 9,300-8000 calibrated BP, are contemporaneous with the burials found at PC-343 and represent some of the oldest known and highest-altitude human remains in the world (Francken et al. 2018; Rademaker and Hodgins 2018). A weighted mean of three dates for each EH Burial place the interments around 9133-8788, 8986-8691, and 8536-8386 calibrated years BP. The remaining two individuals date to the Late Holocene, around 4287-4085 and 3361-3182 calibrated years BP. The expansion of raw material types and the interment of human remains signifies a change in site-use starting in the Holocene. These records reflect emerging mobility strategies or trade relations, familiar with lower elevation resources and people.

2.1.3 Outstanding Research at Cuncaicha

2.1.3.1 Site Seasonality

Seasonality at Cuncaicha was assessed using palaeobotanical and zooarchaeological measures. Macro botanical methods have identified organic remains that are only available when plants flower during the wet season (Furlotte, In Progress). Tooth eruption data from Cuncaicha's juvenile fauna corroborate the botanical assessment of a wet season occupation,

placing site occupation between March-April (Moore 2016b). Faunal measurements of tooth eruption and wear have been applied successfully in the northern Junín region of the Central Andes to accurately identify the seasonality and duration of the earliest occupations at Panaulauca (Moore 1998). However, applying the method at Cuncaicha may reveal less accurate results due to the small sample size and differences in regional seasonality and animal behavior (Katherine Moore, personal communication). As such, Moore (2016) proposed an isotopic study to determine the time of harvest for the adult animals at the site. Such an approach exists in the stable isotopic literature (Balasse et al. 2002; Balasse et al. 2003; Eerkens et al. 2014; Green et al. 2018; Knudson et al. 2007; Koch et al. 1989) but will require species- and location-specific developments.

Preliminary faunal analyses conducted in 2012, 2015, and 2018 (Kate Moore, personal communication) revealed three primary species of suitable fauna: vicuña, guanaco, or taruca. Vicuña appear the best suited for a new seasonality proxy for four reasons: (1) vicuña compose 85% of the faunal assemblage, suggesting they were the primary prey for the residents of Cuncaicha (Moore 2013, 2016b); (2) vicuña maintain territories at high-altitude throughout the year; (3) vicuña are obligate drinkers and ingest water and plants directly from their surrounding habitat (Hillson 2005; Moore 2013, 2016a, 2016b; Tomka 1992); and (4) vicuña are the only known ungulate with ever-growing incisors (Figure 7). If there is isotopic variability between seasons vicuña incisors should (A) record local isotopic seasonality and (2) reveal an isotopic signal that records multiple months preceding their death—enabling an accurate estimate of the time of year they died and by proxy, the season of human activity in the area. A preliminary scan of the Cuncaicha faunal materials by Milton and Moore in 2018 suggests

suitable archaeological material may be available for the TP (pending a secure date on dentine) and are abundant for the EH. The first stage of developing a new proxy necessitates the establishment of a seasonal isotopic baseline for the local environment. Because of the wet and dry nature of seasons in the region, such data collection will need to target local surface waters.

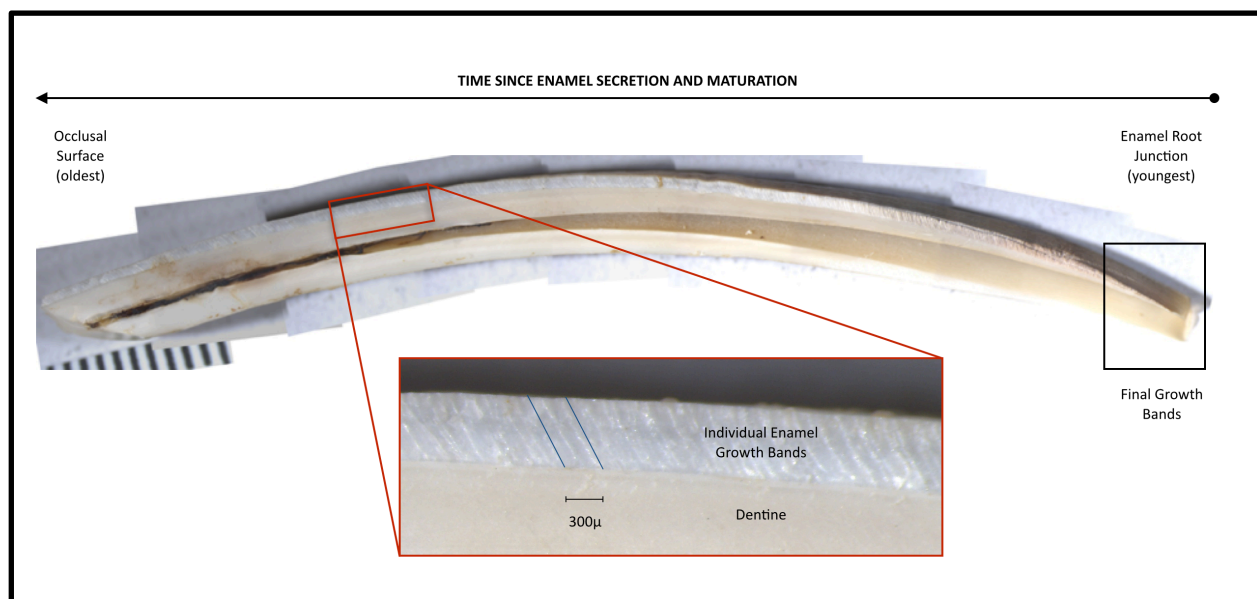


Figure 7: Cross-section of an adult vicuña incisor showing parallel enamel growth lines characteristic of an ever-growing tooth.

2.1.3.2 Human Provenance

The introductory section 1.2 reviewed that $^{87}\text{Sr}/^{86}\text{Sr}$ and $\delta^{18}\text{O}$ analyses have been applied to the human teeth of the Cuncaicha humans to determine the childhood provenance of each individual (Chala-Aldana 2017). In addition to these analyses, three bones from each of the five individuals were isotopically analyzed for $\delta^{13}\text{C}$, $\delta^{15}\text{N}$, and $\delta^{34}\text{S}$ as a means to assess the locality and composition of their adult diet (Haller von Hallerstein 2018). Bone remodels throughout the life of an individual, therefore isotopic values sampled from bone reflect the last 7-10 years of an individual's diet (DeNiro and Epstein 1978; Passey et al. 2005; Sponheimer

and Cerling 2014; Tanz and Schmidt 2010). Comparing both the adolescent values derived from teeth and later life stages recorded in bone could reveal whether the humans of Cuncaicha represent individuals adapted to and persisting at high-altitude or mobile individuals who transitioned between different ecological zones and lived at multiple elevations.

For the dietary analysis, $\delta^{13}\text{C}$, $\delta^{15}\text{N}$, and $\delta^{34}\text{S}$ were measured on bone collagen from the humans remains, as well as a small sample of modern and archaeological fauna. By sampling fauna restricted to high-altitude ecosystems the researchers were able to characterize a local and elevation-restricted dietary signal. The initial assays suggest that the humans buried at Cuncaicha consumed diets consistent with local resources, including viscacha and camelid, during their adult years of life (Haller von Hallerstein 2018).

For both the dietary and provenance studies, some uncertainties for local isotopic patterning remain. Confirming the locality of the Cuncaicha humans during adolescence will require revised interpretations based on isotopic data compiled from the local environment. This research provides the first phase of this work by establishing the $\delta^{18}\text{O}$ values of surface waters in the immediate elevation zones surrounding Cuncaicha.

2.1.4 Section Summary

Obsidian and petrified wood in the Terminal Pleistocene and Early Holocene components of the coastal sites Quebrada Jaguay 280 and Pampa Colorada 343 link the coast to interior ecosystems. Seasonality and provenance data from Cuncaicha could help to resolve site-specific questions. By comparing the data from Cuncaicha with seasonality and provenance data from the coast, it might be possible to reveal the regional settlement strategies active

during the Terminal Pleistocene and Early Holocene. While both studies have been initiated, seasonality data are incomplete, and the provenance study uncertain. For both studies a seasonal and elevation oxygen isotope baseline, constructed from the available surface waters linking the coastal and highland sites, as presented herein, will provide the data necessary to enter the next phase of research. The next section reviews the geologic and ecologic make-up of that study area.

2.2 Study Area

The Cuncaicha rock shelter is located in the Pucuncho Basin ~150 kilometers northwest of the city of Arequipa (Figure 8). The basin is a stable landscape of water, fauna, and flora and is separated from lower-elevation topography. At the eastern extent of the basin, the north-facing rock shelter sits atop a hill, overlooking a flat plain and the perennially flowing *Quebrada Cuncaicha* below.

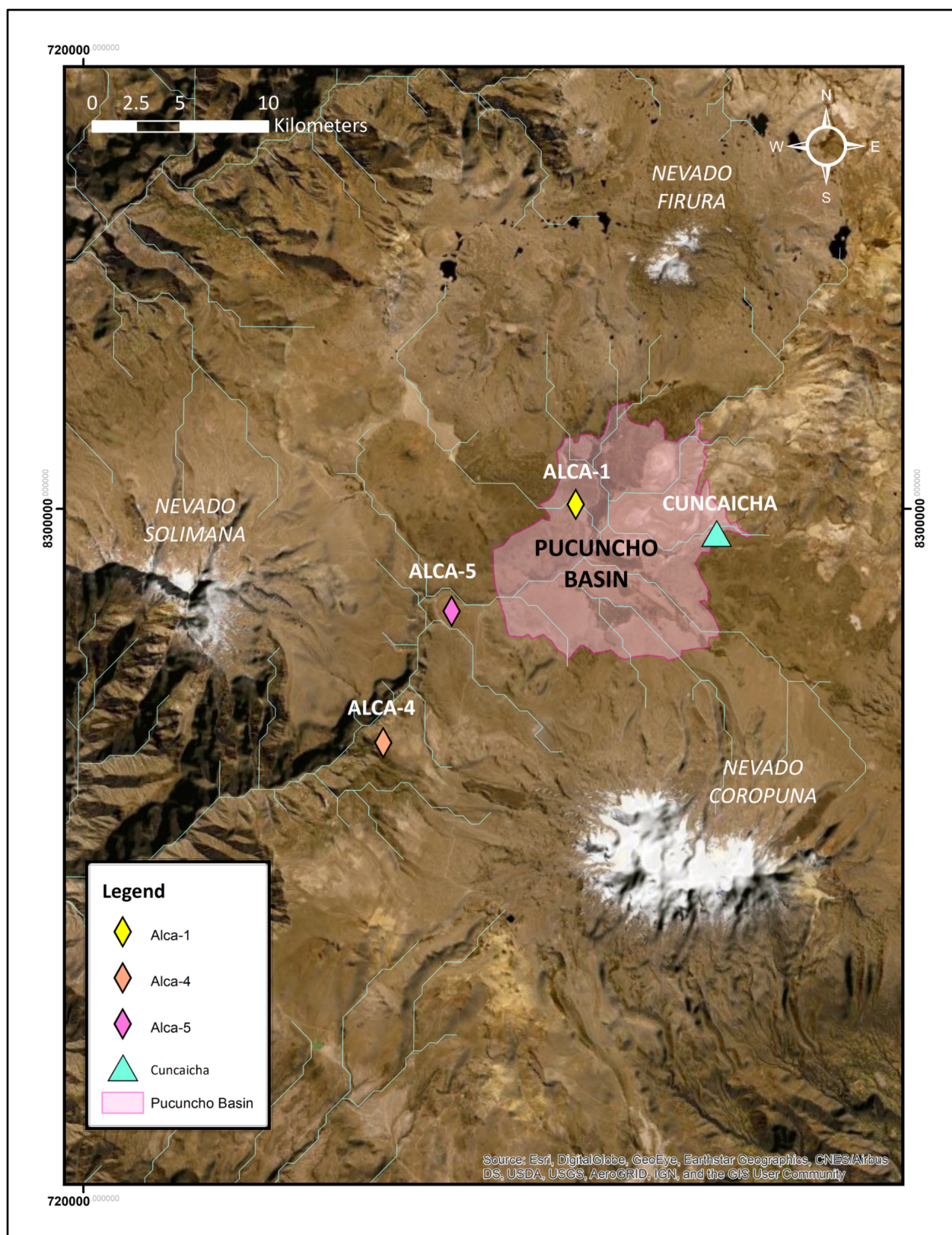


Figure 8: Map of Cuncaicha rock shelter, Pucuncho Basin, and Alca-1, 4, and 5 sources.

2.2.1 Local Geology

Pucuncho is a high-altitude (~4300-4600 masl) basin at the northernmost edge of the Altiplano in southern Peru. The basin appears as a flat plain in the *puna* ecological zone, between three prominent glaciated volcanos: Nevado Firura (5498 masl; 15°14'S, 72°48'W) to the north, Nevado Solimana (6093 m.a.s.l; 15°24'S, 72°52'W) to the west, and the Miocene-age Nevado Coropuna (6405 masl; 15°33'S, 72°53'W) to the south (Bromley 2010). The prominent stratovolcano, Nevado Coropuna was last active during the Early Holocene. Nevados Solimana and Firura are both considered extinct (Venturelli et al. 1978).

Volcanic and glacial processes characterize the geomorphology of the basin. The basin is situated atop an ignimbrite plateau. Initial geologic formation involved volcanic deposits of andesite and basalt throughout the Miocene and Pleistocene. Pliocene-age Grupo Barroso flows compose the area around Cuncaicha, including the shelter itself (Galaś 2011). The area surrounding Cuncaicha has lacustrine and fluvial features. In front of the site, to the north, is a Pleistocene-Holocene alluvial plain.

Extensive glacial activity during the Pleistocene formed the present-day landscape. Moraines, boulders, and glacial outwash (sandy gravel and rock) characterize the area surrounding the shelter. During the Pleistocene, the glaciers of Coropuna, Solimana, and Firura extended 9-12 kilometers further from the termini of present day (Bromley 2010; Bromley, Hall, Rademaker, et al. 2011; Bromley, Hall, Schaefer, et al. 2011). Ice from all three mountains reached elevations as low as 4540 meters, approximately 1000 meters lower than the present-day elevations, between ~20-25 thousand years ago (Bromley 2010; Bromley et al. 2011). Helium and Beryllium dates from the terminal moraines indicate glaciers began retreating

shortly thereafter, well before the arrival of humans (Bromley et al. 2009; Rademaker et al. 2014).

2.2.2 Hydrology

From west to east, the study area encompasses the Ocoña (15,459.9 km²), Jaguay (1,064.3 km²), and Majes (16,935.7 km²) watersheds (Figure 9). Freshwater on the plateau consists primarily of seasonal springs and perennial *bofedales* (wetlands), *quebradas* (streams), and *ríos* (rivers) (Figure 10). Seasonal precipitation and underground aquifers feed the local surface waters (Fonkén 2014). Though the surrounding mountains are glaciated, field inspection has revealed minimal direct meltwater inputs into the basin regardless of season (Bromley and Rademaker 2018, personal communication). Highland springs and streams concentrate into rivers before discharging over the plateau rim. East of Coropuna waters drain to the Colca canyon and discharge as the Río Majes. At lower elevations, water bodies comprise small order streams and large rivers; canals divert waters to surrounding towns.

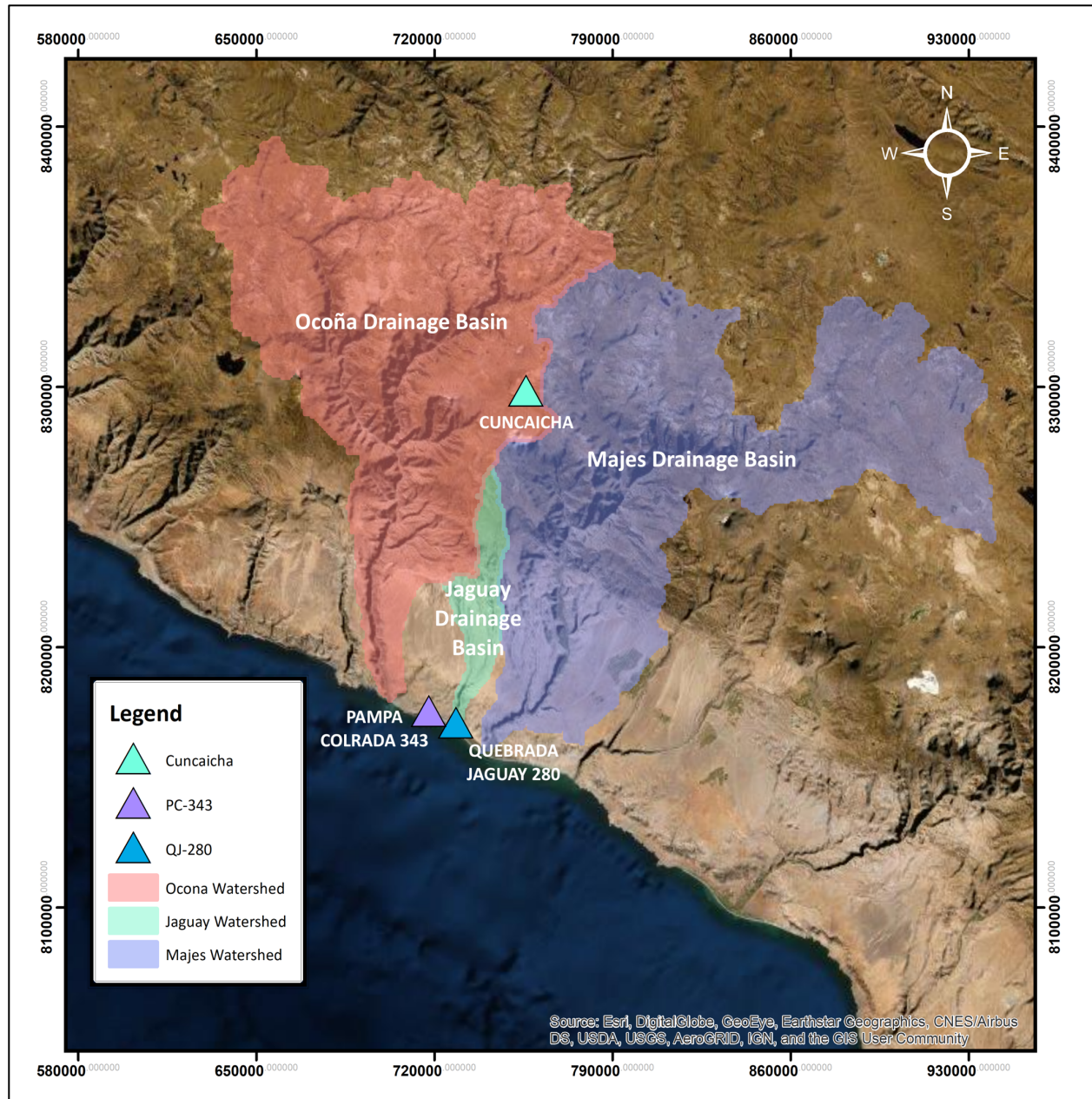


Figure 9: Map of Ocoña, Jaguay, and Majes watersheds.

The Pucuncho Basin lies in the Ocoña watershed. The basin shows a similar configuration to the perched wetland identified by Sitzia et al. (2019). Sitzia et al. describe a high-altitude wetland on an impermeable ignimbrite substrate. The geology results in a near-surface water table and perennial wetlands. The comparable surface geology of the Pucuncho Basin to Sitzia's

study might explain the abundance of perennial freshwater near the surface. Waters from the Pucuncho Basin merge at the Río Arma before discharging over the plateau edge. Below the plateau, the Río Arma becomes the fifth-order Río Ocoña, which empties into the Pacific.

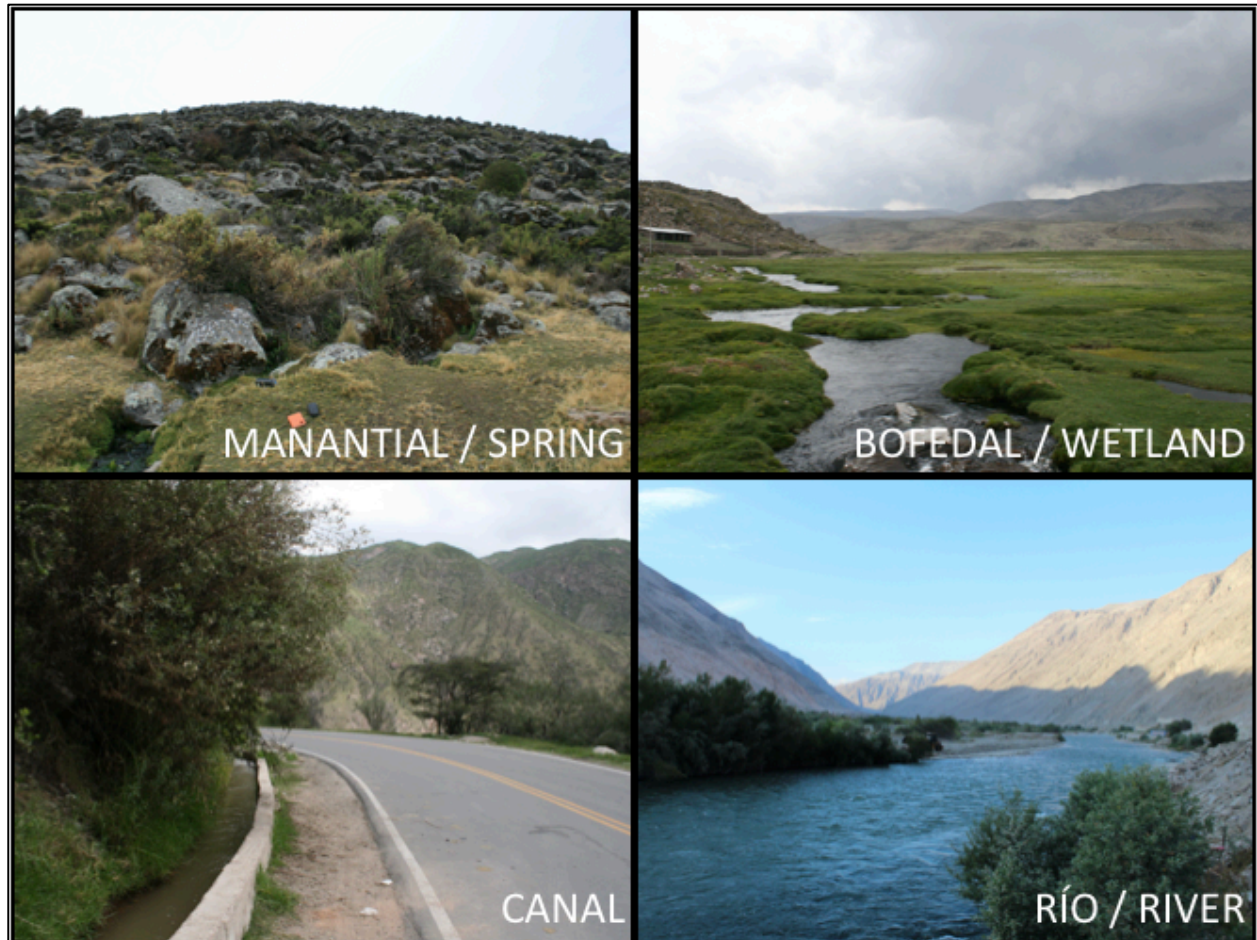


Figure 10: The prominent water bodies of the study area. These include high-altitude springs (upper right, dry season) and wetlands (upper left, wet season); as well as canals (lower left, dry season) and rivers and streams (lower right, dry season) found at all elevations.

2.2.3 Highland Ecology

At 15°S, low seasonal fluctuations in temperature and the perennial availability of water support a stable high-altitude ecological zone, known as the *puna*. The *puna* zone begins around 3200-3700 masl and ends below snow line (5000+). Latitudinally the *puna* zone extends

from approximately 10-30°S latitude (Troll 1968). *Puna* habitats comprise grasses and shrubs. The wetter latitudes in the north are warmer and wetter, demonstrating greater primary productivity. The arid dry and salt *puna* to the south receive diminished annual precipitation. During the first human occupation at the end of the Pleistocene, wetter conditions may have extended a sense of fixed habitats, like those of the wet and dry *puna*, to the southern salt *puna* (Blard et al. 2011).

2.2.3.1 Fauna

Local fauna includes medium-bodied camelids, deer, *Hippocamelis antisensis* (taruca), the small mammal *Lagidium peruanum* (viscacha), and wild birds. Today, four camelid species inhabit the puna: these include the wild *Vicugna vicugna* (vicuña) and *Lama guanicoe* (guanaco), and the domesticated *Lama glama* (llama) and *Vicugna pacos* (alpaca) (Moore 2016a). Only the wild camelid species would have been present during the Terminal Pleistocene and Early Holocene, and important distinctions exist between them. The larger-bodied guanaco is dry-adapted, allowing it to move freely between ecological and altitudinal zones (Tomka 1992). The smaller vicuña (Figure 11) is restricted to high-altitude >3200 masl and is an obligate drinker, making it unsuited to occupy arid environments (Franklin 1983; Moore 2016a).

Genetic evidence suggests that vicuña populations rapidly expanded on the Andean Plateau at the end of the Pleistocene (Marín et al. 2007; Marín et al. 2017). This may have resulted from climatic amelioration, as abundant pasturage and charged aquifers would have allowed vicuña to range into the lower latitudes of the modern dry and salt *punas* (Blard et al. 2011). Annually fed surface waters have allowed vicuña herds to occupy and maintain highland territories year-round (Marín et al. 2017; Moore 2016a; Yann et al. 2016).



Figure 11: A herd of vicuña on the Andean Plateau, posed in front of Nevado Coropuna. Image shows llareta cushion plants and bunch grasses during the dry season.

2.2.3.2 Flora

The flora of the *puna* includes shrubs, grasses, mosses, and cacti. Microhabitats vary across space because of changes in soil type, elevation, and geographic position. Furlotte (2018) prepared an extensive, site-specific report for Cuncaicha and the surrounding Pucuncho Basin. Furlotte identified multiple perennial grasses, woody shrubs, and cushion plants. Common grasses include *ichu* bunch grass including *Festuca*, *Stipa*, and *Calamagrostis*; and small-to-medium shrubs such as *Parastrephia lucida* and *Parastrephia quadrangularis* (Szpak et al. 2013). The cushion plant, *Azorella compacta*, common name, *llareta*, is the most probable fuel for the inhabitants of Cuncaicha (Figure 11). To the west, the *quenual* tree may have

served as a second important resource. The modern elevation limit for local *quenual* falls between 4000-4200 masl.

2.2.4 Section Summary

The surface waters of the study area transect three prominent watersheds populated by various water body types. Available waters support plants and animals in a high-altitude ecological zone, the puna, before discharging southwest to the Pacific coast. The next section reviews the principles of stable isotopes and outlines the specific controls for oxygen isotopes in the region.

2.3 Stable Isotopes

An isotope refers to the different atomic masses of a single element. The variation in weight is driven by the number of neutrons in the atom's nucleus, which is denoted by the number to the upper right of an element (Kendall and Caldwell 1998). Unlike radioactive isotopes, stable isotopes do not decay over time. Different elements occur in predictable ratios throughout the global environment. Typically, the most stable weight of an isotope is found in the greatest abundance (Kendall and Caldwell 1998). The relative abundances of certain isotopes are controlled by specific geologic, biologic, or atmospheric processes (Luz et al. 2009; Luz et al. 1984). Fractionation processes result in the enrichment of one stable isotope over another, where lighter isotopes react more readily to kinetic processes. The processes driving fractionation differ between elements.

2.3.1 Stable Oxygen

There are three stable forms of oxygen atoms, each containing eight protons and between eight and ten neutrons (Kendall and Caldwell 1998). Oxygen-16 (^{16}O) constitutes 99.76% of available oxygen, oxygen-18 (^{18}O) 0.2%, and oxygen-17 (^{17}O), the rarest, comprises only 0.04%. The standard notation for oxygen, $\delta^{18}\text{O}$, expresses the measured ratio of heavy to light isotopes in a sample, $^{18}\text{O}/^{16}\text{O}$, as compared to a standard (Craig 1961b). The global standard for oxygen isotopes is the Vienna Standard Mean Ocean Water (VSMOW).

^{18}O varies with meteoric processes including distance from source, latitude, altitude, aridity, temperature, and precipitation (Craig 1961a; Dansgaard 1954, 1964; Gat 1996, 2000).. Oxygen fractionation occurs during multiple phases of the water cycle including evaporation, transportation, and condensation. Craig (1961a) demonstrated a linear relationship exists between δD and $\delta^{18}\text{O}$ in precipitation, known today as the *meteoric water line (MWL)*. Building on Craig's research, Dansgaard (1964) showed that the $\delta^{18}\text{O}$ of precipitation increases in value with increasing temperature and vice versa.

2.3.2 Oxygen Isotopes for Archaeological Research

The predictability of $\delta^{18}\text{O}$ across a landscape allows for reconstructions of human and animal movement and regional assessments of short- (seasonal) and long-term (decadal) climate change (Bowen 2010; Bowen and Revenaugh 2003; Bowen and Wilkinson 2002); principles adapted for archaeological research. Living terrestrial organisms assimilate the isotopic ratios of their local ecosystems via eating, breathing, and drinking (Passey et al. 2005; Sponheimer and Cerling 2014). Advances in paleontological research have revealed the

potential of using organic and inorganic human and animal tissues as records of ecological change (Bocherens et al. 1996; Cerling and Harris 1999; Cerling and Sharp 1996; Drucker et al. 2008; Fry 1991; Iacumin et al. 2000; Koch et al. 1998), diet (Bocherens et al. 2016; Cerling and Harris 1999; DeNiro and Epstein 1978; Díaz-Zorita Bonilla et al. 2016; Drucker and Bocherens 2004; Passey et al. 2005; Schoeninger and Moore 1992; Somerville et al. 2015; Sponheimer and Cerling 2014), health and life history (Smith et al. 2018), and geographic movement (Balasse et al. 2002; Chala-Aldana 2017; Dufour et al. 2014; Knudson 2009; Knudson et al. 2009; Price et al. 2002; Santana-Sagredo et al. 2018; Zazzo et al. 2006).

Metabolized oxygen isotopes are incorporated into tooth and bone apatite (Lee-Thorp and Sponheimer 2003). The high organic content of bone is more susceptible to diagenic change and heating alterations than the mineral portion of teeth, therefore bones are rarely used for stable oxygen analyses (DeNiro 1985; Lee-Thorp 2002; Lee-Thorp and Sponheimer 2003; Schoeninger et al. 2003; Schoeninger and Moore 1992; Schwarcz and Schoeninger 1991; van Klinken 1999; Zazzo et al. 2013). The highly mineralized nature of tooth enamel leaves it resistant to diagenic processes, making it the preferred tissue for stable oxygen analysis (Bocherens et al. 2011; Lee-Thorp et al. 2003).

The use of oxygen isotopes in archaeological provenance research in the Andes is a relatively recent development (Knudson 2009). Oxygen isotopes are assumed to reflect regional seasonal or spatial variations in imbibed waters, as humans and animals primarily consume oxygen via drinking (Longinelli 1984; Luz et al. 1984). Archaeologists estimate local climate, migration between areas, and provenance during early life using the $\delta^{18}\text{O}$ of human tissues as a proxy for drinking water (Daux et al. 2008; Kennedy et al. 2011; Luz et al. 1984).

2.3.2.3 Analytical Interpretations

Culture and biology present challenges to interpreting the oxygen values derived from human tissues. Water storage, rainwater collection, and preparation techniques (boiling) would all alter the composition of local waters and result in a value that does not exactly match the local environment. The metabolic processes contributing to the observed $\delta^{18}\text{O}$ in biologic tissues varies with species and individual consumption. The formula adjusts for an observed enrichment in $\delta^{18}\text{O}$ resulting from ingested food. Iacumin et al. (1996) developed a formula to convert $\delta^{18}\text{O}$ enamel carbonate (C) to $\delta^{18}\text{O}$ phosphate (P). The formula is printed in *Equation 1*.

Equation 1: Conversion for Enamel Carbonate to Phosphate

$$\delta^{18}\text{O}_\text{P} = 0.98 \delta^{18}\text{O}_\text{C} - 8.5$$

Daux et al. (2008) developed a formula to convert the $\delta^{18}\text{O}$ of human phosphate ($\delta^{18}\text{O}_\text{P}$) to $\delta^{18}\text{O}_\text{W}$ (drinking water). The formula is provided in *Equation 2*.

Equation 2: Conversion for Enamel Phosphate to Drinking Water

$$\delta^{18}\text{O}_\text{W} = 1.54 (\pm 0.09) * \delta^{18}\text{O}_\text{P} - 33.72 (\pm 1.51) \text{ (DAUX)}$$

2.3.3 Section Summary

Stable oxygen values from teeth should reflect the regional landscape, but interpreting those values requires environmental mapping and considerations of both cultural adaptations and species biology. A baseline needs to contend with both spatial change across elevations in the region, as well as seasonal change driven by climate. The next section reviews isotopic inputs to the study area to support the predictions for oxygen isotope patterning in the region.

2.4 Stable Isotopic Inputs to the Study Area

The study area extends from the Pacific coastal sites, Quebrada Jaguay 280 and PC-343, transects through the Majes Valley, and ends in the Pucuncho Basin on the Andean Plateau. The two research objectives include a stable oxygen elevation baseline for provenance analyses, as well as a preliminary seasonality baseline data for the surface waters of the plateau. This section reviews the climate literature to set predictions for both studies.

The temporal and spatial controls of stable isotopes in the environment include (1) input source(s) and (2) fractionation processes. To develop a targeted sampling strategy for the surface waters of southern Peru, I identify potential input source(s) of stable oxygen to the study area, the temporal variability of these sources, and the fractionation effects determining the $\delta^{18}\text{O}$ of Andean surface waters. I briefly review the paleoclimate literature to explore the suitability of a modern baseline for accurately interpreting materials accumulated at regional archaeological sites over the past ~13 thousand years.

2.4.1 Input Sources for the Pucuncho Basin and Western Slope

The isotopic composition of a substrate reflects various geophysical processes or fractionation effects. Water molecules, composed of hydrogen and oxygen, are sensitive to atmospheric and hydrological processes. Seasonal and source inputs are important controls for the isotopic composition of surface waters in the study area. Seasonal atmospheric change manifests as a fluctuation in temperature or precipitation. Oxygen should therefore record the change between wet and dry seasons in the study area.

Next, it is important to control for the fractionation processes that control the isotope. Multiple sources or fractionation may complicate analysis. As a regional example, competing stable oxygen inputs from the Pacific and Atlantic could attenuate a seasonal signal in the high-Andes.

Climate variability in the study area reflects the specific air circulation active in the geographic location. South American climate encompasses tropic, subtropic, and extra-tropic zones; the seasonal, annual, and inter-decadal climate regimes vary between regions (Bershaw et al. 2010; Blard et al. 2011; Garreaud et al. 2003). The Andes pose a distinct orographic barrier to atmospheric circulation and moisture transport, especially between the latitudes of 0-40°S where the Andean mountain belt frequently rises above 4km in elevation (Garreaud et al. 2009; Vimeux et al. 2009).

The geographic focus for seasonality is the Pucuncho Basin, a high-altitude, tropical basin at 15°S, the northern edge of the Altiplano. The Altiplano is a meteorologically distinct region of the Central Andes between 15-22°S where the Andes reach their widest lateral extent (Garreaud et al. 2003). Often referred to as the Andean Plateau, the elevation averages >3,700 masl, constituting the highest, uninterrupted territory outside of the Himalayas. The tropics experience relatively stable temperatures year-round; precipitation constitutes the predominant mode of atmospheric change, and seasons are characterized as wet or dry (Vuille et al. 2012). In the Andean sub-tropics, diurnal changes in temperature are more significant than annual change (Thompson et al. 2000; Vuille and Bradley 2000).

In the study area, weather station data from the Pucuncho Basin demonstrate small seasonal amplitudes in temperature, but considerable change in precipitation. Mean

temperature in sub-tropical Andes (>3500 masl) is low (~7°C) and varies between ~25°C during the day, but only ~1-8°C over the course of the year, whereas precipitation increases by as much as 800 mm during the wet season (Dornbusch 1998). Competing moisture sources could complicate predictions for both seasonal and spatial signals (Vuille et al. 2012). Two sources dominate the precipitation inputs for the South American continent: the Atlantic and Pacific Oceans. I discuss both below.

2.4.1.1 Pacific Inputs

Pacific moisture does not contribute much to the composition of water in the Andes (Abbott et al. 2003; Garreaud et al. 2003). Despite the proximity of the Pacific Ocean to the Altiplano, it is not the dominant input source of meteoric waters to the landscape. The topography of the western continent restricts lateral transport of Pacific moisture and an atmospheric temperature inversion at 800 meters above sea level inhibits vertical movement (Rutllant and Ulriksen 1979). The temperature inversion results from subsiding air masses in the southeast Pacific and is responsible for the hyper-arid conditions of the Atacama desert on the southwestern coast. Sporadically, dry air masses from the Pacific will reach the Altiplano. Herreros et al. (2009) identified Pacific marine aerosols and pollen from southern Patagonia in an ice core from Coropuna. Both aerosols and pollen are interpreted as chemical indicators of El Niño events rather than moisture transported from the Pacific. Together the regional temperature inversion and local topography suggest the Pacific does not contribute to the moisture in the Pucuncho Basin. This leaves the Atlantic Ocean as the dominant source of incoming stable oxygen to the study area.

2.4.1.2 The Atlantic Source

The South American Summer Monsoon system (SASM) transports Atlantic moisture across the South American continent to the high Andes. The SASM is a prominent internal mode of climate variability in the southern hemisphere (Vuille et al. 2012). The monsoon originates in the west Atlantic, south of the Intertropical Convergence Zone (ITCZ) in the Atlantic (Garreaud et al. 2009; Garreaud et al. 2003). During peak activity, the SASM transports air masses west across the South American continent, distributing precipitation along the way. While fractionation effects spatial change in meteoric compositions of $\delta^{18}\text{O}$, various climate regimes impact temporal patterns of moisture transport to the area.

2.4.2 Stable Isotopic Controls

2.4.2.1 Fractionation

Precipitation constitutes the primary source for Andean surface waters, though groundwater and meltwater may also contribute to annual flow. The isotopic composition of surface waters reflects upstream processes of air masses prior to final rainout in the depositional environment. A Rayleigh Distillation model is used to describe the isotopic controls of the water cycle (Vuille et al. 2012). Rayleigh fractionation refers to the preferential expulsion of heavier nuclides during condensation and lighter nuclides during evaporation (Dansgaard 1964). For example, evaporated surface waters exhibit more enriched (higher) values than the depleted (lower) values of incoming precipitation. In the low-latitude tropics, the primary controls for the stable isotopic composition of water include altitude, distance, and rainout effects (Dansgaard 1954, 1964; Gat 1996, 2000).

In the tropical Andes, δ values of surface waters reflect the amount of isotopic rainout, or transport efficiency across the monsoon region. The *amount effect* refers to the decrease of stable isotopic values as rainout increases. The continental effect predicts that waters farther from the source (Andes) are lower than those closer to the Atlantic coast. Similarly, waters at higher elevations present lower values than those at low elevation, because rainout increases with elevation. In the research area, rainout increases with *distance* from the Atlantic source and with *altitude* as air masses move up the leeward side of the Andes (Garreaud et al. 2003). Therefore, the stable isotopic composition of precipitation becomes lower as it moves farther into the Altiplano.

2.5 Climate Variability

2.5.1 Annual Variability, Seasonality

The South American Summer Monsoon is a seasonal phenomenon. Annually, increased solar forcing and the displacement of the ITCZ result in the enhanced lofting of air masses over the Andes and increased moisture transport across the continent (Garreaud et al. 2003). The SASM emerges around October, in the austral spring, reaches peak intensity between December and February, and subsides in April, late in the austral fall (Vuille et al. 2012). While active, the SASM pushes Atlantic moisture westward across the South American continent. During this period, northern latitudes and the eastern Amazon Basin receive abundant rainfall. Intra-seasonal oscillations force wet and dry pulses, typically lasting around two weeks ($T \sim 15$ days). In the Altiplano, precipitation varies on a northeast to southwest gradient, where locations closer to the source receive more moisture (Garreaud et al. 2003; Vuille et al. 2012).

The Pucuncho Basin experiences a wet season during the mature phase of the SASM. Seventy percent of local precipitation (600-1000mm) collects between late December to mid-to-late March. The Online Isotopes in Precipitation Calculator (OIPC) predicts the incoming isotopic value of precipitation for the study area (Figure 12) (Bowen 2017). $\delta^{18}\text{O}$ in precipitation is lower during the wet season months and higher during the dry season. As a reflection of local precipitation, surface waters in the Pucuncho Basin should become lower during the wet season as depleted incoming precipitation replenishes the local water table. In contrast, surface waters should demonstrate lower values during the dry months as discharge lowers the water level and evaporation gradually removes lighter isotopes (Bowen 2017).

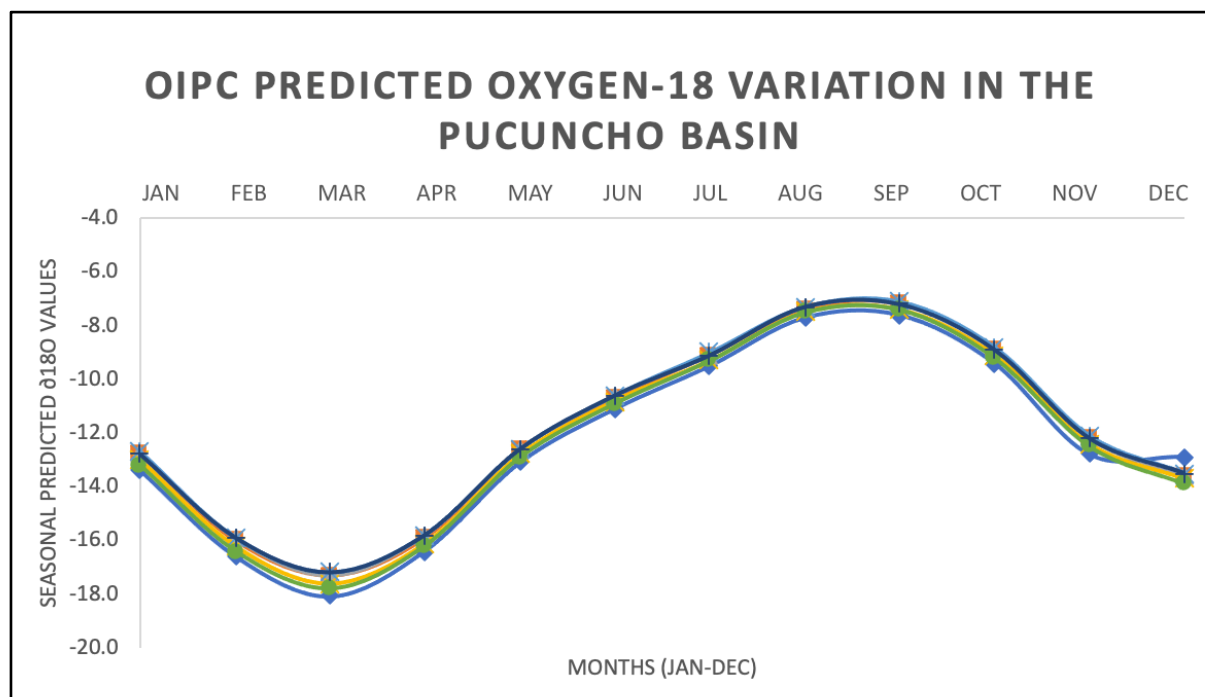


Figure 12: Predicted seasonal variation in $\delta^{18}\text{O}$ in precipitation for the Pucuncho Basin based on OIPC modeled values for water sampling locations of Chala-Aldana et al., 2018.

2.5.2 Inter-Annual Variability

The primary inter-annual mode of climate variability in the area is the El Niño Southern Oscillation (ENSO) phenomenon. ENSO is an internal mode of climate variability. It manifests as multi-year reversals in sea surface temperatures and atmospheric circulation across the tropical and subtropical Pacific. ENSO effects global climate (Garreaud et al. 2009). Climate records suggest the Altiplano is sensitive to significant ENSO activity. The moisture supply to the Altiplano is driven by upper-level atmospheric circulation, which correlates with changes in Pacific sea surface temperature (SST) driven by latent heat flux (Vimeux et al. 2009). The relationship between Pacific SSTs and Atlantic precipitation is indirect (Garreaud et al. 2003).

During ENSO, the Altiplano mirrors the response of the west coast; El Niño events warm the troposphere leading to decreases in precipitation, while La Niña events result in cooler and wetter conditions (Vimeux et al. 2009). Rainfall and ice core data collected between 1955 and 2003 indicate the reverse conditions on the Altiplano during significant El Niño events. In 1982-3 and 1992, El Niño conditions resulted in a 48-100% *decrease* in precipitation. Similarly, an ice core from the saddle of Coropuna showed an enrichment of local pollen and dust for the 1982-3 and 1992 events. However, during the 1998 event, five out of seven local meteoric stations recorded a 5-51% *increase* in the amount of precipitation (Silverio and Jaquet 2012). The rain gauge data indicate a strong ENSO event might temporarily ($\sim T=1-2$ years) attenuate a seasonal signal driven by incoming precipitation.

2.6 Proposed Study and Predictions

I have identified two outstanding data requirements for interpreting the archaeological at Cuncaicha (1) an exacting provenance reassessment of Cuncaicha's human burials and (2) the development of a stable isotopic method to study records of seasonality in the highlands.

Oxygen isotopes have been proposed as an excellent candidate for both studies for three practical reasons: (1) direct and daily ingestion via drinking will reliably capture changes in environment and behavior through time, (2) reliable consumption by both humans and animals, and (3) preservation in the mineral component of tooth enamel will results in reliable preservation. For the study region, oxygen isotopes are bioavailable to humans and animals in the surface waters between the coast and highlands. A dataset constructed from observed values remains to be developed.

As the first phase of research, I propose to construct this baseline from surface water samples collected between the Pacific coast and the high altitude Pucuncho Basin in southern Peru. I offer predictions for seasonal and elevation-based results.

2.6.1. Predictions

Two hypotheses underlie the expected outcome for an elevation transect and seasonal sampling. I back each with a set of predictions that lead me to this hypothesis.

2.6.1.1 Andean Surface Water Seasonality

Hypothesis 1: the $\delta^{18}\text{O}$ of surface waters in the study area will demonstrate lower values during the wet season (Dec-April) and higher values during the dry season.

I used the oxygen predictors in precipitation calculator (OIPC) to estimate the contributions of $\delta^{18}\text{O}$ in precipitation to Pucuncho Basin surface waters during the wet season (Figure 12). The OIPC suggests $\delta^{18}\text{O}$ in precipitation will be 11‰ lower in the wet season; therefore, $\delta^{18}\text{O}$ in surface waters should be lower during the wet season and higher during the dry season. The onset of the wet season is defined by the onset of precipitation. However, stream gauge data from the *Servicio Nacional de Meteorología e Hidrología* (SENHAMI) indicate regional waters do not register incoming rains until mid-January.

I also predicted that surface waters would demonstrate an attenuated seasonal signal when compared to the OIPC, as surface waters average the incoming $\delta^{18}\text{O}$ in precipitation with existing $\delta^{18}\text{O}$ in surface waters. I further predicted that lower order streams (smaller volumes of running water) should be more sensitive incoming $\delta^{18}\text{O}$ in precipitation.

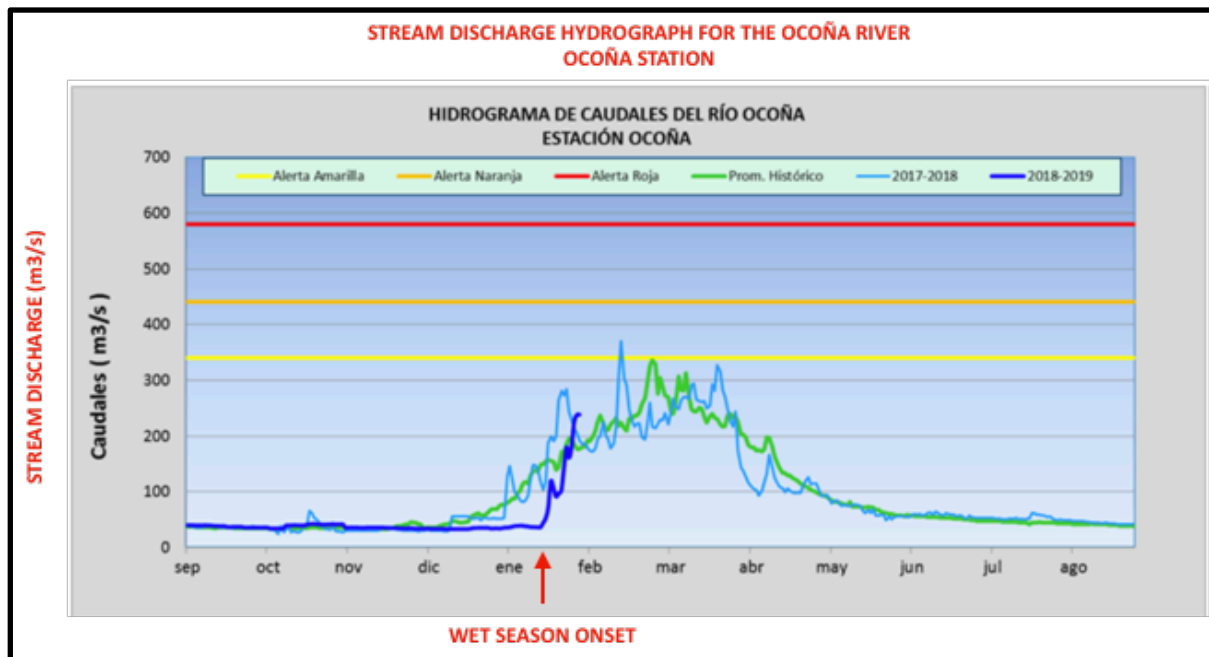
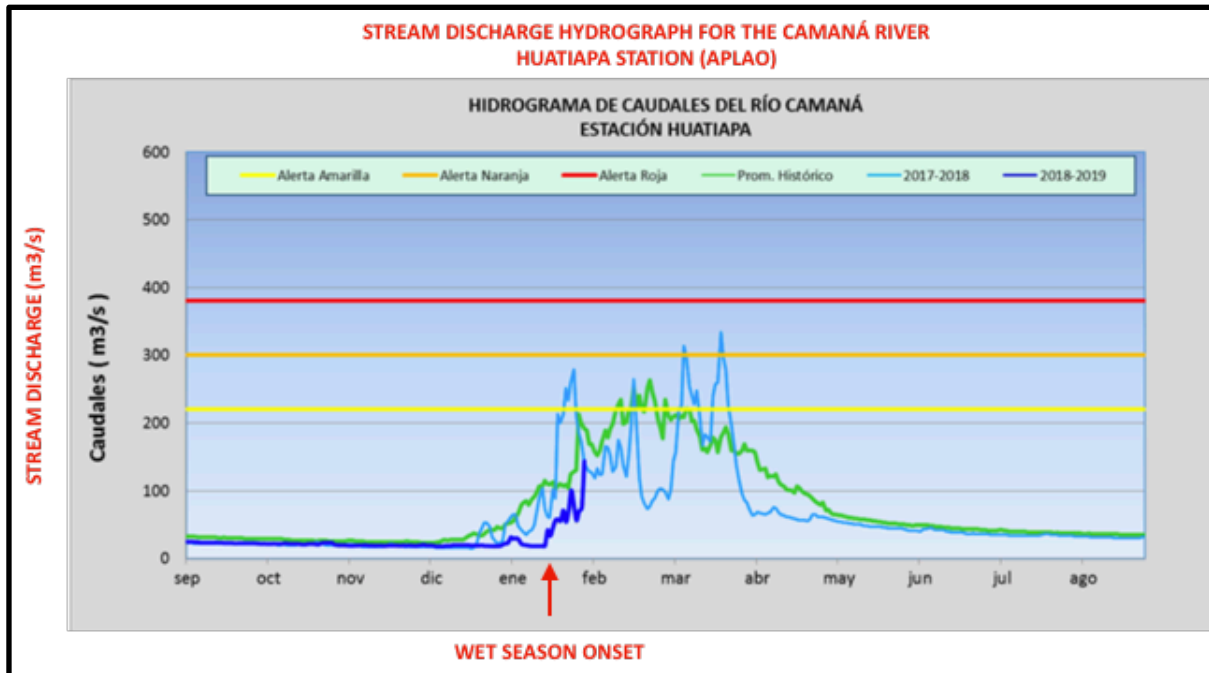


Figure 13: SENAMHI stream gauge data for 2018-2019 in the Majes (top) and Ocoña (bottom) watersheds. Each graph shows volume of stream discharge (left axis) over time (bottom axis). Together these images show the complete onset, peak, and decline of the 2018-2019 wet and dry seasons in the study area.

2.6.1.2 The Elevation Transect

Hypothesis 2: the $\delta^{18}\text{O}$ in surface waters in the study area will be lower in the Andes and higher at the coast—except where lower elevation waters represent large highland discharges.

The altitude effect predicts that the $\delta^{18}\text{O}$ values of surface waters will become lower with increasing elevation. The amount effect predicts that the $\delta^{18}\text{O}$ values of meteoric waters will become lower with increasing distance from the Atlantic coast, as heavier isotopes rain out (the amount and continental effects). On the windward side of the Andes, both effects result in the depletion of meteoric waters. On the leeward side, the effects directly conflict until about 800 meters above sea level (where Pacific inputs may complicate the signal). I predicted that the altitude effect would have a stronger control on surface waters along an elevation transect based on previous work by Mark and McKenzie (2007).

However, I also predicted that larger water bodies (with greater discharge and faster moving waters) might demonstrate a less predictable pattern, as they are less susceptible to evaporation processes.

CHAPTER 3: METHODS

3.1 Field Methods and Collection Procedure

3.1.1 Elevation Sampling

Surface waters were collected from perennial waters throughout multiple elevation zones between the Pacific coast and the highland Pucuncho Basin. The survey extent was determined by the location of three archaeological sites, Cuncaicha, Pampa Colorada-343, and Quebrada Jaguay (Figure 14). The transect represents approximately 150 kilometers from coast to highlands and nearly 5000 meters of vertical elevation.

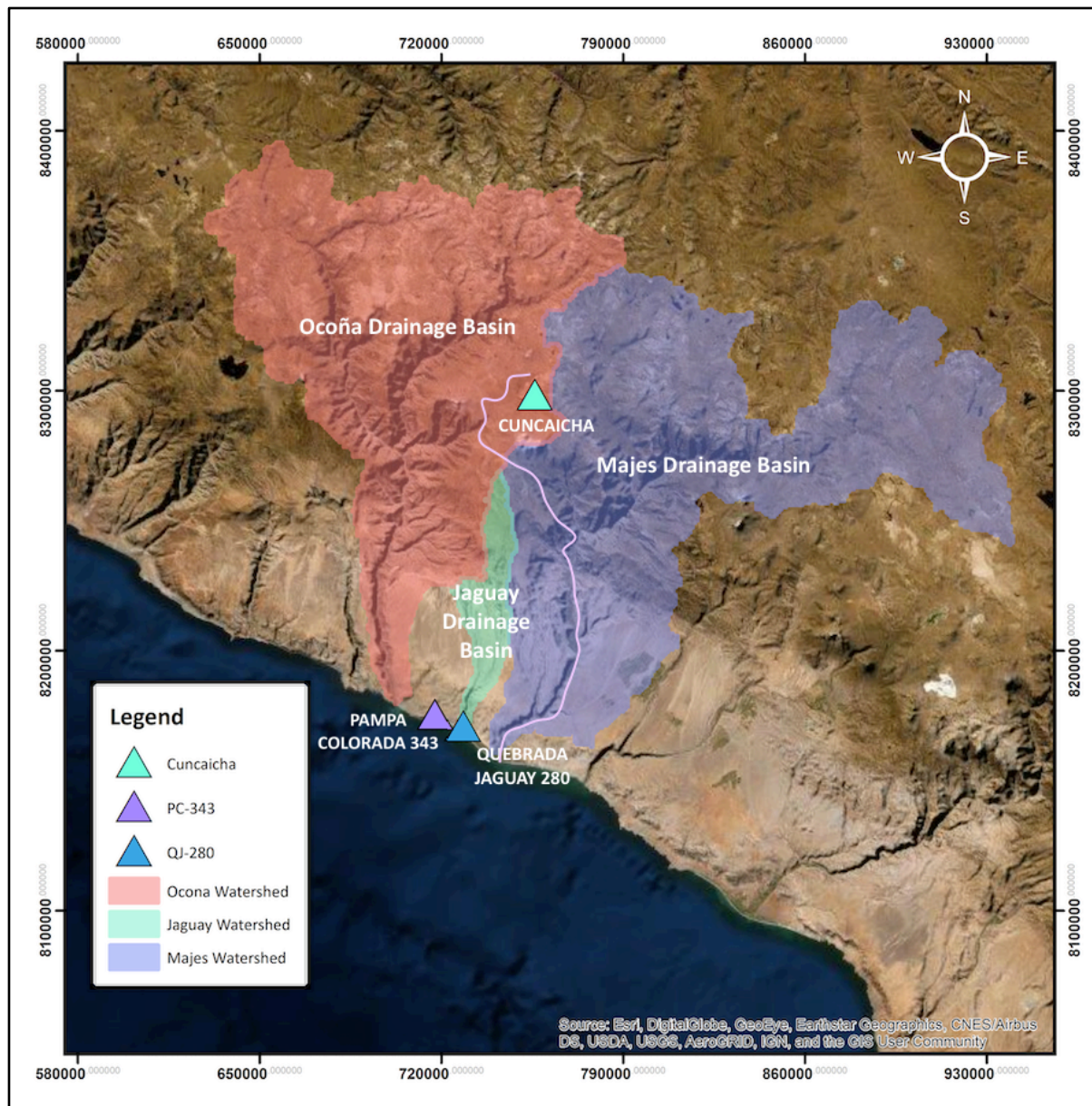


Figure 14: Map of the Survey Area. The survey route (light pink line) extends from Pampa Colorada 343 and Quebrada Jaguay 280 to Cuncaicha. Sampling crossed three watersheds, the Ocoña, Jaguay, and Majes Drainages.

Below the plateau, sampling followed waters from the Ríos Majes and Blanco and human-made canals. Río Majes samples extended from the Camaná River Delta (36 masl) to the confluence of the Río Colca and Río Capiza (896 masl) (Figure 14). Between the Río Majes and the edge of the plateau (~1000 to 3400-3800 masl), most waters derived from the Río Blanco

and its associated canals (Figure 15). On the plateau, sampling included any viable drinking source for humans and animals. Waterbodies included springs, streams, wetlands, and rivers.

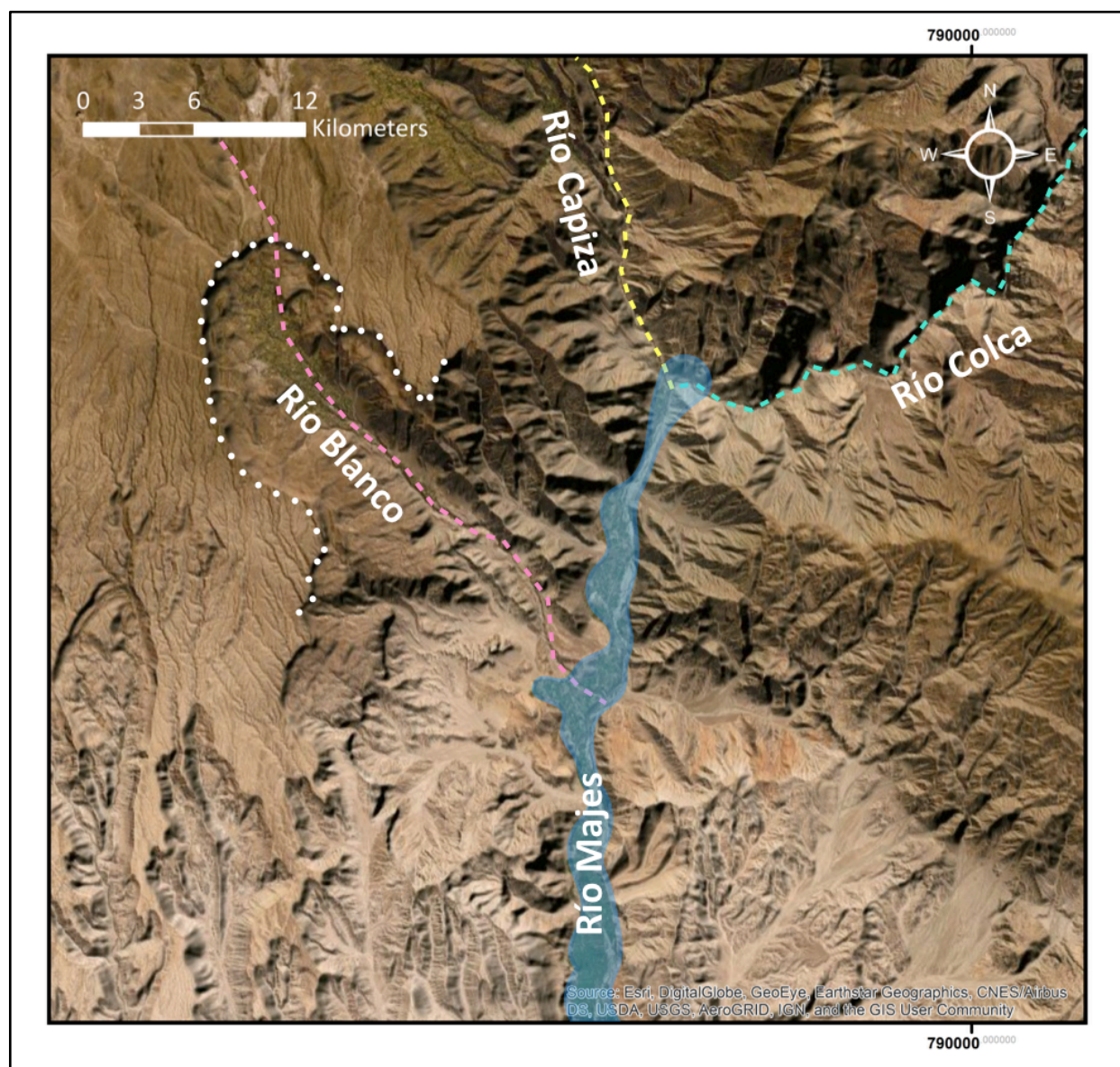


Figure 15: Map of key sampling locations below the plateau. The confluence of Río Capiza (dashed yellow line) and the Río Colca (dashed blue line) mark the beginning of the Río Majes (blue area). The Río Blanco (dashed pink line) discharges over the plateau rim (dotted white line) around ~3500 masl.

3.1.2 Temporal Sampling

Samples were collected along the elevation transect during months that represent both the austral wet and dry season. Seasonal sampling included the collection of wet and dry

season waters over a broad area, and the testing specific water bodies during both seasons. For the general seasonal samples, Dry season samples include any waters collected between June to December, wet season samples represent February and March. Samples were not collected in January, April, or May.

To test for perceptible seasonal change in surface waters, samples were collected to test daily, seasonal, and yearly variation. For each type of comparison, two or more samples were collected from a single water source at the same approximate location. Daily and inter-annual sampling was conducted to measure the magnitude of observable change in local surface waters.

3.1.2.1 Daily Tests

Daily tests included replicated '*simultaneous*' samples, and one test to measure *diurnal* variation. Simultaneous pairs consist of two samples taken from a single water source at the same time during the same test. A *diurnal* test was taken for the same location in the morning and evening.

3.1.2.2 Seasonal Tests

Maximum *seasonal* variation was established through targeted, replicated sampling of easily recognized water bodies during a peak wet (March 2019) and dry (July 2018 or June 2019) seasons.

3.1.2.3 Yearly Tests

Approximate *yearly* variability was determined by comparing samples taken from the same season (dry) during different years. These included one-, three-, and four-year

comparisons. One-year tests compared locations I sampled in both July 2018 and June 2019. Three- and four-year tests compared my July 2018 or June 2019 samples to published values from 2015 that derived from known, easily recognizable locations (Chala-Aldana et al. 2017).

3.1.3 Sampling Procedure

Waters were collected in 30 mL high-density polyethylene Nalgene bottles and sterile 15mL polypropylene Corning tubes. Location data were recorded using a Trimble GeoExplorer II global positioning system (GPS) set to the Universal Transverse Mercator (UTM) coordinate system. Spatial accuracy for X, Y, and Z was <1.5 meters. Water collection followed International Atomic Energy Agency (IAEA) protocol (*Introduction to Water Sampling and Analysis for Isotope Hydrology*). Each container was labeled on the side and cap with the water sample number. Vials were rinsed in the local water, submerged and capped, then inspected. If an air bubble was identified, the sample was recollected. After collection, the vial was dried. Clear tape was placed over the label, and electrical tape around the seal. Each vial was then covered in foil and stored in a dark box in a cool location. Location, date, time, temperature, relative humidity, weather, water body name (if known), and direction of flow was recorded for each sample. Each water source was photographed four times, once in each of the cardinal directions. Vials were sealed with electrical tape, covered in foil, and stored in a dark box. Samples were not permitted to freeze or sit in the sun at any point. All samples were successfully transported to the United States undamaged.

3.1.3.1 Labeling System

I collected 90 samples during my fieldwork. I labeled each vial with a four-digit (YYXX) Water Sample (WS) catalog number. The first two numbers refer to the year I collected the sample (2018 or 2019 = YY). The last two numbers reflect the chronological order of sampling and provide the individual identifier (XX) for the sample. For example, water sample WS 1801 was the first sample collected in 2018.

A local highland family collected monthly five samples between August and December 2018. I include the samples in the analysis but ultimately intend them for a separate study of seasonality not discussed here. The monthly samples received labels with the prefix 'PU' to separate them from transect samples. I labeled the vials with our highland partners for water collection. After the family collected each sample, they wrote the date of sampling under the number using permanent marker. Samples include 01, 03, 04, 05, and 06. Vial 02 was lost or not collected.

Kurt Rademaker collected three samples in December 2018. These samples are labeled with his initials (KR) and two digits to indicate order of collection (01, 02, and 03).

3.2 Laboratory Analysis of Oxygen and Hydrogen

Stable isotopic analysis was conducted at the Environment and Natural Resources Institute Stable Isotope Lab (ENRI SIL) at the University of Alaska, Anchorage. Samples 1801-1815, Pu-XX samples, 2018-KR-XX samples, and 1901-1926 were analyzed on May 5th, 2019. Samples 1927-1970B were analyzed on August 10th, 2019.

Water $\delta^2\text{H}$ and $\delta^{18}\text{O}$ isotope ratios were measured using a Picarro L2130-i WS-CRDS analyzer (Picarro, Sunnyvale, CA). Samples were screened to verify that organic content was low enough to minimize absorption interference spectra. Each sample was then analyzed six times and reanalyzed if the standard deviation of the six replicates was greater than 0.3‰ for $\delta^{18}\text{O}$ and/or 3‰ for $\delta^2\text{H}$, or if the internal standard for the run differed from the accepted value by greater than $\pm 0.2\text{‰}$ or 2‰ , for $\delta^{18}\text{O}$ and $\delta^2\text{H}$, respectively. International reference standards (IAEA, Vienna, Austria) were used to calibrate the instrument to the VSMOW-VSLAP scale and working standards (USGS45: $\delta^2\text{H} = -10.3\text{‰}$, $\delta^{18}\text{O} = -2.24\text{‰}$ and USGS46 : $\delta^2\text{H} = -235.8\text{‰}$, $\delta^{18}\text{O} = -29.8\text{‰}$) were used with each analytical run to correct for instrumental drift. Long-term mean and standard deviation records of a purified water laboratory internal QA/QC standard ($\delta^2\text{H} = -149.80\text{‰}$, $\delta^{18}\text{O} = -19.68\text{‰}$) yield an instrumental precision of 0.93 ‰ for $\delta^2\text{H}$ and 0.08 ‰ for $\delta^{18}\text{O}$. Water measurements are reported in standard delta (δ) notation as the per mil (‰) deviation from Vienna Standard Mean Ocean Water (VSMOW).

Equation 3: Delta Notation (Craig 1961b)

$$\delta = ((R_{\text{sample}}/R_{\text{standard}}) - 1) * 1000$$

R = ratio of heavy to light isotopes ($^{18}\text{O}/^{16}\text{O}$)

3.3 Calculated Change for Temporal Tests

The temporal dataset was divided into subtests based on sampling location. Samples for the temporal tests were grouped by test type (simultaneous, daily, seasonal, or inter-annual). Entries were ordered by elevation (lowest to highest) then chronological sequence.

The per mil $\delta^{18}\text{O}$ difference between pairs was calculated to measure temporal change. To do this, the smaller of the two $\delta^{18}\text{O}$ values in a pair was subtracted from the larger $\delta^{18}\text{O}$ value. Once calculated, the difference values were compiled into a new table for analysis in RStudio. Targeted temporal tests were compared within groups (daily vs. daily) and between groups (daily vs. seasonal) to assess the time frame that results in maximum variation in surface water $\delta^{18}\text{O}$ values.

3.4 Software Analyses

Measured $\delta^{18}\text{O}$ and δD values were added to a geospatial database in a Geographic Information System (GIS) and mapped in ESRI ArcMap 10.6.1. Hydrological data were derived from the HydroSHEDS (**H**ydrological data and maps based on **S**huttle **E**levation **D**erivatives at multiple **S**cales) South American River Networks and HydroBASINS 30 second shapefiles. Data plots and statistical summaries were created in RStudio 3.3.2 with the ggplot2 and Tidyverse packages.

3.4.1 Watershed and Stream Order Classifications

Each location datum was assigned to the Ocoña, Jaguay, or Majes watersheds based on the HydroBASIN shapefile. Field observation was used to assign each water body as either human modified (HUM) or natural (NAT). Stream order classification (1-5) was assigned to each sample using the ORD_STRA field in the HydroSHEDS River Networks shapefile (Figure 16). Canal samples were assigned a Strahler order based on the nearest order of stream in the GIS. Stream order identifications are based on the Strahler classification system, where two streams of the same order must merge to generate the next size class. The Strahler system reduces

the chance that unmapped or misidentified first order streams will lead to the resulting misclassification of higher order streams.

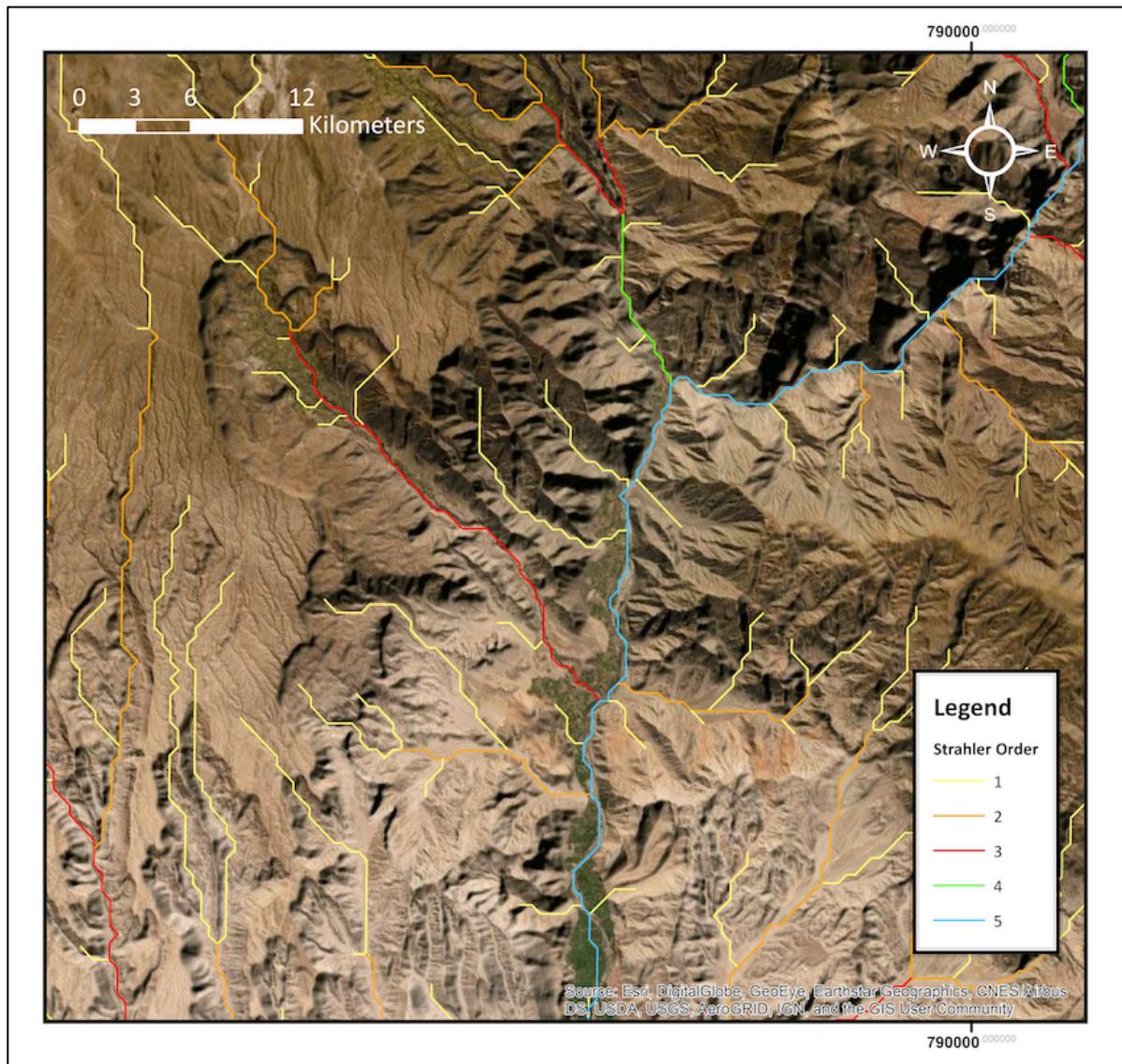


Figure 16: Map provides an example of stream orders in the study area.

CHAPTER 4: RESULTS

Chapter 4 reviews the results of the seasonal and spatial studies. Section 4.1 relays $\delta^{18}\text{O}$ results in terms of other research investigating meteoric waters in the region. Section 4.2 reviews the results of temporal testing. Sections 4.3 and 4.4 explore the spatial distribution of surface water $\delta^{18}\text{O}$ in the study area and examine these findings in terms of the archaeological research objectives for a provenance marker.

4.1 General Results

4.1.1 Results of Sample Collection

The final sample set comprises 98 surface water samples collected over 12 months. Ninety-four samples were compiled as part of the elevation transect and temporal testing. Four samples represent the high-elevation samples obtained by local collaborators on a month-to-month basis from September to December 2018. Together, the data represent approximately 4000 square kilometers of area (Figure 17) collected during two dry seasons (July-December 2018; June 2019) and one wet season (February- March 2019). Samples derive from the Jaguay, Majes, and Ocoña drainage basins at elevations between 36 and 4938 meters above sea level (masl).

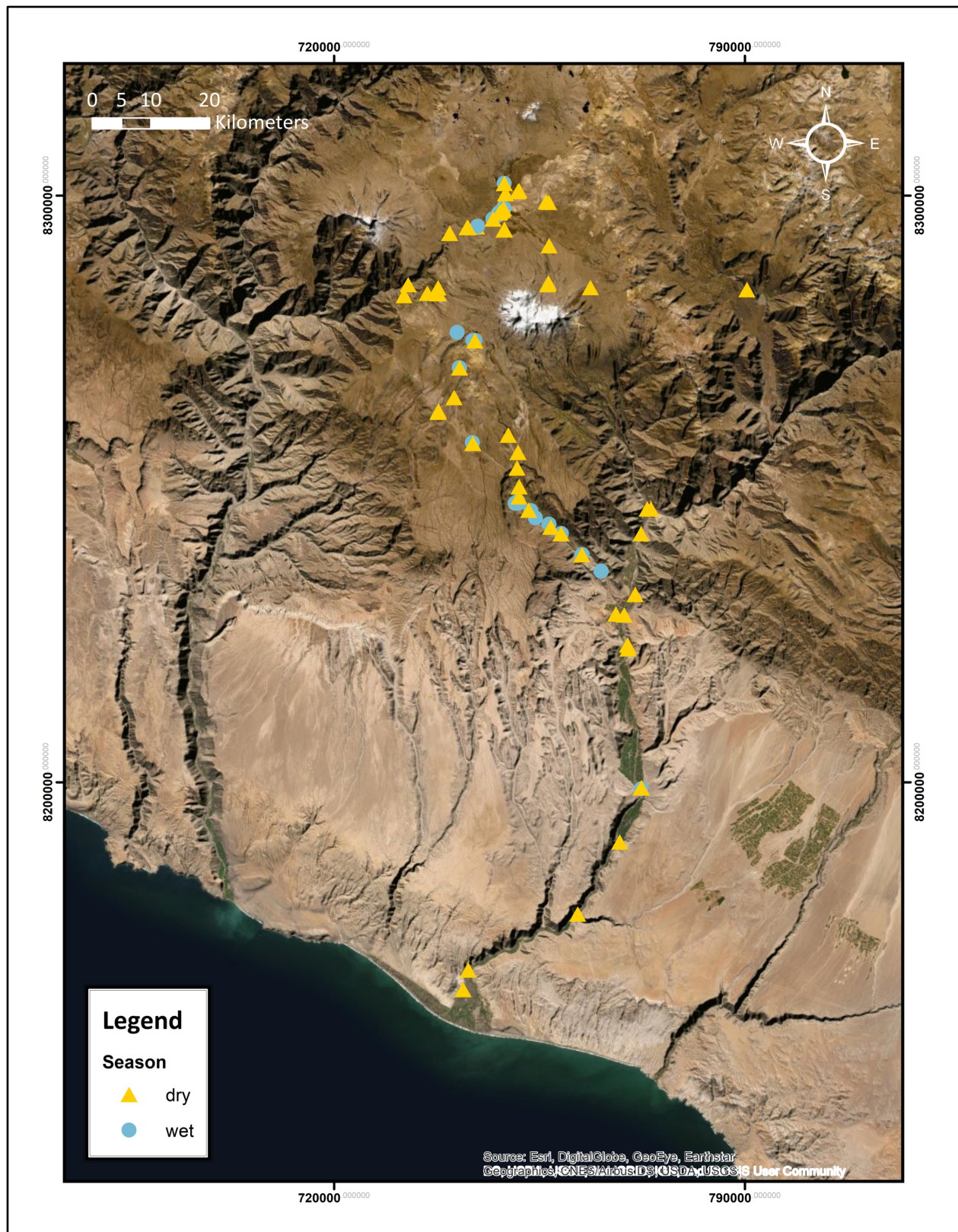


Figure 17: Map of all sample locations within the survey area. Yellow triangles show dry season testing and blue circles indicate wet season sampling.

The initial (2018) dry season sampling was restricted to natural streams above 2500 MASL, because the original project aimed to investigate only seasonal variation for high-elevation waters. The 2018 dry-season dataset comprises 15 samples (1801-1815) collected between 3070 and 4896 MASL. These samples comprise areas on the western and northern margins of Nevado Coropuna. The lowest sample from the 2018 dataset came from the Colca Canyon (3070 MASL) in late July. It is the only 2018 sample gathered from the Majes Watershed.

The four month-to-month samples derive from highland wetlands, or *bofedales*, which reflect the drinking-water source of a single alpaca purchased and monitored for a separate study. These samples were included in the general analysis. The precise sampling locations are unknown; therefore, the values are excluded from the more detailed seasonal and stream-class analyses.

In 2019, the aims expanded to include identifying variation between seasons, in multiple elevation zones. The second field collection occurred from February 27th to March 1st, 2019, during the peak of the Andean wet season. Twenty-six samples (1901-1926) represent elevations between 383 and 4719 MASL. Fifteen of the transect samples constitute the *puna* zone at the southeast edge of the plateau. The other 11 locations reflect waters from below the plateau rim between the highland town of Chuquibamba (2950 MASL) and the lower Majes River valley town of Aplao (620 m.a.s.l.).

Humans have modified the surface waters below Andean Plateau. Waters from the Río Grande are redirected by canals to the terraces of the surrounding towns. A network of canals feeds these waters from Chuquibamba to Aplao. It was necessary to collect from canals to

capture a representative sample of the surface water variation between ~1000 and 3000 MASL. Canals only divert natural waters, so should record changes in elevation and season.

The 2019 dry season transect comprises 49 samples (1927-1970B) collected over two days in June 2019. Collection during the final season extended from the mouth of the Majes River at the Pacific coast to the center of the *puna*. The total range of elevation in 2019 was between 36 and 4720 MASL. 2019 sampling targeted former wet and dry season sample points and under-sampled elevation zones. For example, the first two collection surveys lacked samples from elevations between 3000-4000 MASL. The June 2019 sampling transect targeted waters in this elevation range.

A second focus to the June 2019 dry season included retesting the three lowland values omitted by Chala-Aldana (2017 et al. 2019), as discussed in Chapter 1. The samples in question, Out-wa-011, Out-wa-012, and Out-wa-013, derived from waters below 700 MASL and yielded results more depleted than the values predicted using the Oxygen Isotopes in Precipitation Calculator (OIPC). Chala-Aldana also rejected three highland values from his analysis, Out-wa-002, Out-wa-004, and Pu-wa-021, that were not retested. Each of these values represented saline or standing waters, which are not suitable drinking sources for humans.

Figure 18 shows the density of samples collected between seasons and across elevations. The graph indicates a bimodal distribution for the dry-season sampling, with nodes at both lowest (0-1000 masl) and highest (4000-5000 masl) elevation ranges. The wet season plot is unimodal and skewed to the left. For both seasons most samples were collected from high elevation (>3500 masl), creating a bias. The data are also biased between seasons. The dry season (June-December) comprises 73% of samples.

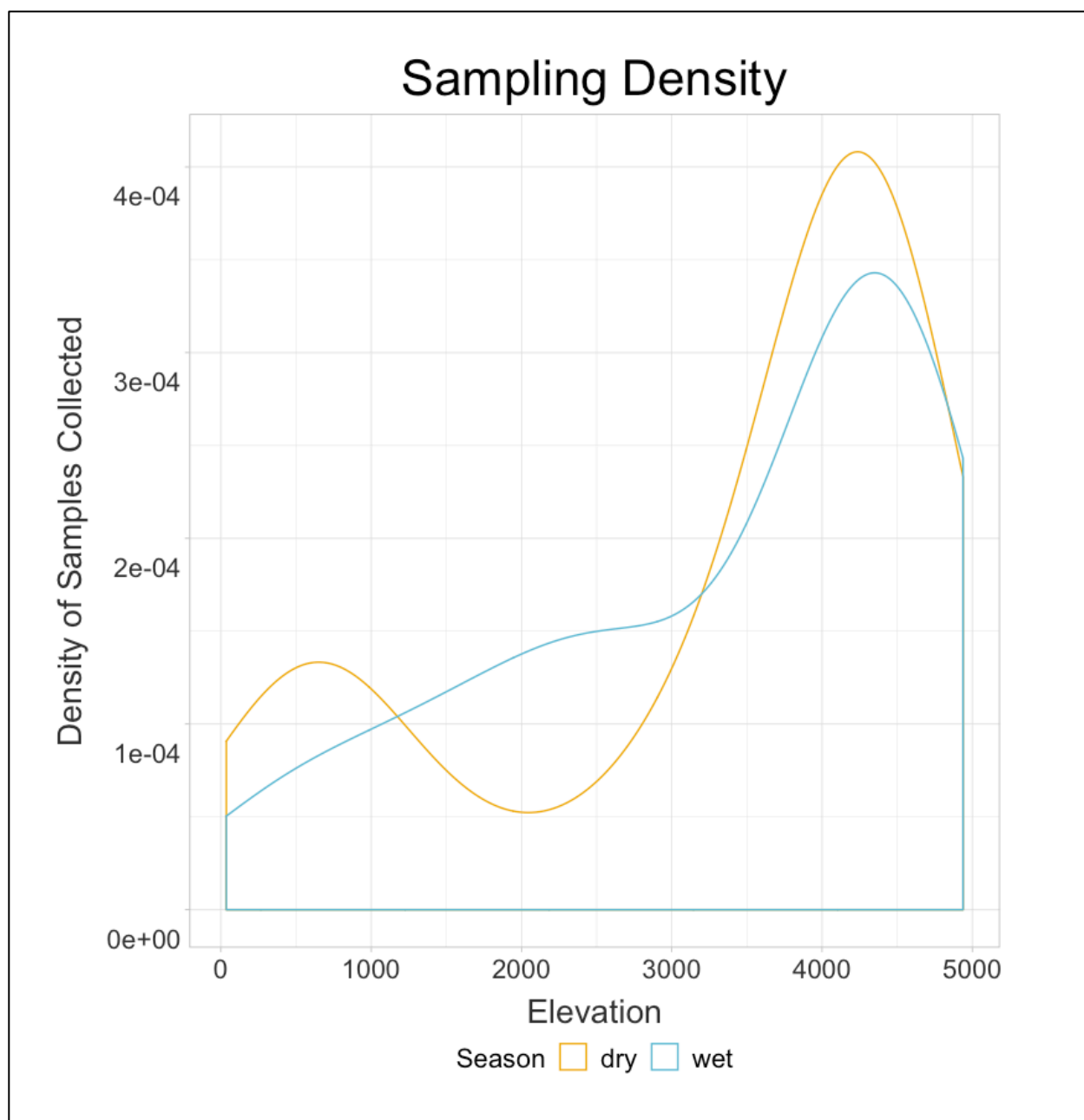


Figure 18: Density of samples collected for wet (blue line) and dry (yellow line) seasons. The dry season shows a bimodal distribution of samples; most were collected below 1000 masl or above 3500 masl. The wet season shows a unimodal distribution with most samples collected from above 3500 masl.

4.1.2 Results of $\delta^{18}\text{O}$ and δD Analysis

Results of hydrogen and oxygen analysis are reported in delta-notation (δ) (**Error! Reference source not found.**) relative to the Vienna Standard Mean Ocean Water (VSMOW)

standard and displayed in Table 1. $\delta^{18}\text{O}$ is $^{18}\text{O} / ^{16}\text{O}$ and $\delta^2\text{H}$ or δD $^2\text{H} / ^1\text{H}$. δ ratios for both oxygen and hydrogen are presented in per mil (‰) units. Standard mean machine precision for $\delta^{18}\text{O}$ measurements was 0.03‰ and range from 0.00 to 0.22‰. The mean δD precision was 0.16‰, with a range of 0.00 to 1.24‰. Overall instrumental precision was good; all samples were retained for further analyses. Results of the δD measurements are considered in the general results but not considered the seasonal or elevation analyses.

Table 1: Summary of Results. In order of increasing elevation. Water Sample (WS) number indicates the year the sample was collected.

WS Number	Water Body	Season	Easting	Northing	Elevation (masl)	$\delta^{18}\text{O}$ (VSMOW)	$\delta^{18}\text{O}$ St. Dev.	δD (VSMOW)	δD St.Dev.	Strahler Order	Type	On / Off plateau
1927	Majes mouth	dry	741970	8164671	36	-16.40	0.03	-123.51	0.25	5	Natural	OFF
1928	Irrigation canal	dry	742862	8168020	67	-16.48	0.03	-124.04	0.15	5	Canal	OFF
1929	Majes	dry	761492	8177561	184	-16.41	0.01	-124.06	0.07	5	Natural	OFF
1930	Irrigation canal with plants	dry	768669	8189857	296	-15.19	0.02	-116.14	0.06	5	Canal	OFF
1925	Majes (Punta Colorada)	wet	772350	8198886	383	-16.49	0.00	-128.21	0.13	5	Natural	OFF
1926	Majes (Punta Colorada)	wet	772350	8198886	383	-16.60	0.02	-129.44	0.00	5	Natural	OFF
1932	Majes (Punta Colorada)	dry	772321	8199060	383	-16.37	0.08	-124.10	0.23	5	Natural	OFF
1931	Majes canal	dry	772371	8199063	387	-16.29	0.04	-123.79	0.13	5	Canal	OFF
1933	Majes at Aplao	dry	770100	8222763	631	-16.81	0.06	-126.58	0.15	5	Natural	OFF
1934	Majes (bridge of stix)	dry	769426	8228514	707	-16.78	0.03	-126.49	0.09	5	Natural	OFF
1939	Chuiqui stream in canal	dry	770003	8223428	711	-15.62	0.03	-118.58	0.05	5	Canal	OFF
1935	Majes before Castillo	dry	771300	8232016	731	-16.74	0.02	-125.87	0.03	5	Natural	OFF
1940	Quebrada del Castillo canal	dry	767998	8228684	800	-16.49	0.01	-124.82	0.04	1	Canal	OFF
1936	Northeast Majes	dry	772316	8242386	866	-16.95	0.02	-127.36	0.04	5	Natural	OFF
1937A	Colca feed into Majes	dry	774003	8246601	896	-17.09	0.01	-128.70	0.11	5	Natural	OFF
1937B	Colca feed into Majes	dry	774003	8246601	896	-17.10	0.03	-128.70	0.04	5	Natural	OFF
1938	Rio Capiza (Coropuna Viraco input)	dry	773348	8246630	937	-13.39	0.00	-95.97	0.23	4	Natural	OFF
1924	Canal Mascapmpa	wet	765517	8235969	1128	-12.56	0.05	-92.81	0.27	3	Canal	OFF

Table 1 (Cont'd)												
WS Number	Water Body	Season	Easting	Northing	Elevation (masl)	$\delta^{18}\text{O}$ (VSMOW)	$\delta^{18}\text{O}$ St. Dev.	δD (VSMOW)	δD St.Dev.	Strahler Order	Type	On / Off plateau
1923	Rio Grande	wet	762277	8238806	1379	-12.13	0.02	-89.00	0.55	3	Natural	OFF
1941	Rio Grande	dry	762218	8238811	1379	-9.74	0.03	-72.58	0.10	3	Natural	OFF
1922	Canal de Pacaychacra	wet	758748	8242414	1811	-12.32	0.05	-89.34	0.29	3	Canal	OFF
1942	Canal de Pacaychacra	dry	758672	8242375	1811	-10.83	0.01	-77.78	0.03	3	Canal	OFF
1921	Huacllay canal	wet	756653	8244007	1960	-11.39	0.10	-82.14	0.81	3	Canal	OFF
1943	Huacllay canal	dry	756914	8243520	1960	-10.27	0.03	-74.47	0.04	3	Canal	OFF
1920	Iray canal	wet	754343	8245048	2347	-12.25	0.00	-87.89	0.23	1	Canal	OFF
1919	Iray canal	wet	753554	8246318	2521	-11.87	0.04	-85.85	0.02	1	Canal	OFF
1944	Iray canal	dry	753144	8246407	2521	-11.55	0.01	-82.42	0.08	1	Canal	OFF
1916	Sequia La Rinconada	wet	751338	8247880	2889	-11.92	0.04	-83.68	0.25	2	Canal	OFF
1917	Chucuibamba canal	wet	751394	8247541	2902	-10.85	0.03	-76.70	0.62	2	Canal	OFF
1918	Chucuibamba canal	wet	750888	8247547	2938	-11.39	0.02	-78.99	0.28	2	Canal	OFF
1966	Sequia La Rinconada	dry	751494	8248662	2965	-12.31	0.02	-86.70	0.01	2	Canal	OFF
1967A	Río Grande	dry	751523	8250402	2980	-12.39	0.00	-87.77	0.03	2	Natural	OFF
1967B	Río Grande	dry	751523	8250402	2980	-12.44	0.01	-87.98	0.01	2	Natural	OFF
1815	Rio Andagua	dry	790338	8283984	3070	-16.70	0.04	-127.38	0.01	4	Natural	OFF
1962	Río Arma at Salamanca	dry	732609	8284844	3221	-17.11	0.00	-125.91	0.05	3	Natural	OFF
1968A	Río Blanco	dry	751163	8253578	3396	-13.42	0.01	-94.33	0.01	2	Natural	OFF
1968B	Río Blanco	dry	751163	8253578	3396	-13.49	0.01	-94.49	0.01	2	Natural	OFF

Table 1 (Cont'd)												
WS Number	Water Body	Season	Easting	Northing	Elevation (masl)	$\delta^{18}\text{O}$ (VSMOW)	$\delta^{18}\text{O}$ St. Dev.	δD (VSMOW)	δD St.Dev.	Strahler Order	Type	On / Off plateau
1963	Salamanca Sincha	dry	731929	8282985	3559	-13.58	0.01	-99.87	0.04	1	Canal	OFF
1969A	Río Blanco	dry	751344	8256230	3727	-13.46	0.01	-94.61	0.02	2	Natural	ON
1969B	Río Blanco	dry	751344	8256230	3727	-13.48	0.00	-94.74	0.02	2	Natural	ON
1970A	Río Blanco	dry	749675	8259172	3800	-13.12	0.01	-93.20	0.00	2	Natural	ON
1970B	Río Blanco	dry	749675	8259172	3800	-13.56	0.03	-95.11	0.06	2	Natural	ON
1909	Quebrada de Rata	wet	743603	8257875	3922	-12.77	0.13	-91.45	0.99	1	Natural	ON
1945	Quebrada de Rata	dry	743642	8257759	3936	-9.98	0.01	-77.01	0.01	1	Natural	ON
1965	Quebrada de Rata Nighttime	dry	743642	8257759	3936	-10.14	0.02	-78.18	0.03	1	Natural	ON
1802	Quebrada Pariaviri	dry	737720	8263072	3966	-12.34	0.00	-87.45	0.06	1	Natural	ON
1801	Quebrada Pariaviri	dry	737764	8263279	3967	-12.35	0.02	-87.82	0.17	1	Natural	ON
1964	Quebrada Pariaviri	dry	737764	8263279	3967	-12.30	0.02	-88.97	0.27	1	Natural	ON
1803	Quebrada Huamantirca	dry	735887	8283367	4048	-14.18	0.00	-102.07	0.05	1	Natural	ON
1960	Río Arma Bofedal	dry	739698	8293581	4085	-17.55	0.05	-128.57	0.01	3	Natural	ON
1961	Río Arma	dry	739698	8293581	4085	-17.66	0.01	-129.19	0.03	3	Natural	ON
1946	Quebrada Palljaruta	dry	740453	8265580	4116	-12.10	0.02	-86.30	0.05	1	Natural	ON
1804	Quebrada Sique Grande	dry	737719	8284287	4161	-15.06	0.04	-106.60	0.22	1	Natural	ON
1910	Quebrada Azufrioc	wet	740988	8276666	4186	-13.58	0.02	-96.04	0.20	1	Natural	ON
1806	Quebrada Sique Grande	dry	737687	8283282	4205	-14.57	0.03	-103.53	0.03	1	Natural	ON
1805	Quebrada Sique Grande	dry	737725	8283340	4215	-14.68	0.00	-104.05	0.00	1	Natural	ON

Table 1 (Cont'd)												
WS Number	Water Body	Season	Easting	Northing	Elevation (masl)	$\delta^{18}\text{O}$ (VSMOW)	$\delta^{18}\text{O}$ St. Dev.	δD (VSMOW)	δD St.Dev.	Strahler Order	Type	On / Off plateau
1950	Río Arma	dry	742645	8294544	4272	-17.25	0.02	-127.04	0.11	3	Natural	ON
2018-KR-01	Rio Arma at bridge	dry	742819	8294579	4278	-17.11	0.06	-125.06	0.06	3	Natural	ON
1814	Rio Arma	dry	744278	8294697	4310	-16.97	0.02	-125.63	0.06	3	Natural	ON
1908	Rio Arma	wet	744469	8294780	4310	-17.99	0.02	-133.13	0.29	3	Natural	ON
1951	Río Colunga/ Río de Choriltes	dry	748132	8297085	4327	-17.21	0.03	-129.34	0.46	2	Natural	ON
1959	Río Achala	dry	747064	8296039	4328	-16.28	0.01	-123.01	0.00	2	Natural	ON
1901	Río Colunga/ Río de Choriltes	wet	748128	8297072	4333	-17.39	0.02	-130.03	0.15	2	Natural	ON
1952	Quebrada Chilacala	dry	748268	8297238	4342	-13.88	0.00	-112.29	0.12	1	Natural	ON
1955	Río Grande	dry	748858	8297801	4343	-17.44	0.02	-127.30	0.11	3	Natural	ON
1907	Río Achala	wet	747100	8296023	4345	-16.06	0.03	-122.12	0.13	2	Natural	ON
1954	Auquimanca/Río Cuncaicha	dry	748872	8297784	4347	-13.94	0.03	-113.65	0.02	1	Natural	ON
1902	Auquimanca/Quebrada Cuncaicha	wet	748983.1	8297822	4349	-16.98	0.01	-126.69	0.04	1	Natural	ON
1904	Chalojmarka	wet	748658	8297498	4349	-12.94	0.07	-104.04	0.07	1	Natural	ON
1953	Chalojmarka	dry	748660	8297492	4350	-13.86	0.02	-112.22	0.05	1	Natural	ON
1906	Río Blanco o Mapa Mayo o Quebrada Collpa Huayco	wet	747760	8296537	4352	-17.04	0.07	-125.53	0.01	3	Natural	ON
1903	Rio Grande	wet	748807	8297737	4354	-15.47	0.10	-120.53	0.68	3	Natural	ON
1808	Bofedal Pucuncho	dry	748708	8298933	4359	-14.84	0.01	-114.06	0.02	2	Natural	ON
1958	Capilla; Río Pucuncho	dry	749218	8300353	4375	-17.30	0.00	-126.41	0.02	3	Natural	ON
1956	Río León Huactana	dry	751297	8300700	4383	-17.14	0.01	-126.63	0.05	2	Natural	ON

Table 1 (Cont'd)												
WS Number	Water Body	Season	Easting	Northing	Elevation (masl)	$\delta^{18}\text{O}$ (VSMOW)	$\delta^{18}\text{O}$ St. Dev.	δD (VSMOW)	δD St.Dev.	Strahler Order	Type	On / Off plateau
2018-Pu-01	Quebrada Collpa Huauco	dry	748949	8294183	4390	-16.47	0.02	-124.43	0.11	1	Canal	ON
2018-Pu-03	Quebrada Collpa Huauco	dry	748949	8294183	4390	-17.41	0.00	-128.16	0.28	2	Canal	ON
2018-Pu-04	Quebrada Collpa Huauco	dry	748949	8294183	4390	-17.58	0.05	-128.81	0.05	2	Canal	ON
2018-Pu-05	Capilla; Río Pucuncho	dry	749003	8302075	4390	-17.23	0.10	-125.59	0.05	2	Natural	ON
2018-KR-02	Quebrada Collpa Huauco	dry	748949	8294183	4390	-16.43	0.03	-123.67	0.21	1	Canal	ON
2018-KR-03	Quebrada Collpa Huauco	dry	749028	8294248	4390	-16.32	0.05	-122.90	0.15	1	Canal	ON
2018- Pu-06	Capilla; Río Pucuncho	dry	749003	8302075	4390	-17.36	0.01	-125.92	0.07	2	Natural	ON
1811	Río León Huactana	dry	751509	8300873	4392	-16.96	0.01	-124.25	0.03	2	Natural	ON
1905	Capilla; Río Pucuncho	wet	749003	8302075	4408	-17.42	0.10	-125.89	0.06	2	Natural	ON
1947	Quebrada Japuchaca	dry	741375	8270657	4430	-13.90	0.01	-97.62	0.09	1	Natural	ON
1911	Quebrada Japuchaca	wet	741356	8270635	4437	-14.29	0.08	-102.30	0.69	1	Natural	ON
1912	Quebrada Japuchaca	wet	741387	8270628	4440	-14.00	0.00	-99.58	0.41	1	Natural	ON
1807	Quebrada Cuncaicha (at site)	dry	756111	8298963	4457	-14.73	0.01	-111.25	0.06	1	Natural	ON
1957	Quebrada Cuncaicha (at site)	dry	756557	8298854	4474	-14.39	0.01	-114.32	0.04	1	Natural	ON
1913	Quebrada Pucunchitoyocc	wet	744016	8275307	4539	-14.65	0.04	-105.25	1.18	1	Natural	ON
1813	Rio Agua Caliente	dry	756611	8291491	4567	-17.57	0.04	-128.58	0.13	2	Natural	ON
1915	Road below Q. Pucunchitoyocc	wet	743995	8275275	4699	-15.01	0.07	-109.67	0.24	1	Natural	ON
1948	Quebrada Pucunchitoyocc	dry	743994	8275277	4717	-14.24	0.01	-100.35	0.07	1	Natural	ON
1914	Bofedal Pucunchitoyocc	wet	743670	8275292	4719	-14.57	0.22	-105.95	1.24	1	Natural	ON

Table 1 (Cont'd)												
WS Number	Water Body	Season	Easting	Northing	Elevation (masl)	$\delta^{18}\text{O}$ (VSMOW)	$\delta^{18}\text{O}$ St. Dev.	δD (VSMOW)	δD St.Dev.	Strahler Order	Type	On / Off plateau
1949	Bofedal Pucunchitoyocc	dry	743978	8275286	4720	-13.28	0.01	-95.79	0.04	1	Natural	ON
1812	Quenua Ranra	dry	763669	8284336	4830	-17.74	0.02	-135.92	0.05	1	Natural	ON
1810	Quebrada Ullullo	dry	756489	8285159	4896	-16.84	0.03	-121.49	0.03	1	Natural	ON
1809	Quebrada Ullullo	dry	756375	8284836	4938	-16.75	0.05	-120.58	0.07	1	Natural	ON

4.1.3 Stable Isotopic Variation In Andean Surface Waters

Surface waters in the study area show considerable variability in $\delta^{18}\text{O}$. The total range of $\delta^{18}\text{O}$ is between 17.99 to -9.74‰ and -135.92 and -72.58 ‰ for δD . δD and $\delta^{18}\text{O}$ values for local surface waters were plotted with the Global Meteoric Water Line (GMWL) (Figure 19). The GMWL reflects the highly correlated ($r^2=0.95$) linear relationship between oxygen and hydrogen in precipitation (Craig 1961a). The formula for the GMWL is:

Equation 4: Global Meteoric Water Line

$$\delta\text{D} = 8 (\delta^{18}\text{O}) + 10\text{‰}$$

$$\delta\text{D} = \text{slope} (\delta^{18}\text{O}) + d\text{‰}$$

D is the deuterium excess ($d=\delta\text{D} - 8 \delta^{18}\text{O}$) and represents enrichment from evaporative effects. Evaporative loss causes waters to plot below or to the right of the GMWL. Vapors derived from evaporation plot above and to the right of the line. Waters condensed from the evaporated vapors will plot parallel to the line but demonstrate a greater deuterium excess. The Local Surface Water Line (LSWL) derived from the entire dataset is:

Equation 5: Local Surface Water Line

$$\delta\text{D} = 7.86 (\delta^{18}\text{O}) + 7.08.$$

The LSWL suggests local δD and $\delta^{18}\text{O}$ values are highly correlated ($r^2=0.96$). Data plotting below the LSWL either indicate direct evaporative effects or sources mixed with other evaporated waters (Craig 1961a; Gat 1996, 2000). The plotted data and LSWL show little to no evaporative effects affecting meteoric precipitation prior to deposition in Andean surface waters. Seasonal differences in the local meteoric water line are plotted and discussed in Section 4.2.1.

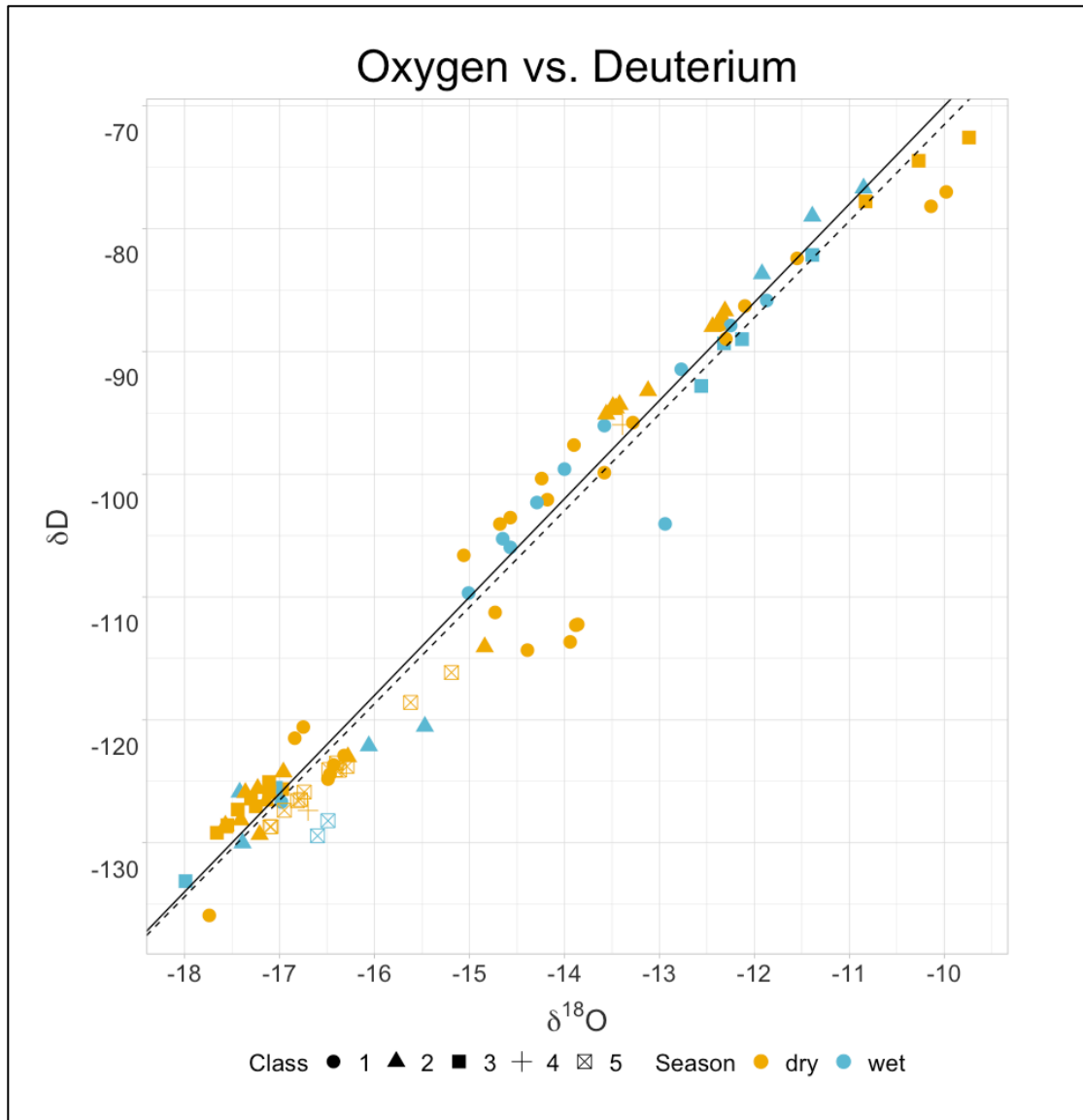


Figure 19: Plot of $\delta^{18}\text{O}$ and δD for all samples. The black line is the Global Meteoric Water Line (GMWL) $\delta\text{D} = 8(\delta^{18}\text{O}) + 10\text{‰}$. The dashed black line reflects the local surface water line (LSWL) $\delta\text{D} = 7.86(\delta^{18}\text{O}) + 7.08\text{‰}$. Class 1-5 indicates stream order, where first order streams are the smallest volume. The enriched samples below the line are discussed in Figure 21.

4.2 Results of Seasonal Sampling

In total, seventy-two samples between 36 and 4938 masl represent the austral dry season and 26 samples between 383 and 4719 masl represent the wet season. Dry season samples include all samples collected from July-December 2018, and June 2019. Wet season samples reflect collection during February-March 2019.

4.2.1 Local Variation in Andean Surface Waters Between Seasons

The range of $\delta^{18}\text{O}$ values observed in Andean surface waters is between -17.37 to -9.74‰ during the austral dry season and -17.99 to -10.84 ‰ in the wet season (Table 2). Seasonal results of δD and $\delta^{18}\text{O}$ values were plotted relative to the Global Meteoric Water Line (GMWL). The plot suggests more evaporated values may occur during the dry season than the wet season (Figure 20), though this may also reflect the dry season sampling bias.

Table 2: Summary of Sampling for Each Field Season.

Season	Year	Samples (n =)	Min Elevation (masl)	Max Elevation (masl)	Min $\delta^{18}\text{O}$ (VSMOW)	Max $\delta^{18}\text{O}$ (VSMOW)	Average $\delta^{18}\text{O}$ (VSMOW)
DRY	2018	23	3070	4938	-17.74	-12.34	-16.01
WET	2019	26	347	4719	-17.99	-10.84	-14.23
DRY	2019	49	36	4720	-17.66	-9.74	-14.59

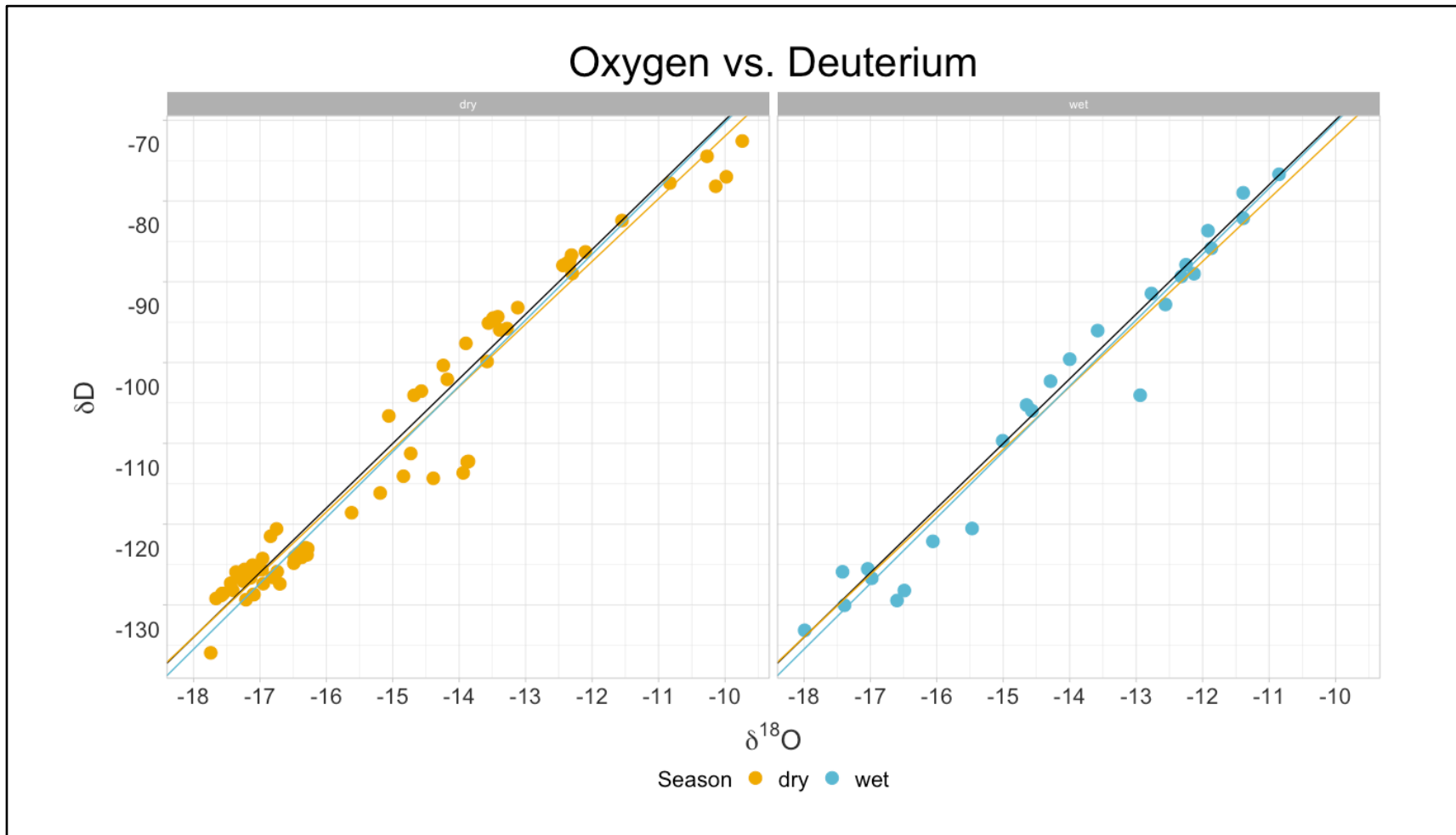


Figure 20: Seasonal datasets plotted with the respective wet and dry season Local Surface Water Lines (LSWL). Dry season samples (yellow dots) and LMWL ($\delta\text{D} = 7.75 * \delta^{18}\text{O} + 5.52\text{‰}$) are presented on the left and wet season samples (blue dots) and LMWL ($\delta\text{D} = 8.15 * \delta^{18}\text{O} + 11.22\text{‰}$) presented on the right. Values that plot below the GMWL and LSWLs reflect enriched waters.

Seasonal Local Surface Water Lines (LSWL) base on all samples are:

$$\text{Dry Season: } \delta D = 7.75 * \delta^{18}\text{O} + 5.52\text{‰}$$

$$\text{Wet Season: } \delta D = 8.15 * \delta^{18}\text{O} + 11.22\text{‰}$$

$$\text{LSWL: } \delta D = 7.86 (\delta^{18}\text{O}) + 7.08.$$

$$\text{GMWL: } \delta D = 8(\delta^{18}\text{O}) + 10\text{‰}$$

Both the dry season slope (7.75) and intercept (5.52‰) suggest slightly more evaporated surface waters in the study area during this time. The wet season intercept (11.22‰) indicates that the incoming precipitation may reflect previously evaporated waters carried through transport to the study area. The increased intercept during the wet season (11.22‰) likely reflects the influx of precipitation from evaporative vapors transported from the east.

To adjust for the difference in sample size between seasons, the plot was recreated using only samples that were replicated during both the wet and dry season (n=24 samples, n=12 per season) (Figure 21).

$$\text{Dry Subset: } (\delta D = 7.64 * \delta^{18}\text{O} + 3.14\text{‰})$$

$$\text{Wet Subset: } (\delta D = 8.10 * \delta^{18}\text{O} + 10.83\text{‰})$$

In a subset test, the dry season slope and intercept are both decreased indicating more evaporated waters than the wet season samples from the same locations. Some waters appear more affected by evaporation during the dry season than others (Figure 21). For example, sample location 2, 4, 6, and 9 all fall below the GMWL during the dry season, indicating waters susceptible to evaporative processes. Sample location 1, the Majes River, falls to the right of the line during both the wet and dry seasons. Sample locations 2 (Río Grande; 1379 masl), 4 (Huacllay Canal; 1960 masl), and 9 (Río Cuncaicha; 4348 masl) fall to the right of the GMWL, suggesting enrichment occurs at these locations during the dry season.

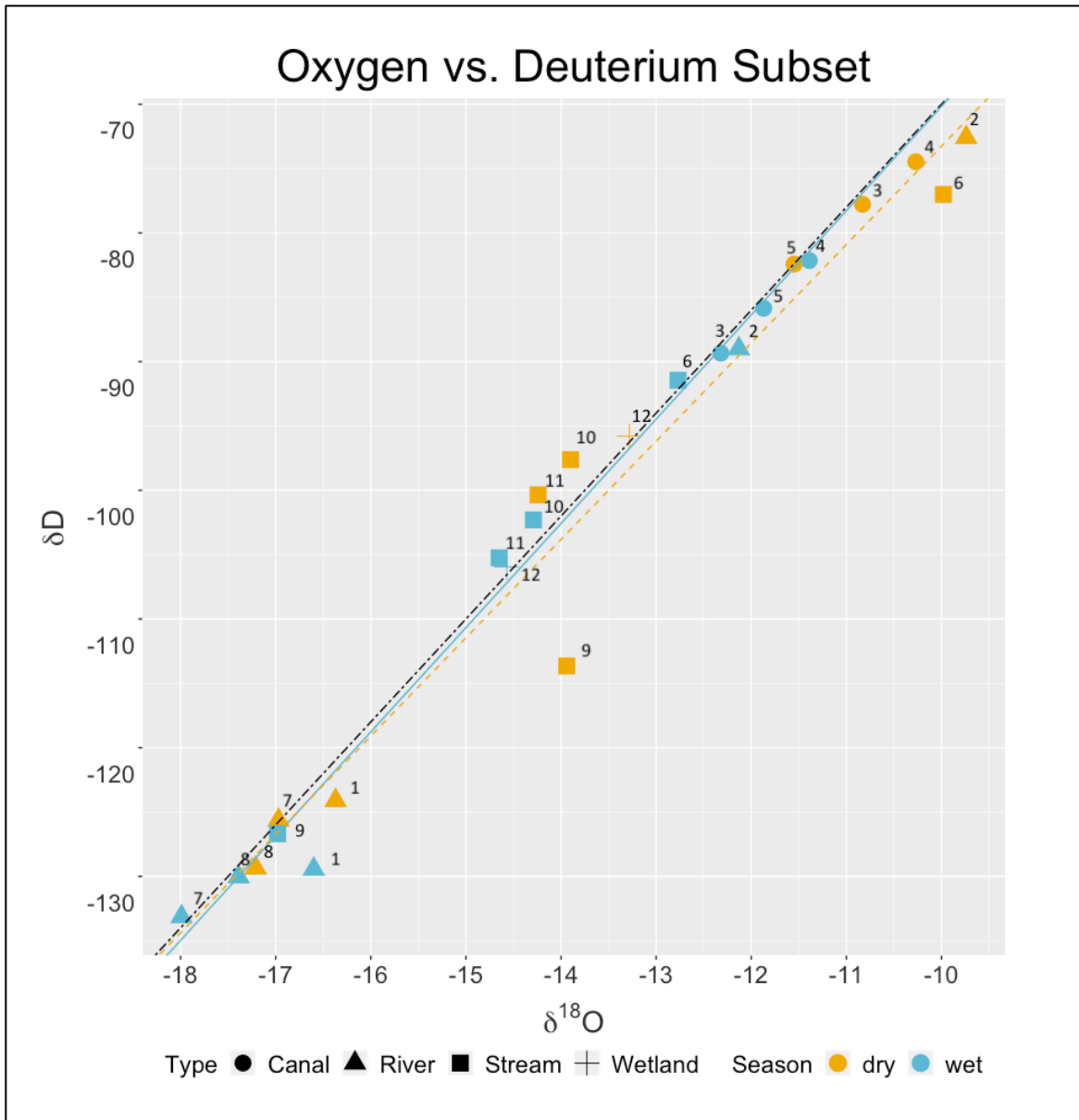


Figure 21: $\delta^{18}\text{O}$ plotted against δD for sample locations replicated as part of the seasonality study. Dashed black line indicates the global meteoric waterline $\delta\text{D} = 8.0 * \delta^{18}\text{O} + 10.00\text{‰}$. Blue solid line $\delta\text{D} = 8.10 * \delta^{18}\text{O} + 10.83\text{‰}$. indicates the local meteoric water line during the wet season. Yellow dashed line represents the local meteoric water line during the dry season $\delta\text{D} = 7.36 * \delta^{18}\text{O} + 3.14\text{‰}$. More samples appear to plot below the line during the dry season.

4.2.2 Results of Temporal Testing

To test for measurable variation in surface waters at multiple time scales, samples were collected daily, seasonally, and yearly from the same water bodies. The resulting temporal

dataset consists of 29 paired samples. Seven simultaneous tests represent samples taken from the same locations at the same time. To estimate the degree of diurnal change in surface waters, one pairing was collected from the Quebrada de Rata in both the morning and evening. Seasonal samples include 12 pairs acquired during the dry seasons of 2018 or 2019 and the wet season of 2019. Three paired samples collected during both the 2018 and 2019 dry seasons test same-season variation during different years. Finally, six tests compare waters collected in 2018 or 2019 with published (Chala-Aldana et al. 2018) 2015 dry season values.

4.2.2.1 Boxplot Assessment for All Temporal Tests

Per mil (‰) differences in $\delta^{18}\text{O}$ between temporal pairs are presented in Tables 3, 5, 7, and 9. Potential outliers for all subsets were identified using the boxplot method to assess the change in $\delta^{18}\text{O}$ across the time scales (Figure 22). The simultaneous test revealed one outlier (difference = 0.44‰) from water sample pairs WS1970A and WS1970B from the Río Blanco at 3800 masl (Table 3) the pair was removed prior to further analysis. This Río Blanco at this elevation is a waterfall and presents fast moving, highly aerated waters; this is the likely cause of the increased difference between replicate samples.

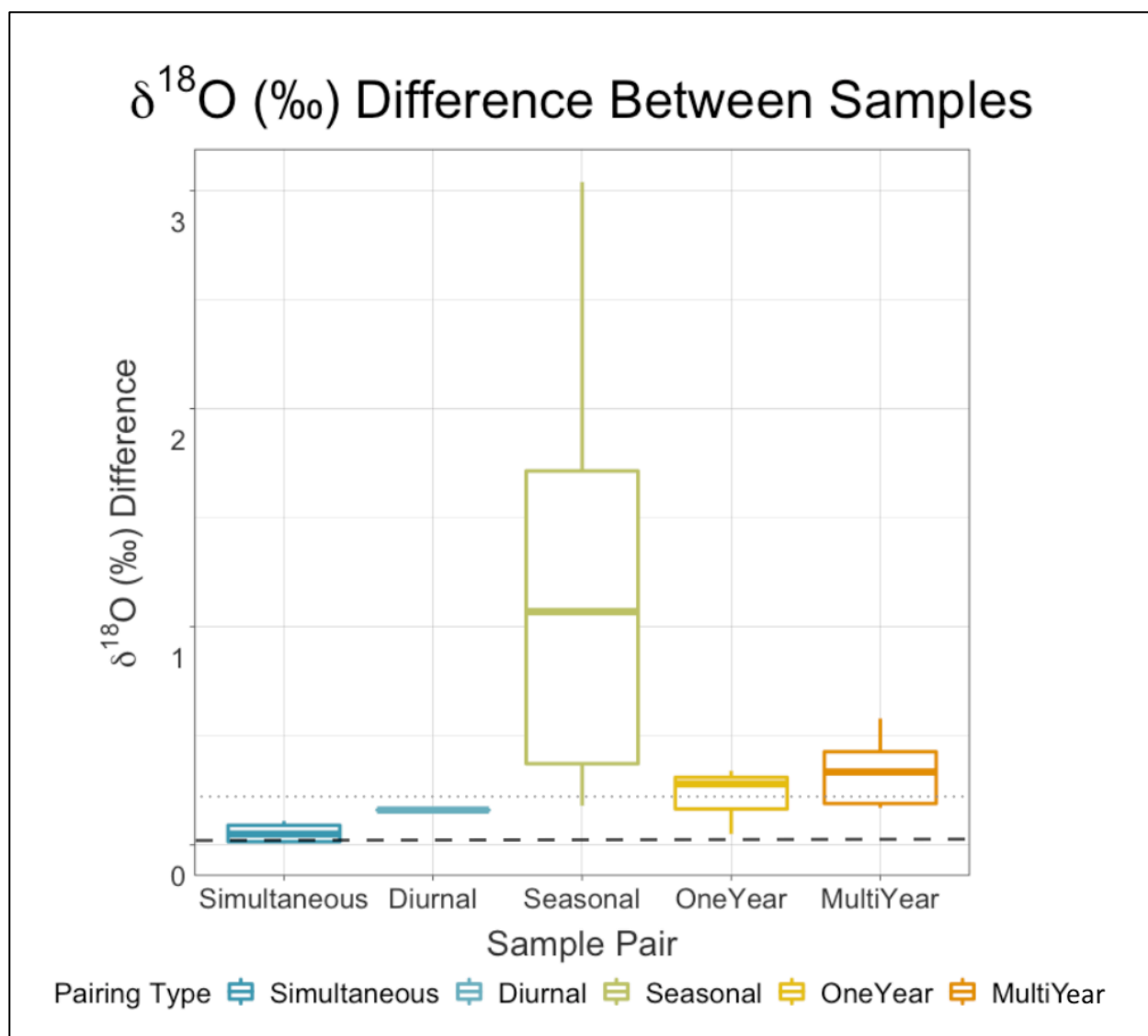


Figure 22: Box plot assessment for the per mil $\delta^{18}\text{O}$ difference between paired temporal samples. Mean instrumental precision (0.03‰) shown by the dashed black line. Maximum instrumental precision (0.22‰) indicated by the dotted grey line.

4.2.3 Daily Tests

4.2.3.1 Simultaneous Tests

Results of simultaneous testing are provided in Figure 1. The same-time dataset (n=14) represents paired samples of water taken from seven locations between 383 and 4085 masl. The first same-time pair (SIM-01) was collected from highland waters, at the rim of the plateau,

from a class-two stream on July 11th, 2018 (1801 and 1802) in the dry season. The second same-time test (SIM-02) was collected below the plateau from the Majes River at the Punta Colorada bridge, west of the town of Aplao, on March 1st, 2019 (1925 and 1926) in the wet season. The remaining six simultaneous pairs were collected from rivers in the low- and highlands during the 2019 dry season. Replicate test SIM-06 from the Rio Blanco (Table 3) is considered an outlier and is not included in the data plots. The observed $\delta^{18}\text{O}$ values for each daily pair are plotted in Figure 24. Per mil difference between daily samples is shown in Figure 25.

Little to no variation was expected for samples taken during the same day, regardless of time. The per mil difference between same-day tests, including the outlier, ranges between $\delta^{18}\text{O}$ 0.00‰ to 0.44‰. Excluding the outlier, the range is 0.00‰ to 0.11‰. The mean standard machine error for $\delta^{18}\text{O}$ was 0.03‰, range 0.00 to 0.22‰. The mean is less than the difference for four simultaneous samples and all observed daily variation is less than the maximum possible standard machine error.

Table 3: Results of Daily Tests.

Sample ID	Pairing ID	Test Type	Location	Time	Elevation (masl)	Measured $\delta^{18}\text{O}$ (VSMOW)	$\delta^{18}\text{O}$ Average (VSMOW)	$\delta^{18}\text{O}$ Difference (‰)	Date
1925	SIM-01	Simultaneous	Majes River	15:30	383	-16.49	-16.55	0.11	3-Mar-19
1926				15:32		-16.60			
1937A	SIM-02	Simultaneous	Río Colca Feed into Majes River	12:00	896	-17.09	-17.10	0.01	13-Jun-19
1937B				12:02		-17.10			
1967A	SIM-03	Simultaneous	Río Grande	9:20	2980	-12.39	-12.42	0.05	15-Jun-19
1967B				9:22		-12.44			
1968A	SIM-04	Simultaneous	Río Blanco	12:00	3396	-13.42	-13.46	0.07	15-Jun-19
1968B				12:02		-13.49			
1969A	SIM-05	Simultaneous	Río Blanco	13:00	3727	-13.46	-13.47	0.02	15-Jun-19
1969B				13:02		-13.48			
1970A	SIM-06	Simultaneous (outlier)	Río Blanco	13:30	3800	-13.12	-13.34	0.44	15-Jun-19
1970B				13:32		-13.561			
1801	SIM-07	Simultaneous	Quebrada Pariaviri	9:42	3967	-12.35	-12.35	0.01	11-Jul-18
1802				9:53		-12.34			
1960	SIM-08	Simultaneous	Río Arma	15:30	4085	-17.55	-17.61	0.11	14-Jun-19
1961				15:32		-17.66			
1945	DIUR-01	Diurnal	Quebrada de Rata	8:23	3936	-9.98	-10.06	0.16	14-Jun-19
1965				19:20		-10.14			

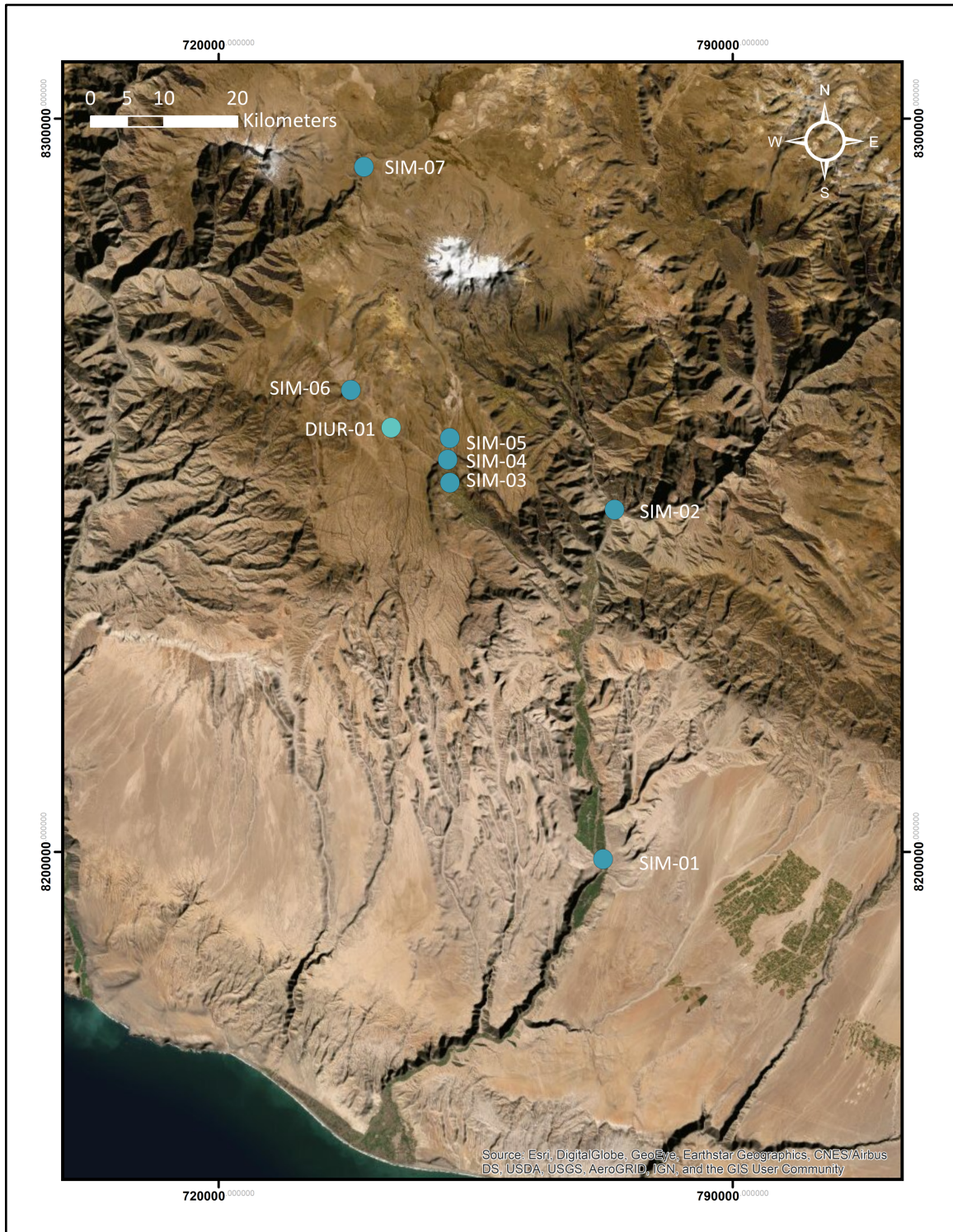


Figure 23: Map of daily sampling locations. Replicate tests are dark blue: the Río Majes, SIM-01 (383 masl); The Río Colca, SIM-02 (896 masl); the Río Grande, SIM-03 (2980 masl), SIM-04 (3396 masl), and SIM-05 (3727 masl); Quebrada Pariaviri, SIM-06 (3967 masl); and the Río Arma, SIM-07 (4085 masl). The diurnal sample (lighter blue), DIUR-01 (3936 masl) derives from the Quebrada de Rata.

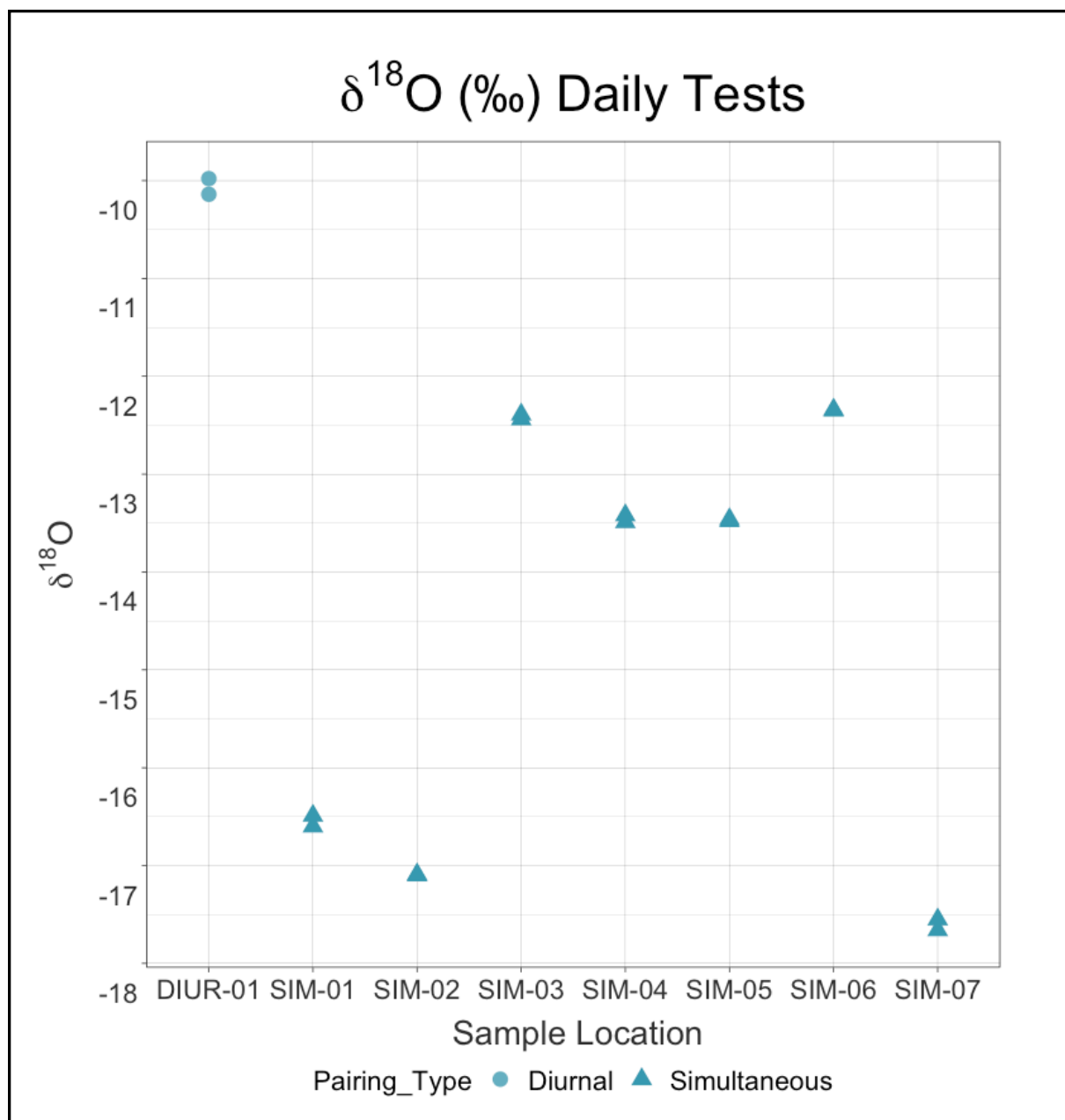


Figure 24: Observed $\delta^{18}\text{O}$ for simultaneous (dark blue triangles) and diurnal (light blue circles) pairs. Samples include the Río Majes, SIM-01 (383 masl); The Río Colca, SIM-02 (896 masl); the Río Grande, SIM-03 (2980 masl), SIM-04 (3396 masl), and SIM-05 (3727 masl); Quebrada Pariaviri, SIM-06 (3967 masl); and the Río Arma, SIM-07 (4085 masl). The diurnal sample, DIUR-01 (3936 masl) derives from the Quebrada de Rata.

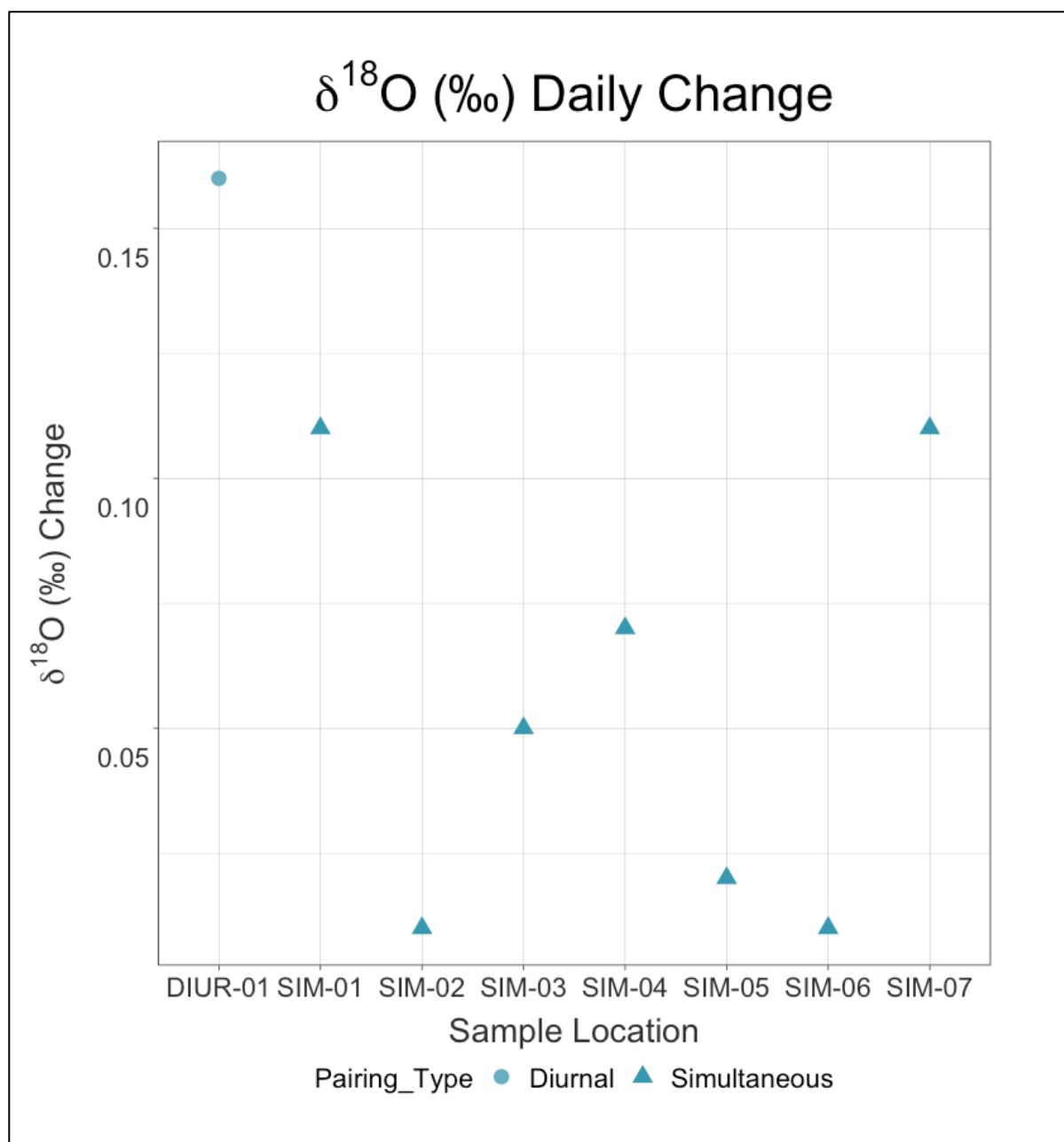


Figure 25: Change in $\delta^{18}\text{O}$ between pairs collected for daily tests. Replicate tests (dark blue triangles) include the Río Majes, SIM-01 (383 masl); The Río Colca, SIM-02 (896 masl); the Río Grande, SIM-03 (2980 masl), SIM-04 (3396 masl), and SIM-05 (3727 masl); Quebrada Pariaviri, SIM-06 (3967 masl); and the Río Arma, SIM-07 (4085 masl). The diurnal sample (light blue circle), DIUR-01 (3936 masl) derives from the Quebrada de Rata. All demonstrate less change than the maximum machine error (0.22‰).

The boxplot for $\delta^{18}\text{O}$ difference between same-time samples taken at a single location revealed one outlier with larger than expected variance. The sample collection, from Location 6, Río Blanco, utilized identical conical 15 mL Corning vials and the analytical machine precision

for both samples was good. To understand the impact of the outlying value on the dataset, the value was removed and the range and mean recalculated. The adjusted range for same-time tests is: $\delta^{18}\text{O}$ 0.00‰ to 0.11‰ (Figure 24).

Locations 3 (Río Grande) and 5 (Río Blanco) of the same-time tests utilized different vial types to test for variation between sampling containers; these pairs utilized one 30 mL Nalgene tube and one 15mL Corning vial. No significant variation was expected between vials, and no significant variation was identified (0.05‰ and 0.01‰). The statistical summary of results provided in Table 4 considers all daily samples to provide the most conservative simultaneous baseline variation possible. The range of difference for $\delta^{18}\text{O}$ was 0.43‰. The interquartile range for per mil variation was 0.09‰.

Table 4: Statistical Results for Simultaneous Tests.

Pairing Type	Samples (n =)	Mean Change (‰)	Standard Deviation	Minimum Change (‰)	Maximum Change (‰)	Range (‰)	Q1	Q3	IQR
Simultaneous Tests	8	0.10	0.14	0.01	0.44	0.43	0.02	0.11	.09

4.2.3.2 Diurnal Test

A single test was conducted during June 2019 to examine diurnal variation for a single location, as shown in Figure 24. Water sample numbers 1945 and 1965 were collected approximately 11 hours apart from the Quebrada de Rata at the edge of the Andean Plateau. The test indicates little difference between water collected from a single location at different times of day. Variation for the diurnal test was 0.16‰ for $\delta^{18}\text{O}$ (Figure 24). This value falls slightly outside of the range of per mil difference for the simultaneous tests. It is less than the range for machine precision error. Therefore, diurnal variance is negligible.

4.2.4 Seasonal Tests

Fifteen locations were sampled during both the wet and dry seasons. Three sample pairs were excluded from the seasonal analysis due to the uncertainty of their locations after a visual inspection in the GIS. Seasonal sample locations represent elevations between 383 and 4720 masl. The final seasonal test dataset is provided in Table 5 and shown in Figure 26.

Twelve locations were sampled during both the wet (2019) and dry (2018 or 2019) seasons (Figure 26). Two seasonal locations incorporated samples collected as part of the daily testing (SEAS-01) Río Majes and (SEAS-06) Quebrada de Rata. For these seasonal tests, three values were available for comparison. To reduce the comparative sample to two, the samples with the greatest difference was selected for comparison. For example, two samples were collected from the Río Majes during the wet season (2019), and one during the dry season (2019). The two wet season samples provided $\delta^{18}\text{O}$ values of -16.60‰ (WS1926) and -16.49‰ (1925). The dry season value was -16.37‰ (WS1932). Water Samples 1926 and 1932 were used for the seasonal analysis because they reflect the greatest difference possible between seasons for waters collected at this location.

Table 5: Results of Seasonal Sampling.

WS Number	Pairing ID	Location	Season	Elevation (masl)	$\delta^{18}\text{O}$ (VSMOW)	Average $\delta^{18}\text{O}$ (VSMOW)	Difference $\delta^{18}\text{O}$ (‰)
1926	SEAS-01	Majes (Punta Colorada)	wet	383	-16.60	-16.49	0.23
1932			dry		-16.37		
1923	SEAS-02	Río Grande	wet	1379	-12.13	-10.94	2.39
1941			dry		-9.74		
1922	SEAS-03	Canal de Pacaychacra	wet	1811	-12.32	-11.58	1.49
1942			dry		-10.83		
1921	SEAS-04	Huacclay canal	wet	1960	-11.39	-10.83	1.12
1943			dry		-10.27		
1919	SEAS-05	Iray canal	wet	2521	-11.87	-11.71	0.32
1944			dry		-11.55		
1909	SEAS-06	Quebrada de Rata	wet	3929	-12.77	-11.38	2.79
1945			dry		-9.98		
1814	SEAS-07	Río Arma Quebrada Ocoruru	dry	4310	-16.97	-17.48	1.02
1908			wet		-17.99		
1901	SEAS-08	Río Colunga/ Río de Choriltes	wet	4330	-17.39	-17.30	0.18
1951			dry		-17.21		
1902	SEAS-09	Auquimanca/Río Cuncaicha	Wet	4348	-16.98	-15.46	3.04
1954			dry		-13.94		
1911	SEAS-10	Quebrada Japuchaca	Wet	4434	-14.29	-14.10	0.39
1947			dry		-13.90		
1913	SEAS-11	Quebrada Pucunchitoyocc	wet	4628	-14.65	-14.50	0.41
1948			dry		-14.24		
1914	SEAS-12	Bofedal Pucunchitoyocc	wet	4720	-14.57	-13.92	1.29
1949			dry		-13.28		

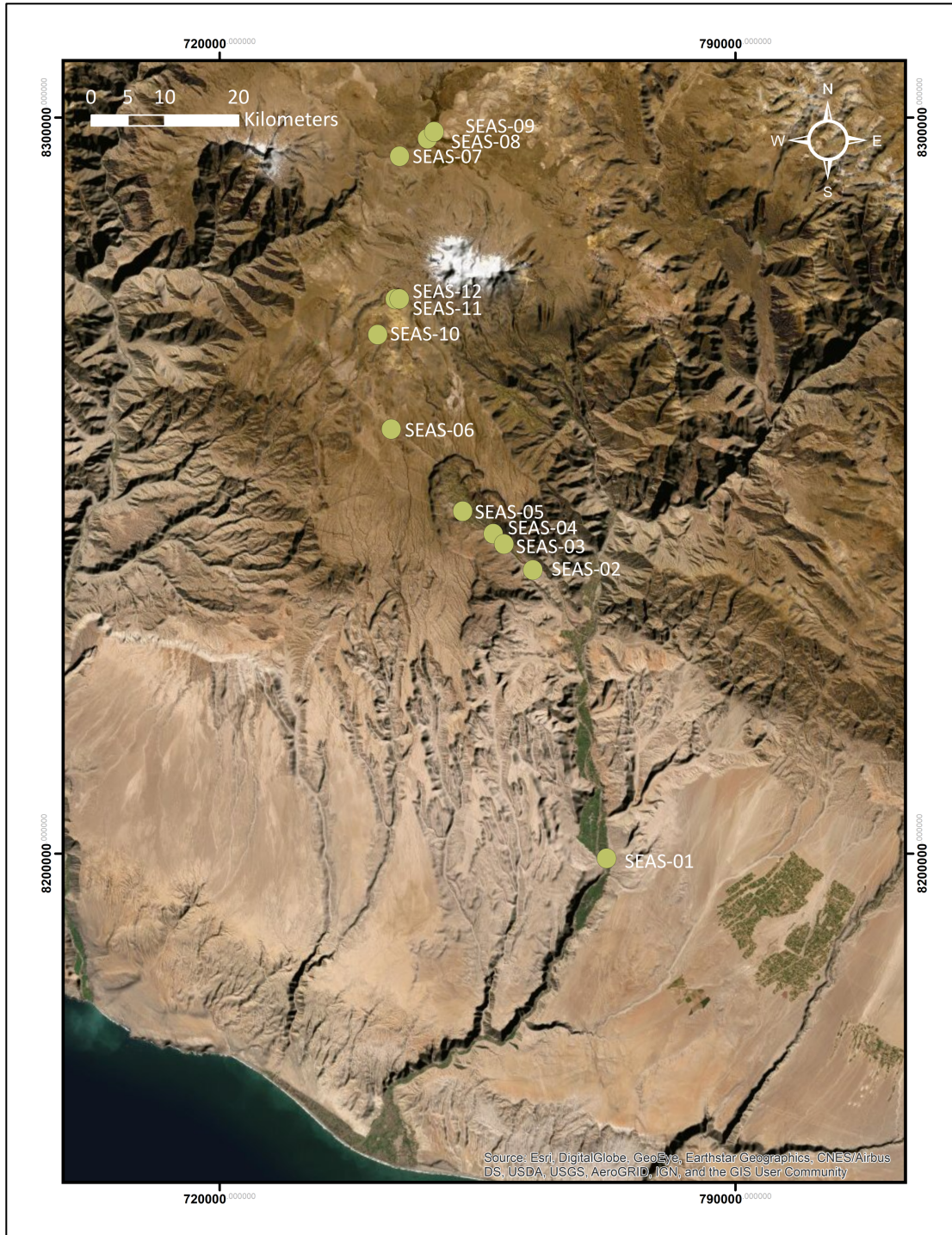


Figure 26: Map of the seasonal sample locations: the Río Majes, SEAS-01 (383 masl); The Río Grande, SEAS-02 (1379 masl); the Canal de Pacaychara, SEAS-03 (1811 masl); Huacclay Canal, SEAS-04 (1960 masl); Iray Canal, SEAS-05 (2521 masl); Quebrada de Rata, SEAS-06 (3936 masl); the Río Arma, SEAS-07 (4310 masl); Río Colunga, SEAS-08 (4333 masl); Río Cuncaicha, SEAS-09 (4347 masl); Quebrada Japuchaca, SEAS-10 (4435 masl); Quebrada Pucunchitoyocc, SEAS-11 (4717 masl); and Bofedal Pucunchitoyocc, SEAS-12 (4720 masl).

Sample pairs 1-5 were acquired from below the plateau rim. Samples 3-5 represent canals that channel waters down to the city of Aplao from the town of Chuquibamba. The remaining two samples (pairs 1 and 2) derive from the Majes River (383 masl) and Río Grande (1379 masl), Order 5 and Order 4 rivers respectively. The remaining seven pairs (6-12) represent waters collected from the Andean Plateau. The boxplot assessments (Figure 22) identified no outliers in the seasonal test dataset; therefore all 12 values were retained for further assessment. The $\delta^{18}\text{O}$ for each sample collected as part of a seasonal pairing is presented in Figure 27.

All dry season samples demonstrate slightly higher $\delta^{18}\text{O}$ values than the wet season samples from the same locations. All Class 3 streams demonstrate an appreciable amount of variation. The degree of $\delta^{18}\text{O}$ change in is variable among first order streams. For example, sample location SEAS-06, Quebrada de Rata, demonstrates a 2.97‰ shift between seasons. But sample location SEAS-10, Quebrada Japuchaca, only demonstrates a 0.39‰ change. All seasonal samples demonstrate more $\delta^{18}\text{O}$ change than daily samples (Table 5).

Table 6: Statistical Results of Seasonal Sampling.

Pairing Type	Samples (n =)	Mean Change (‰)	Standard Deviation	Minimum Change (‰)	Maximum Change (‰)	Range of Change (‰)	Q1	Q3	IQR
Seasonal Tests	12	1.21	1.01	0.18	3.04	2.86	0.39	1.49	1.10

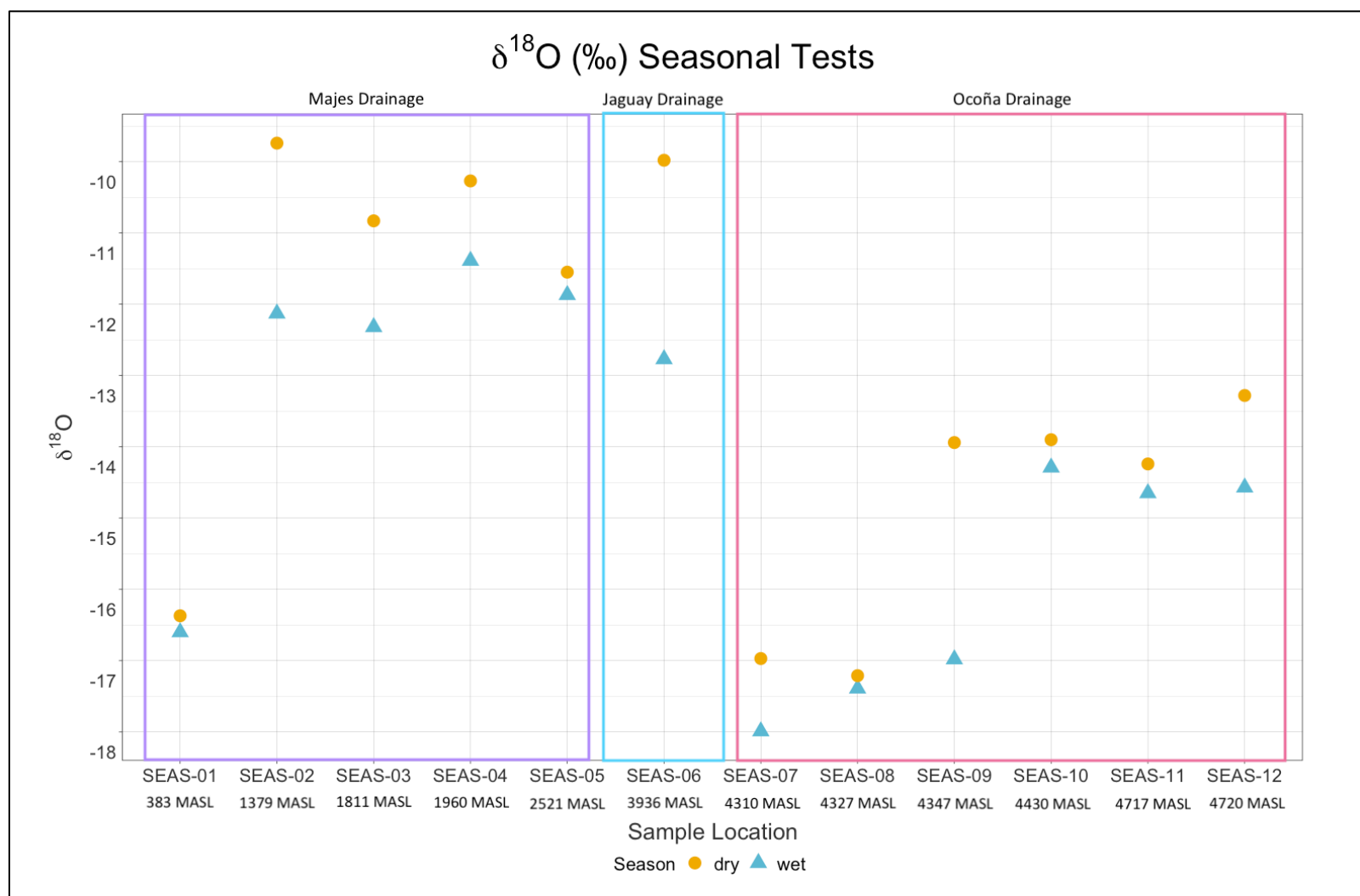


Figure 27: Plot showing $\delta^{18}\text{O}$ values for each sample in the seasonal pairs. Data are coded by wet (blue triangles) and dry (yellow circles) seasons. The Majes (purple), Jaguay (blue), and Ocoña (coral) drainages are indicated. Location codes reflect: the Río Majes, SEAS-01; The Río Grande, SEAS-02; the Canal de Pacaychara, SEAS-03; Huacllay Canal, SEAS-04; Iray Canal, SEAS-05; Quebrada de Rata, SEAS-06; the Río Arma, SEAS-07; Río Colunga, SEAS-08; Río Cuncaicha, SEAS-09; Quebrada Japuchaca, SEAS-10; Quebrada Pucunchitoyocc, SEAS-11; and Bofedal Pucunchitoyocc, SEAS-12.

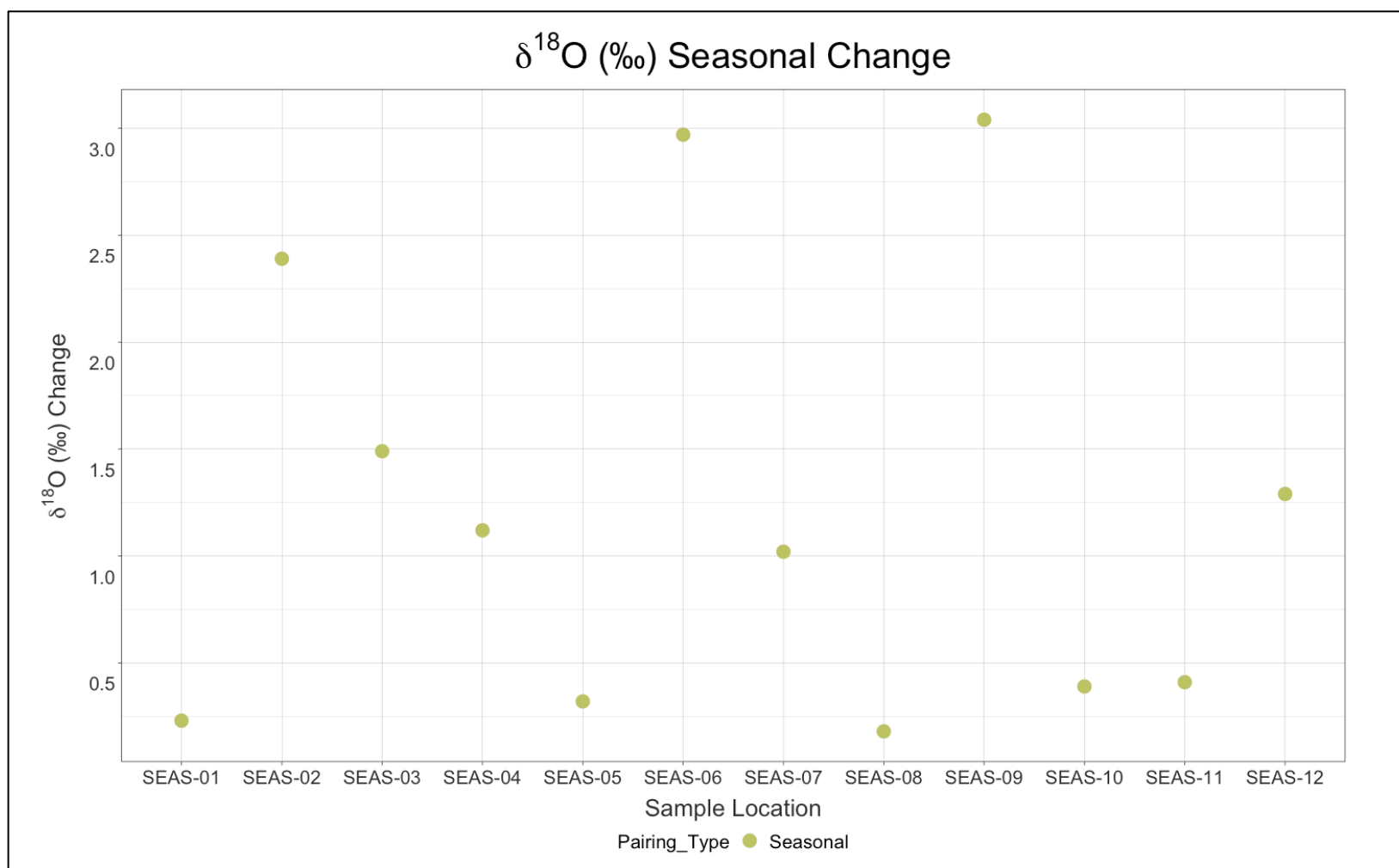


Figure 28: Plot showing the difference in δ¹⁸O (‰) between seasonal sample pairs. Location codes in order of increasing elevation: the Río Majes, SEAS-01; The Río Grande, SEAS-02; the Canal de Pacaychara, SEAS-03; Huacllay Canal, SEAS-04; Iray Canal, SEAS-05; Quebrada de Rata, SEAS-06; the Río Arma, SEAS-07; Río Colunga, SEAS-08; Río Cuncaicha, SEAS-09; Quebrada Japuchaca, SEAS-10; Quebrada Pucunchitoyocc, SEAS-11; and Bofedal Pucunchitoyocc, SEAS-12. All samples demonstrate more change than maximum machine error (0.22‰) and maximum daily change (0.16‰).

4.2.5 Yearly Tests

A second threshold for identifying significant seasonal variation comes from the results of yearly sampling, where the same location is sampled during the same (dry) season in different years. These tests provide an insight to whether the observed variation in seasonal will be greater than inter-annual variation. Results of annual testing are reported in Table 7 and locations presented in (Figure 30). Yearly tests are divided into single year (<1 year; “YR1”) and multi-year (>3 years; “MYR”) groupings. The amount of time between samples is presented for the multi-year groupings. Single year groupings were sampled 11 months apart and represent samples from July 2018 and June 2019. Figure 28 demonstrates the per mil difference between yearly samples.

Table 7: Results of Annual Sampling.

WS number	Pairing iD	Location	Date	Average Elevation (masl)	$\delta^{18}\text{O}$ (VSMOW)	Average $\delta^{18}\text{O}$ (VSMOW)	$\delta^{18}\text{O}$ Change (‰)
1801	YR-01	Quebrada Pariaviri	July 2018	3967	-12.35	-12.33	0.05
1964			June 2019		-12.30		
1814	YR-02	Río Arma	July 2018	4291	-16.97	-17.11	0.28
1950			June 2019		-17.25		
1807	YR-03	Quebrada Cuncaicha	July 2018	4465	-14.73	-14.56	0.34
1957			June 2019		-14.39		

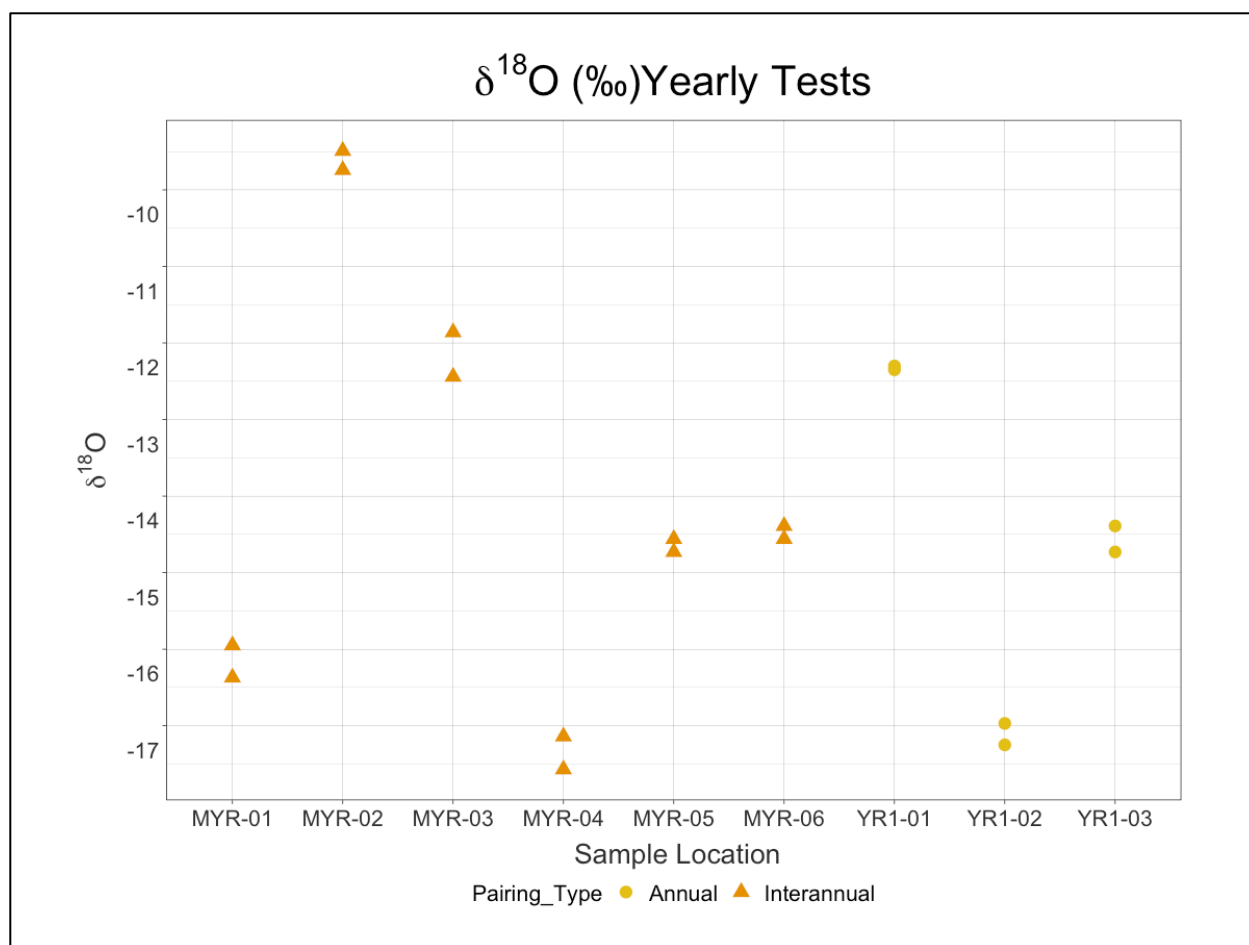


Figure 29: The δ¹⁸O of surface waters sampled during the dry season in multiple years. Annual samples (<1 year; yellow circles) include: Quebrada Pariaviri, YR1-01 (3966 masl); Río Arma, YR1-02 (4300 masl); and Quebrada Cuncaicha, YR1-03 (4457 masl). Multiyear samples (>3 years; orange triangles) include the Río Majes, MYR-01 (383 masl); The Río Grande, MYR-02 (1379 masl); Río Grande, MYR-03 (2980 masl); Río León Huactana MYR-04 (4384 masl); Quebrada Cuncaicha (3-year) MYR-05 (4457 masl); and Quebrada Cuncaicha (4-year) MYR-06 (4474 masl).

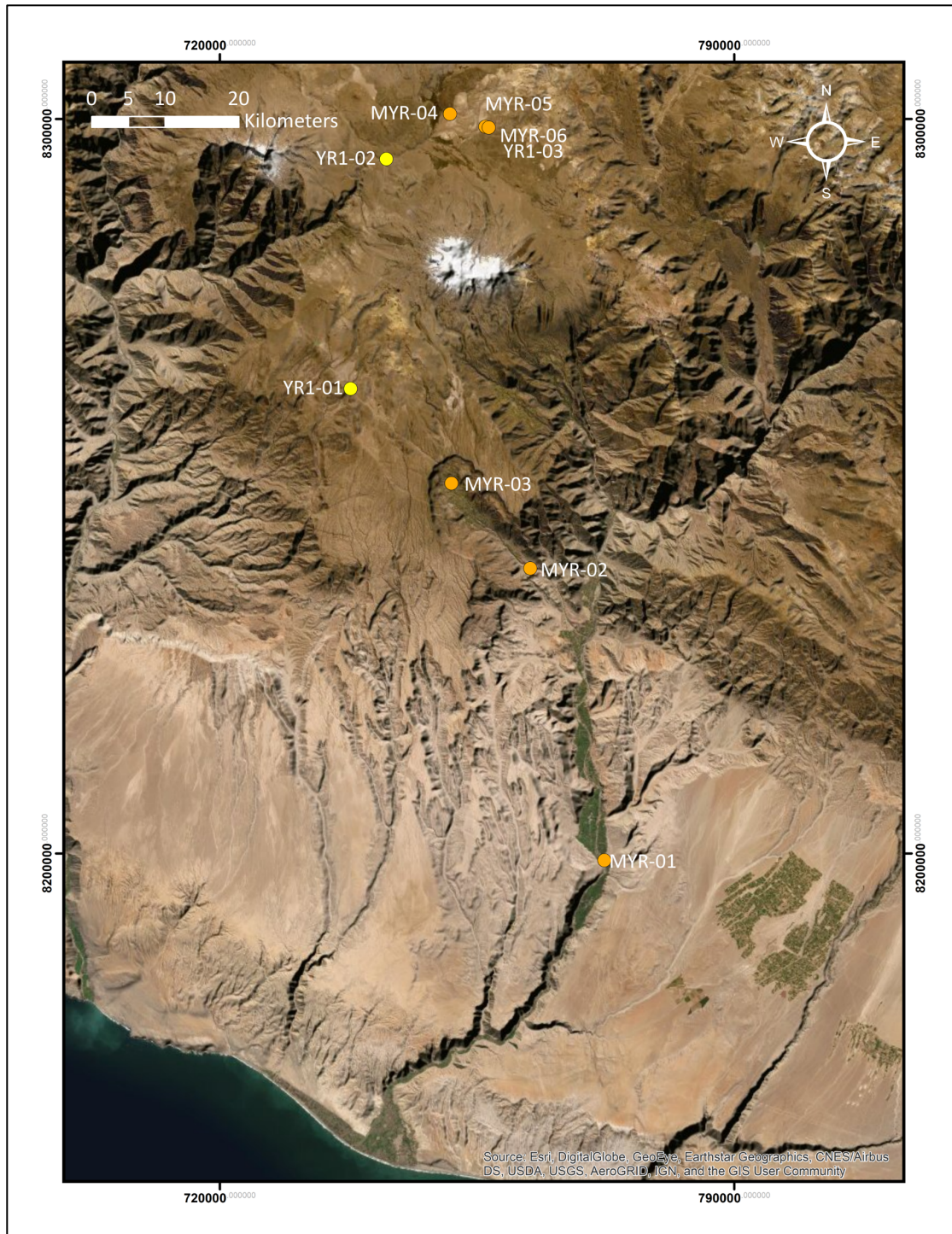


Figure 30: Map of the yearly sample locations. Annual samples (<1 year) include: Quebrada Pariaviri YR1-01 (3966 masl); Río Arma, YR1-02 (4300 masl); and Quebrada Cuncaicha, YR1-03 (4457 masl). Multiyear samples (>3 years) include the Río Majes, MYR-01 (383 masl); The Río Grande, MYR-02 (1379 masl); Río Grande, MYR-03 (2980 masl); Río León Huactana MYR-04 (4384 masl); Quebrada Cuncaicha (3-year) MYR-05 (4457 masl); and Quebrada Cuncaicha (4-year) MYR-06 (4474 masl).

4.2.5.1 Annual Tests

Annual tests represent sample locations that were replicated during the dry seasons of 2018 and 2019. The dry seasons occurred in different months (*July* 2018 and *June* 2019); however, minimal change is expected at such a short time scale. Three annual tests were recorded within the dataset, two from second order streams (pairings YR1-01 and YR1-03) and one from a fourth order river (pairing YR1-02). All three pairings derive from plateau waters. Notable in this dataset is the Quebrada Cuncaicha (pairing YR1-03) that runs in front of the archaeological site. All three pairs show remarkably little per mil variation. Results of annual statistical tests are reported in Table 8. Measured change between tests ranged from 0.05 to 0.34‰, with a mean change of 0.22‰. These data suggest annual change in surface waters is minimal; however, (1) interannual variation and (2) a larger sample set remain to be tested.

Table 8: Results of Annual Statistical Tests.

Pairing Type	Samples (n =)	Mean (‰)	Standard Deviation	Minimum Change (‰)	Maximum Change (‰)	Range of Change (‰)	Q1	Q3	IQR
One Year	3	0.22	1.01	0.05	0.34	0.29	0.17	0.31	0.14

4.2.5.2 Interannual Tests

Some water samples taken by Chala-Aldana in 2015 overlap the locations in the 2018-2019 sample set. Potential interannual samples were identified by converting Chala-Aldana's (2018) sample locations to UTM and comparing them to the 2018-2019 dataset in a GIS. The six potential interannual locations identified are presented in Table 9.

Table 9: Results of Interannual Tests.

WS number	Pairing ID	Location	Season & Year	Elevation (masl)	Oxygen (VSMOW)	Average (VSMOW)	$\delta^{18}\text{O}$ Difference (‰)
OUT-WA-011	MY-01	Majes (Punta Colorada)	Dry 2015	371	-15.95	-16.16	0.42
1932			Dry 2019		-16.37		
OUT-WA-014	MY-02	Río Grande	Dry 2015	1379	-9.49	-9.62	0.25
1941			Dry 2019		-9.74		
OUT-WA-017	MY-03	Río Grande	Dry 2015	2887	-11.86	-12.15	0.58
1967B			Dry 2019		-12.44		
PU-WA-009	MY-04	Río León Huactana	Dry 2015	4383	-17.57	-17.36	0.43
1956			Dry 2019		-17.14		
PU-WA-005	MY-05	Quebrada Cuncaicha	Dry 2015	4463	-14.56	-14.65	0.17
1807			Dry 2018		-14.73		
PU-WA-005	MY-06	Quebrada Cuncaicha	Dry 2015	4475	-14.56	-14.48	0.17
1957			Dry 2019		-14.39		

Six interannual samples span elevations between 371 and 4475 masl representing waters from both on and off the Andean Plateau. The interannual difference between surface waters range from 0.17 to 0.58‰ with a mean of 0.34‰.

Table 10: Results of Interannual Statistical Tests.

Pairing Type	Samples (n =)	Mean Change (‰)	Standard Deviation (s)	Minimum Change (‰)	Maximum Change (‰)	Range (‰)	Q1	Q3	IQR
Per mil Difference (‰)	6	0.34	0.17	0.17	0.58	0.41	0.19	0.43	0.22

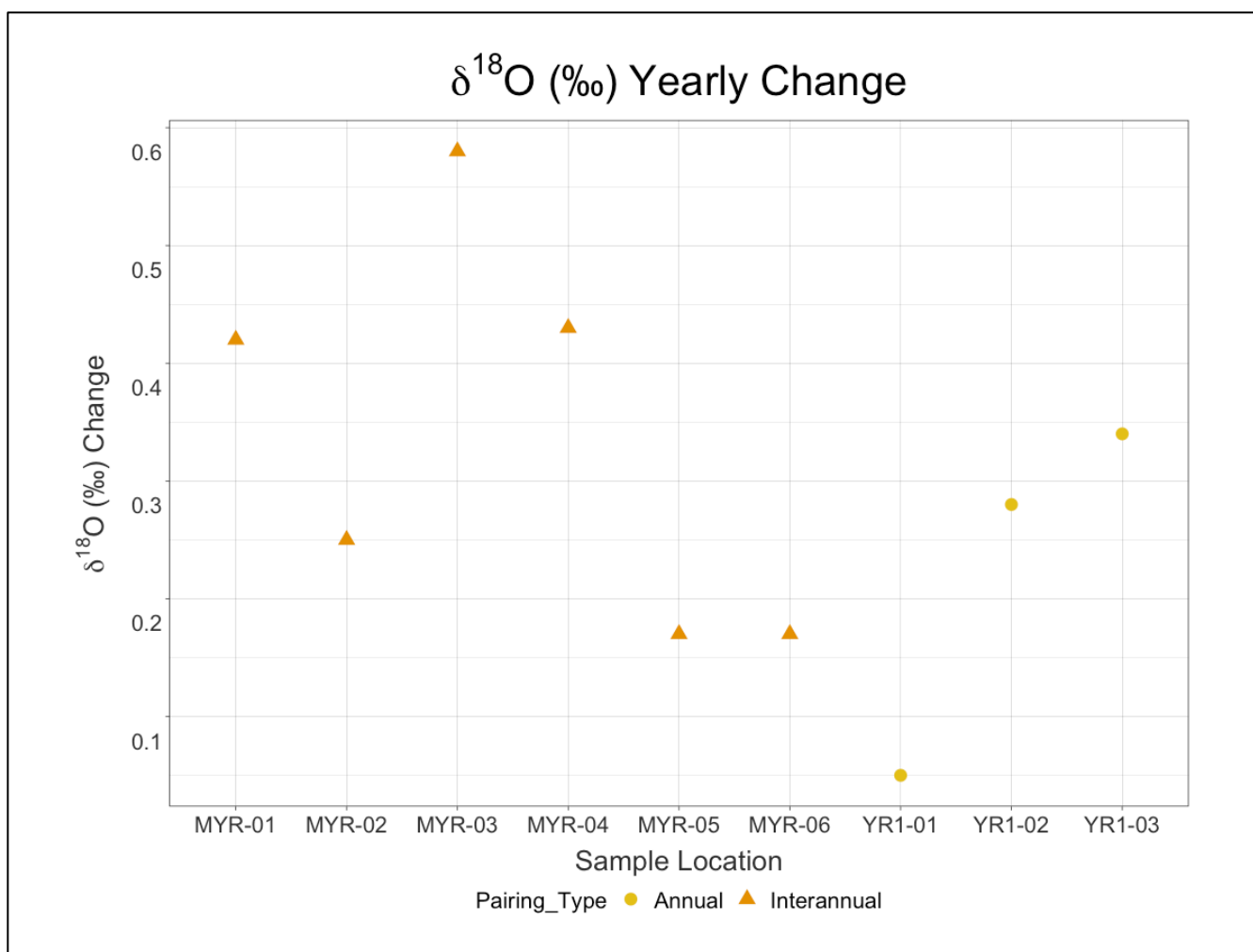


Figure 31: Per mil difference in $\delta^{18}\text{O}$ between surface waters sampled during the dry season in multiple years. Annual samples (<1 year; yellow circles) include: Quebrada Pariaviri, YR1-01 (3966 masl); Río Arma, YR1-02 (4300 masl); and Quebrada Cuncaicha, YR1-03 (4457 masl). Multiyear samples (>3 years; orange triangles) include the Río Majes, MYR-01 (383 masl); The Río Grande, MYR-02 (1379 masl); Río Grande, MYR-03 (2980 masl); Río León Huactana MYR-04 (4384 masl); Quebrada Cuncaicha (3-year) MYR-05 (4457 masl); and Quebrada Cuncaicha (4-year) MYR-06 (4474 masl).

4.2.6 Results of Temporal Comparisons

Results of the comparison for difference values between daily, seasonal, and yearly changes in stable oxygen of surface waters for the study area are depicted in Figure 32. Because Andean surface waters may be susceptible to changes in $\delta^{18}\text{O}$ over multiple time scales, it is important to consider both daily and annual change in determining whether seasonal change registers at the greatest magnitude in Andean surface waters.

Daily and yearly tests set two rhythmic baselines for non-seasonal variation in the study area. Figure 32 plots all temporal data by sample location to demonstrate the measured change in $\delta^{18}\text{O}$ values of surface waters over multiple time intervals. The dashed line indicates the greatest change observed in a non-seasonal pair (0.58‰; multi-year). Surface waters in the study area appear to reflect the greatest degree of $\delta^{18}\text{O}$ change at the seasonal level. A final test explores different levels of temporal variation for controlled locations.

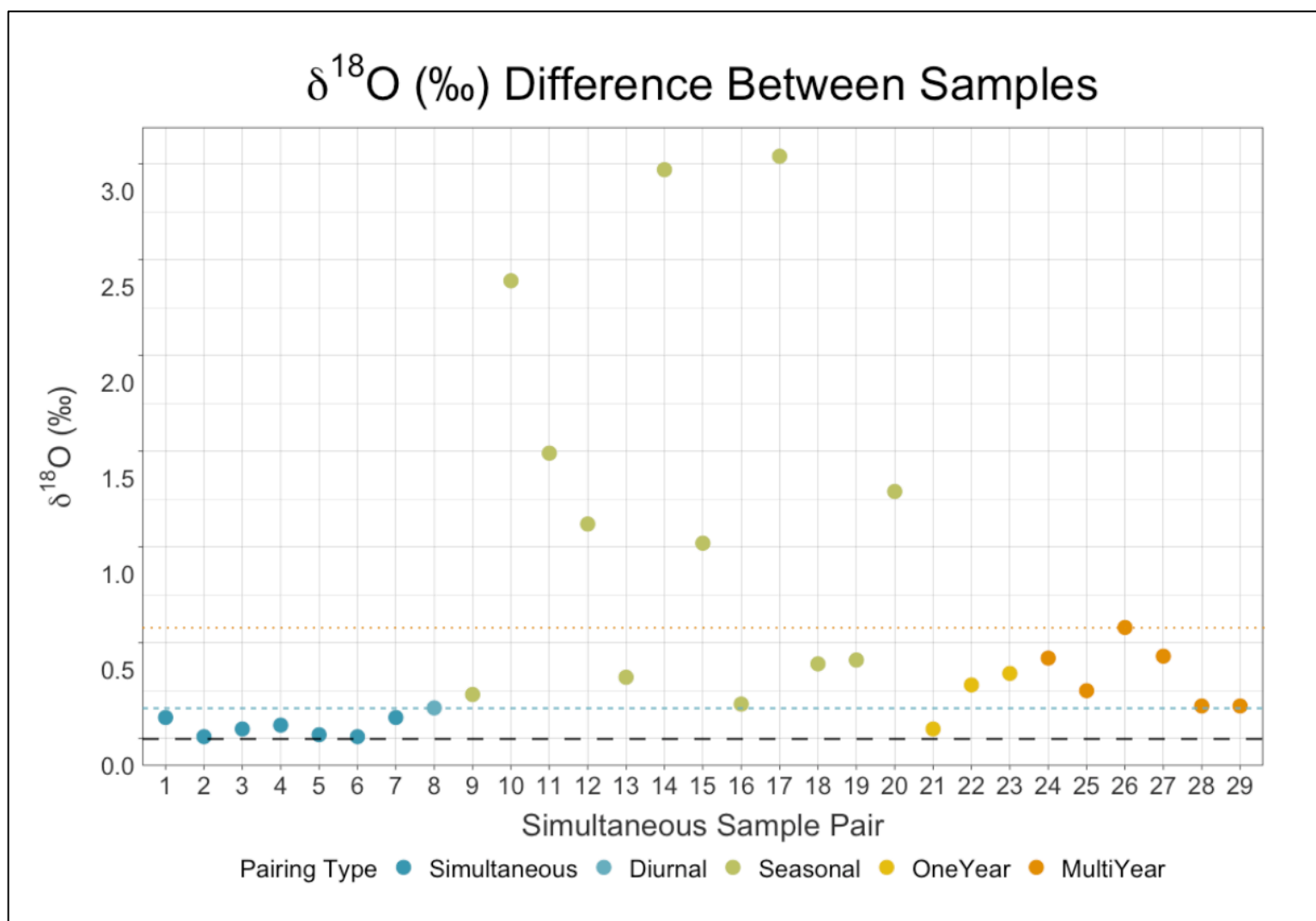


Figure 32: Per mil $\delta^{18}\text{O}$ change for simultaneous (dark blue), diurnal (light blue), seasonal (green), one-year (yellow) and multi-year (orange) tests. Numbers correspond to sampling locations for each test in order of elevation. Maximum observed machine error indicated by the black dashed line (0.22‰). Maximum daily change (0.16‰) indicated by the blue dashed line. Maximum yearly change (0.58‰) indicated by the orange dotted line.

4.2.6.1 Change Over Multiple Time Scales, Controlled for Location

In the first plot, Figure 33, the per mil $\delta^{18}\text{O}$ daily change is compared to $\delta^{18}\text{O}$ seasonal change for three locations. The Quebrada de Rata (a first order stream) is located in the Jaguay drainage at 3936 masl and demonstrates a 0.16‰ change in $\delta^{18}\text{O}$ diurnally, but a 2.79‰ change seasonally. The difference between daily and seasonal change is 2.63‰. Next, the Río Arma (a third order river) is located in the Ocoña drainage system at ~4085 masl. Measured change in $\delta^{18}\text{O}$ between replicate simultaneous tests is 0.11‰ while measured seasonal change is 1.02‰. The $\delta^{18}\text{O}$ per mil change between simultaneous and seasonal samples is 0.91‰. Finally, the Río Majes (a fifth order river) is located at 383 masl in the Majes drainage. Simultaneous change is 0.11‰ and seasonal percent change is 0.23‰. Per mil $\delta^{18}\text{O}$ change is only 0.12‰ for this location.

Comparative daily and seasonal tests from identical locations are limited to three samples; any conclusions will be biased by the small sample size. For these locations, seasonal change is greater than daily change for all locations, though seasonal change in the Río Majes is considered negligible. The percent of seasonal change decreases with increasing stream order for this dataset (n=3).

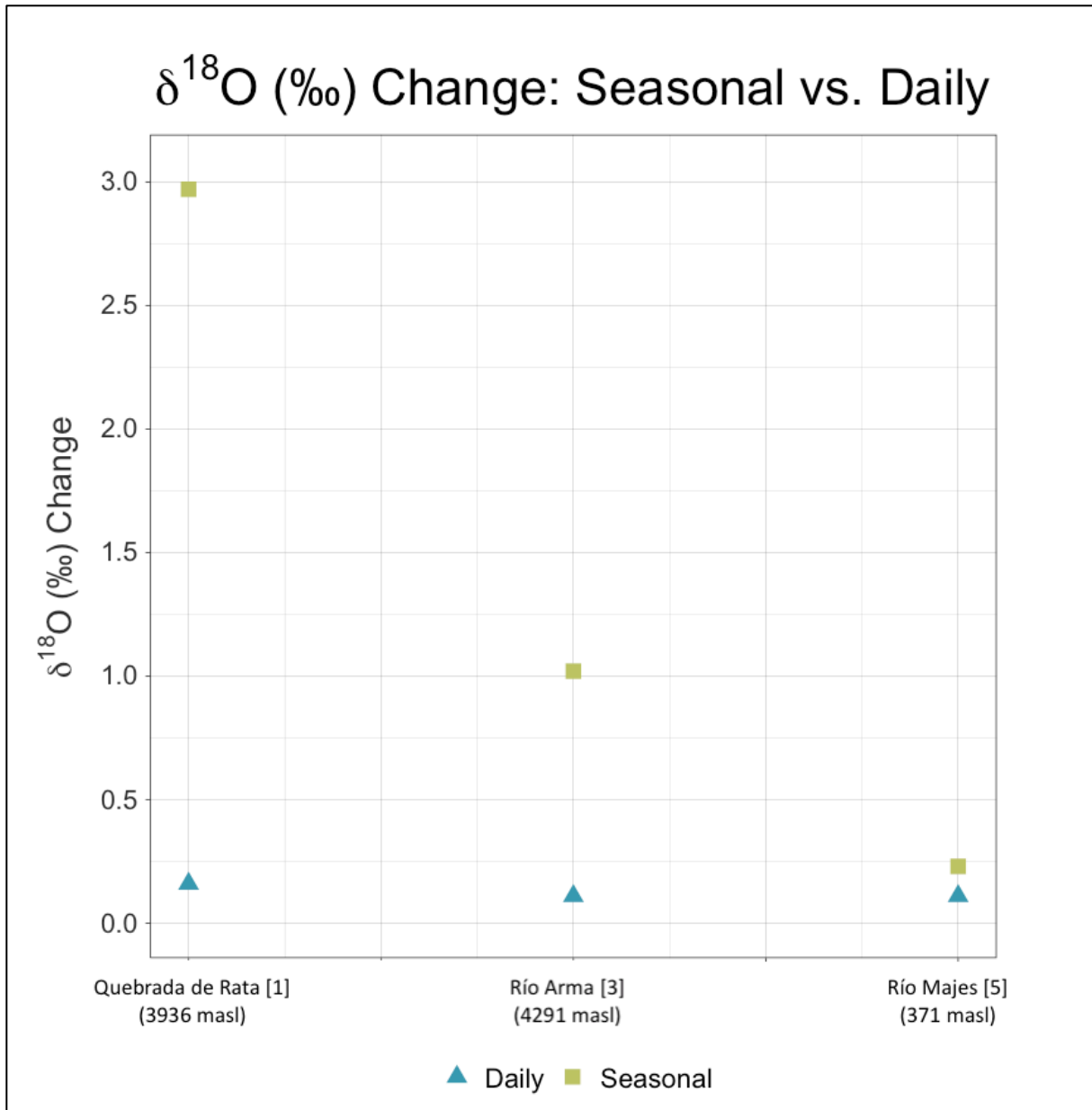


Figure 33: Measured per mil difference in $\delta^{18}\text{O}$ at the daily (yellow) and seasonal (red) scales for the Quebrada de Rata, Río Arma, and Río Majes.

In the plot, Figure 34, per mil daily change in $\delta^{18}\text{O}$ is compared to the seasonal and annual change for two locations. The Río Arma (third order) is located in the Ocoña drainage system at ~4085 masl. The measured change in surface water $\delta^{18}\text{O}$ between simultaneous and annual samples is 0.27‰ and per mil change between seasonal and annual samples is 0.74‰.

For all locations, the change in surface water $\delta^{18}\text{O}$ between seasons is greater than the change measured for single-day samples.

Next, the Río Majes (fifth order) is located at 383 masl in the Majes drainage. For the three locations, the Río Majes demonstrates the greatest change in $\delta^{18}\text{O}$ surface waters at the multi-year scale. Observed seasonal change in $\delta^{18}\text{O}$ for the Río Majes was 0.23‰, while multi-year variation was measured at 0.42‰. Per mil change in the surface water $\delta^{18}\text{O}$ of the Río Majes, compared at the daily and multi-year levels, is low (0.31‰); and even lower when comparing the degree of seasonal and annual $\delta^{18}\text{O}$ change (0.19‰). Multi-year variation is greater than seasonal variation for the Río Majes. The $\delta^{18}\text{O}$ of Majes surface waters are remarkably stable over time.

The Río Grande (third order) at 1379 masl in the Majes drainage provides a third location to compare seasonal and multi-year (4 years) variation. Observed seasonal change in $\delta^{18}\text{O}$ for the Río Grande was 2.39‰, while multi-year variation was measured at 0.25‰. The per mil difference between seasonal and annual change is 2.14‰. Seasonal change is greater than yearly change for this location.

As the final location in this comparative test, the Quebrada Cuncaicha (second order) in the Ocoña drainage was measured at the one-(2018-2019), three- (2015-2018) and four-year (2015-2019) scales. One-year change is 0.34‰, three-year change 0.17‰, and four-year change 0.17‰. The maximum per mil variation observed for the Quebrada Cuncaicha at the yearly scale was 0.34 per mil change between 2018 and 2019.

For these sample locations, smaller order streams demonstrate more change in surface water $\delta^{18}\text{O}$ at the season-year scale than larger order streams.

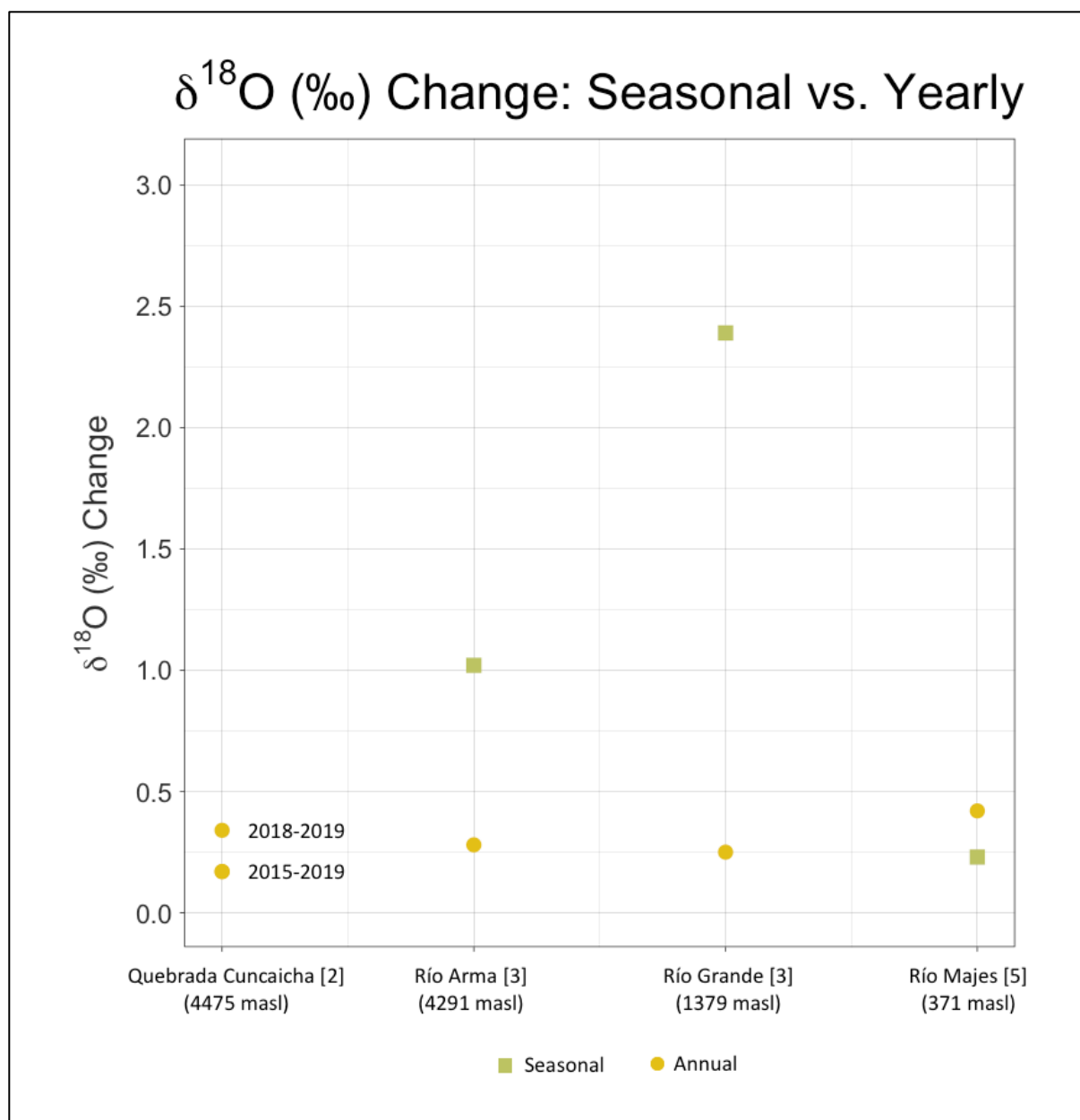


Figure 34: Per mil change in the $\delta^{18}\text{O}$ of surface waters at the daily (yellow), seasonal (red), and annual (blue) scales for the Río Arma, Río Grande, and Río Majes. Pairings from the Quebrada Cuncaicha reflect yearly change at a one- and four-year scale.

4.3 Spatial Variation in Stable Oxygen in Southern Peru

In this section I investigate whether the $\delta^{18}\text{O}$ values of surface waters vary predictably between the Pacific coast and high Andes. I use an elevation transect to assess whether $\delta^{18}\text{O}$ values are distinct among different elevations. As a brief review, the study area begins at the

Pacific coast and extends north-northeast up into the high-altitude Andes mountains. The primary oxygen isotopic input derives from Atlantic precipitation arriving from the east. In the study area, the west coast is the lowest elevation zone, experiences warmest temperatures, and is furthest from the Atlantic system. The targeted Andean high-elevation locations are closer to the input source, receive more precipitation, and are colder overall.

Published studies assume that regional $\delta^{18}\text{O}$ values in meteoric waters will have an inverse relationship with elevation (Chala-Aldana et al. 2018; Haas et al. 2017; Knudson 2009). Specifically, $\delta^{18}\text{O}$ values should decrease with increasing elevation. I measure surface water $\delta^{18}\text{O}$ values to test the assumption that low elevation waters demonstrate higher $\delta^{18}\text{O}$ values than high-elevation waters. This section reviews whether a relationship between elevation and surface water $\delta^{18}\text{O}$ exists in the Study Area.

4.3.1 $\delta^{18}\text{O}$ Variation Across an Elevation Transect

Table 11 and Figure 35 present the results and locations of the elevation transect. The $\delta^{18}\text{O}$ value for each sample was plotted against the elevation of collection (Figure 36). To simplify discussion, elevation changes are discussed in 1000-meter intervals (Table 11).

Table 11: Results of Elevation Subsets.

Elevation Bracket (masl)	Number (n=)	Minimum Elevation (masl)	Maximum Elevation (masl)	Minimum $\delta^{18}\text{O}$ (VSMOW)	Maximum $\delta^{18}\text{O}$ (VSMOW)	1 st Quartile $\delta^{18}\text{O}$ (‰)	3 rd Quartile $\delta^{18}\text{O}$ (‰)	Mean $\delta^{18}\text{O}$ (‰)
< 1000	17	36	937	-17.10	-13.39	-16.78	-16.37	-16.31
1001-2000	7	1128	1960	-12.56	-9.74	-12.22	-10.55	-11.32
2001-3000	9	2347	2980	-12.44	-10.85	-12.31	-11.55	-11.89
3001-4000	15	3070	3967	-17.77	-9.98	-13.53	-12.35	-13.19
> 4000	50	4048	4938	-17.99	-12.10	-17.25	-14.44	-15.83

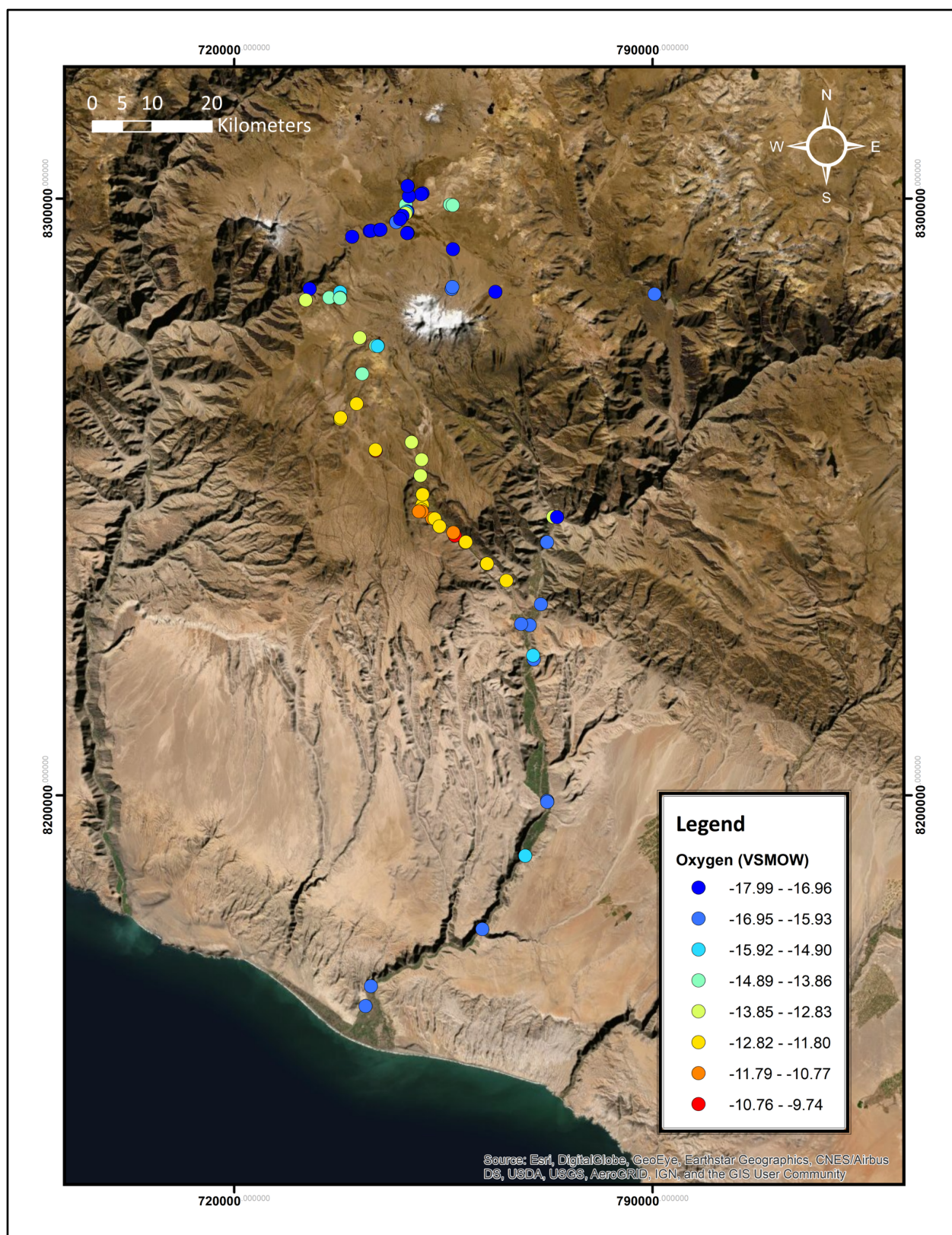


Figure 35: Map of all sampling locations illustrating the $\delta^{18}\text{O}$ values of the collected surface waters.

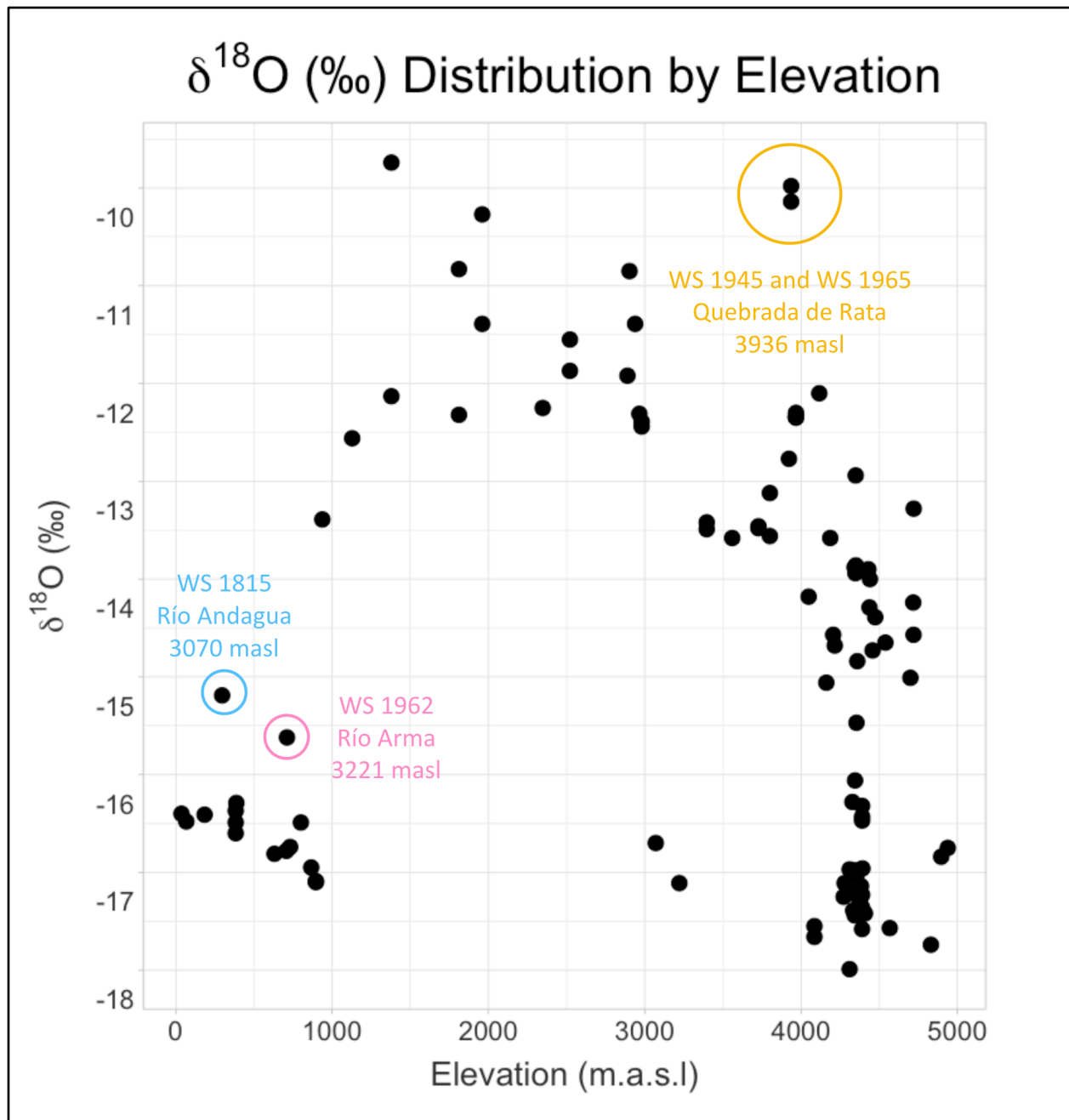


Figure 36: Distribution of $\delta^{18}\text{O}$ across elevation. The plot incorporates all samples. Four outliers include WS1962 (pink) in the Ocoña drainage basin, WS1815 (blue) in the Majes drainage basin, and the paired samples WS1945 and WS1965 (orange) from the Jaguay drainage basin.

Below 1000 meters ($n=17$), $\delta^{18}\text{O}$ ranges from -17.10 to -13.39 ‰, with a mean of -16.31 ‰. The first and third quartile range for samples below 1000 meters is restricted to -16.78 to -16.37 ‰. Between 1000 to 2000 meters ($n=7$), $\delta^{18}\text{O}$ range from -12.56 to -9.74 ‰ and

average -11.32‰. From 2000-3000 meters (n =9) values are restricted to -12.44 to -10.85 ‰, with the mean -11.89‰. The range of $\delta^{18}\text{O}$ values (n=15) in the 3000-4000-meter bracket is the largest, between -17.11 to -9.98 ‰. The mean is -13.19‰ and interquartile range -13.53 to -12.35 ‰. Values above 4000 meters (n=50) are as low as -17.99 and high as -12.10 ‰. The mean is -15.89‰.

Three patterns emerge from the initial investigation. First, the plot shows considerable overlap in stable oxygen for waters below 1000 masl and above 4000 masl for the $\delta^{18}\text{O}$ range between -17.5 to -15‰. Second, there is no appreciable distinction for $\delta^{18}\text{O}$ values between the elevations of 1000 to 4000 masl. Third, between the lowest sample (36 masl) and 3000 meters, the $\delta^{18}\text{O}$ values of surface waters coarsely demonstrate a pattern opposite of expectations: $\delta^{18}\text{O}$ values increase with elevation.

4.3.2 Seasonal Variation in $\delta^{18}\text{O}$ by Elevation

Next, data were examined by season to determine whether $\delta^{18}\text{O}$ patterning across elevations changes annually (Figure 37).

4.3.2.1 Dry Season

Below 1000 meters, the elevation trends remain consistent with the overall results. During the dry season, elevations between 1000-4000 meters demonstrate a clear inverse relationship with $\delta^{18}\text{O}$ values; patterning for this elevation range matches expectations as waters become higher as they decrease in elevation.

4.3.2.2 Wet Season

In the wet season, the small sample size biases the results. Two samples below 1000 meters derive from the Río Majes, which reflects little seasonal change. Between 1000 to 3000 meters, the range of $\delta^{18}\text{O}$ values is more restricted and lower than for the dry season. The same locations in this elevation range were sampled during both seasons; therefore, elevation patterning of $\delta^{18}\text{O}$ changes with season. Between 3000-4000 meters, there are no representative samples. Above 4000 (n=14) the wet season range is $\sim 2\text{‰}$ lower than the dry season. The shift to lower values reflects the influx in precipitation. Waters from the Quebrada de Rata, the two 'outlier' samples, shift to become 2.97‰ higher during the dry season.

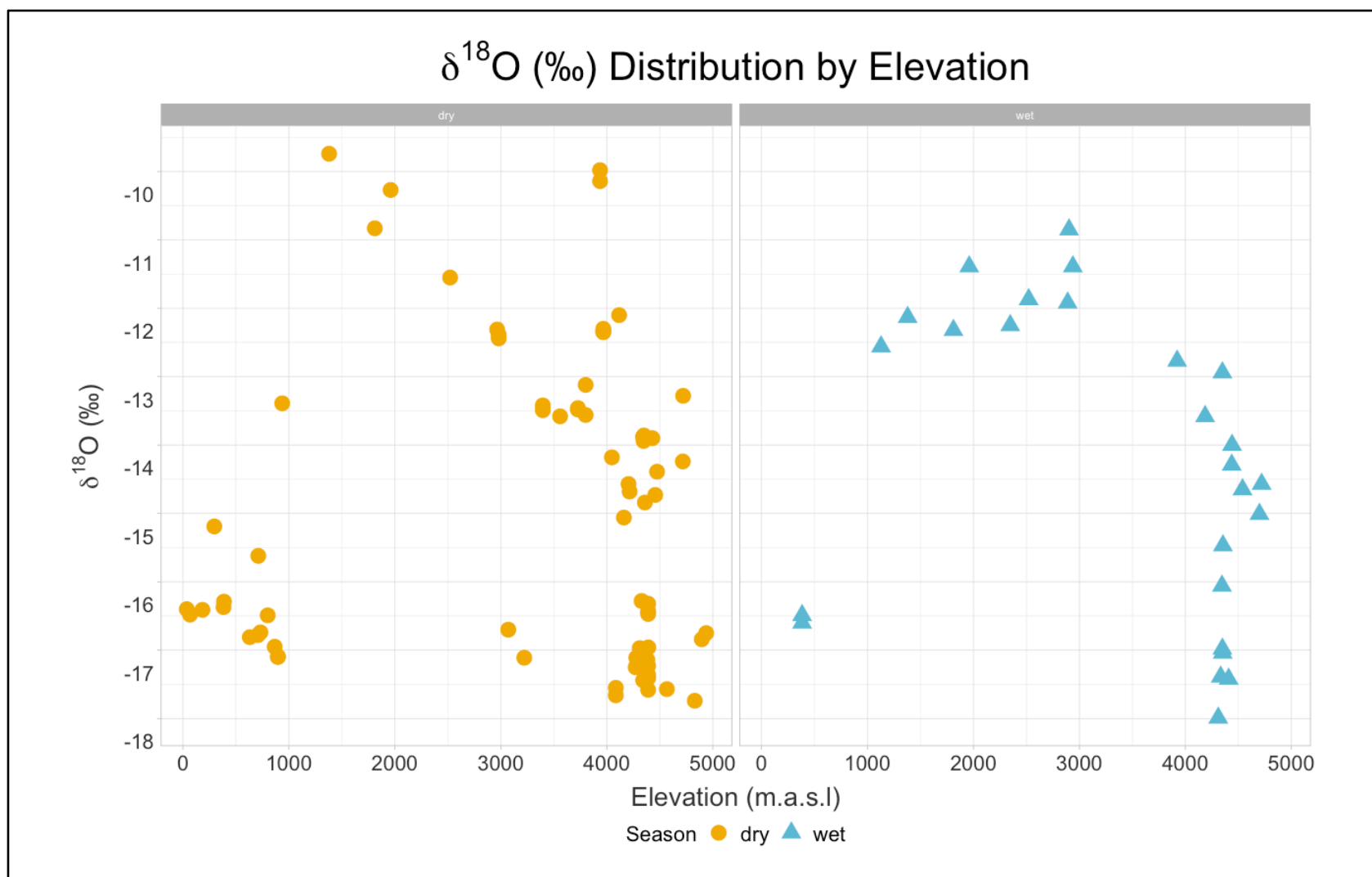


Figure 37: Distribution of $\delta^{18}\text{O}$ of Andean surface waters by elevation. Data are divided by season. Yellow dots (left) reflect the 2018 and 2019 dry season samples and blue triangles (right) the 2019 wet season samples.

4.3.3 $\delta^{18}\text{O}$ Variation Across Watersheds

Data were subdivided into the three watersheds: Jaguay, Majes, and Ocoña. Results are presented in Table 12. A box plot of $\delta^{18}\text{O}$ values for each watershed suggests distinct ranges of $\delta^{18}\text{O}$ (Figure 38). The Ocoña drainage basin comprises 54 samples between 3221 to 4938 masl. The range of $\delta^{18}\text{O}$ in sampled Ocoña surface waters was -17.99 to -12.30‰. Majes samples comprised 40 samples, from 36 to 3800 masl. Sampled Majes waters ranged from -17.10 to -9.74‰, with a mean of -14.02‰. The Jaguay drainage basin contains only four samples. Samples came from 3922 to 4116 masl. The range of sampled Jaguay $\delta^{18}\text{O}$ values was $\delta^{18}\text{O}$ -12.77 to -9.98, and the mean -11.25‰. The elevation range varies significantly across drainage basins. A plot of $\delta^{18}\text{O}$ across elevation is considered for each watershed (Figure 39).

Table 12: Results Divided by Watershed.

Watershed	Number (n=)	Minimum Elevation (masl)	Maximum Elevation (masl)	Minimum $\delta^{18}\text{O}$ (VSMOW)	Maximum $\delta^{18}\text{O}$ (VSMOW)	Mean $\delta^{18}\text{O}$ (VSMOW)
Ocoña Drainage	54	3221	4938	-17.99	-12.30	-15.69
Majes Drainage	40	36	3800	-17.10	-9.74	-14.02
Jaguay Drainage	4	3922	4116	-12.77	-9.98	-11.25

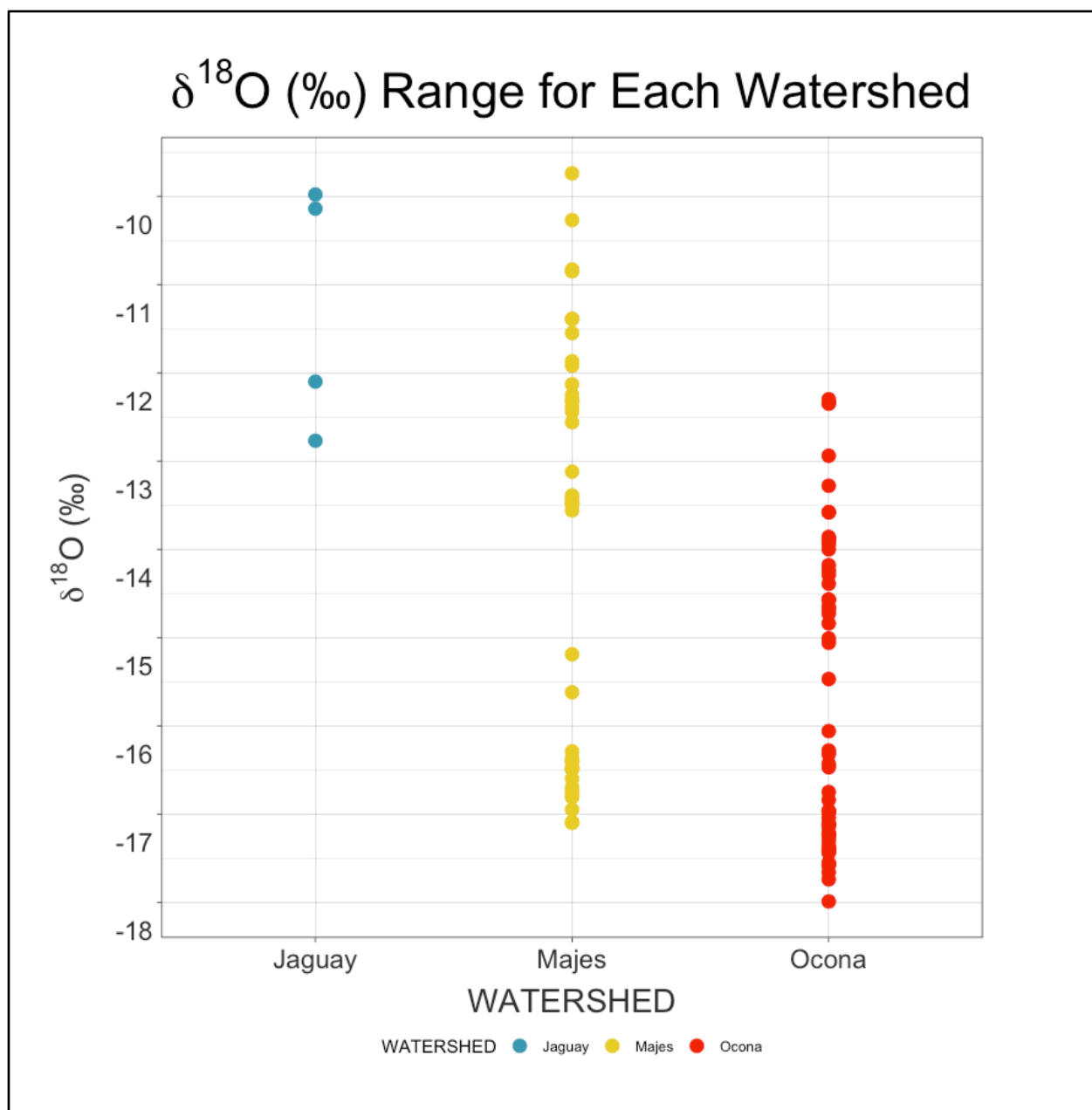


Figure 38: Dot plot of $\delta^{18}\text{O}$ range for the three sampled drainage basins. The Ocoña expresses the most depleted surface water values overall, and the Jaguay the most enriched values.

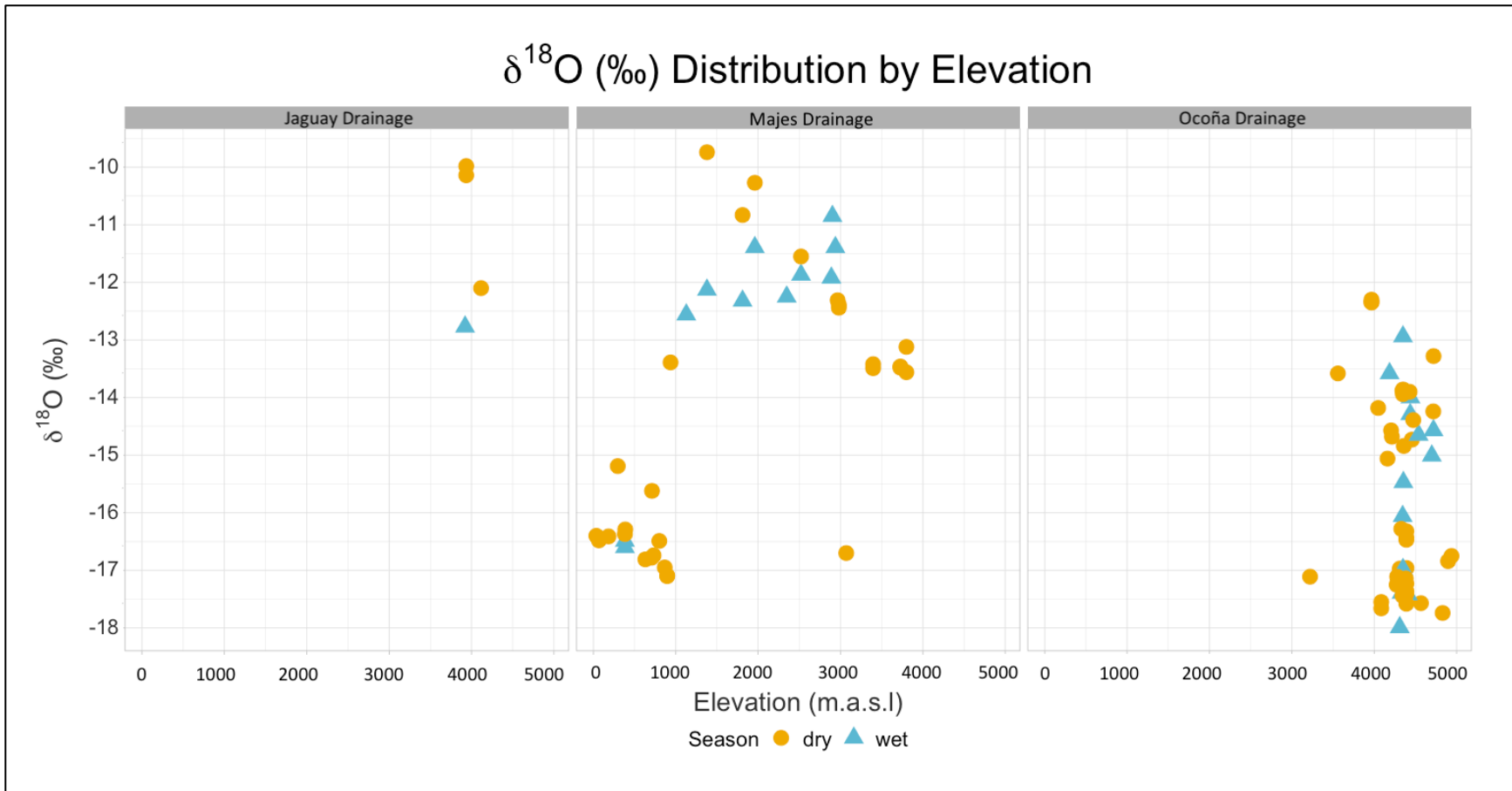


Figure 39: $\delta^{18}\text{O}$ variation by elevation divided by individual watersheds. Jaguay drainage is on the left, Majes center, and Ocoña right. Data are coded by wet (blue triangles) and dry (yellow circles) seasons.

4.3.3.1 Jaguay Drainage Basin

The data for the Jaguay drainage basin is limited by a small sample size ($n=4$). The sample reflects only two distinct water bodies: Quebrada de Rata and Quebrada Palljaruta (Figure 40). The minimum $\delta^{18}\text{O}$ value for Jaguay surface waters was -12.77‰ and maximum -9.98‰ . Both values derive from the Quebrada de Rata. The total range is influenced by seasonal change, not variation across water bodies or elevation.

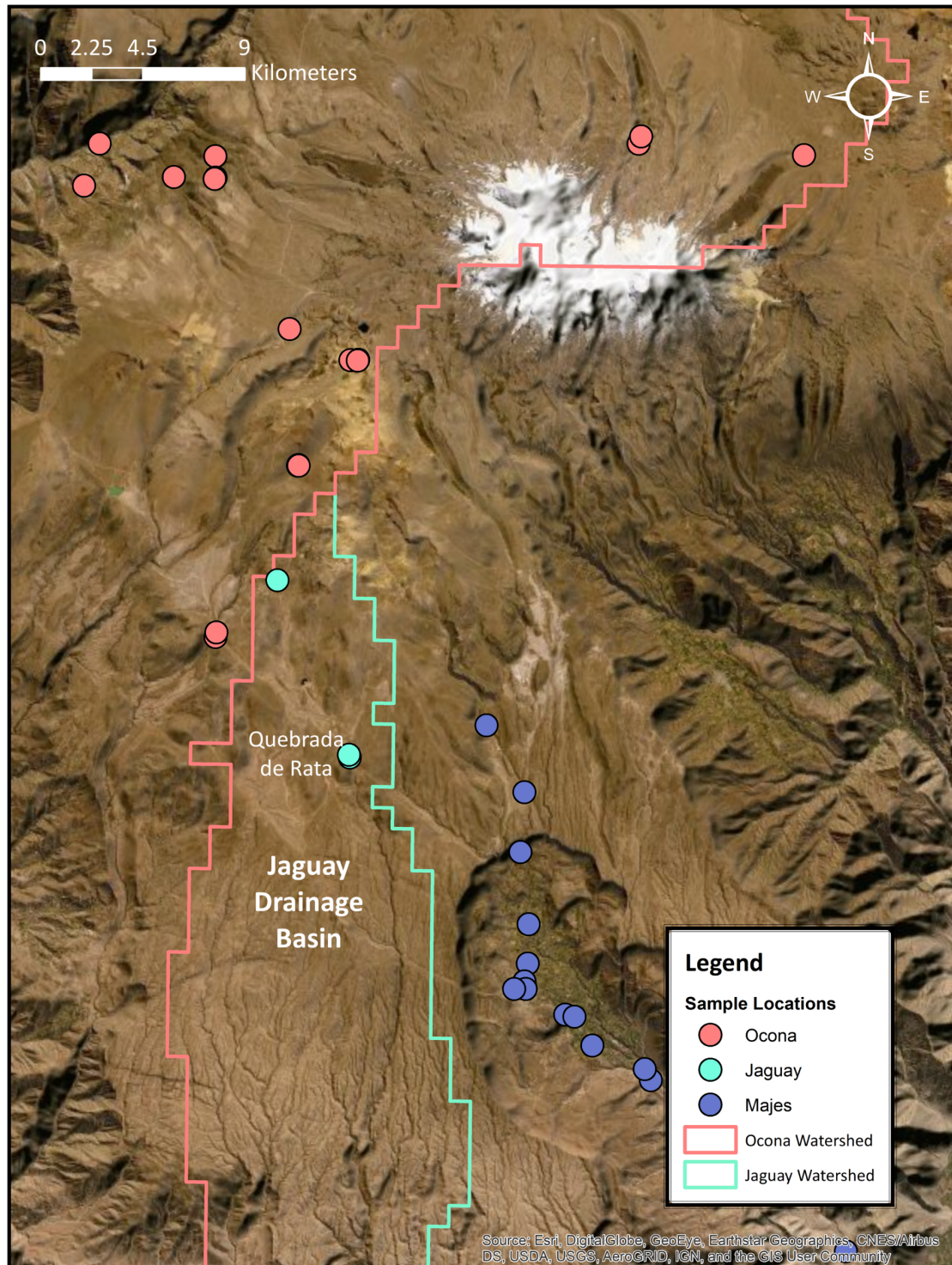


Figure 40: Map of the Jaguay drainage basin and the Quebrada de Rata samples.

4.3.3.2 Majes Drainage Basin

The Majes drainage basin samples were limited to elevations below 4000 meters. Waters follow predicted expectations and become higher with decreasing elevation during the dry season. If seasonal variation is considered, $\delta^{18}\text{O}$ values of surface waters below 3000 meters exhibit a near complete reversal in this pattern and appear to become lower with decreasing elevation. The outlier to this subset is WS1815, a sample from the Río Andagua at 3070 masl I collected the sample further north in the drainage than the other waters in this drainage.

4.3.3.3 Ocoña Drainage Basin

The Ocoña drainage basin sample set is biased toward high elevation locations above 3000 meters, including the Pucuncho Basin. The range of spread for $\delta^{18}\text{O}$ in surface waters is 5.69‰. The Ocoña reflects diverse waterbodies and stream orders, exhibiting the range of variation possible within a single watershed. All waters in this sample set drain into the Río Arma before discharging over the plateau rim. WS1962, the Río Arma in Salamanca (3221 masl), is the lowest water sample collected in the Ocoña drainage.

4.3.4 Variation in $\delta^{18}\text{O}$ by Stream Order

Samples are subdivided their Strahler stream order classification and compared across watersheds (Table 13). A map stream orders sampled within the study area (Figure 41). A plot of $\delta^{18}\text{O}$ values for stream order organized by watershed is presented in Figure 42.

Table 13: Summary of $\delta^{18}\text{O}$ Variation Among Stream Orders.

Strahler Stream Order	Number (n=)	Minimum Elevation (masl)	Maximum Elevation (masl)	Minimum $\delta^{18}\text{O}$ (VMSOW)	Maximum $\delta^{18}\text{O}$ (VSMOW)	Mean $\delta^{18}\text{O}$ (VSMOW)
1	30	3922	4938	-17.74	-9.98	-14.00
2	26	2889	4567	-17.58	-10.85	-14.91
3	17	1128	4375	-17.99	-9.74	-14.86
4	2	937	3070	-16.70	-13.39	-15.04
5	15	36	896	-17.10	-15.19	-16.49

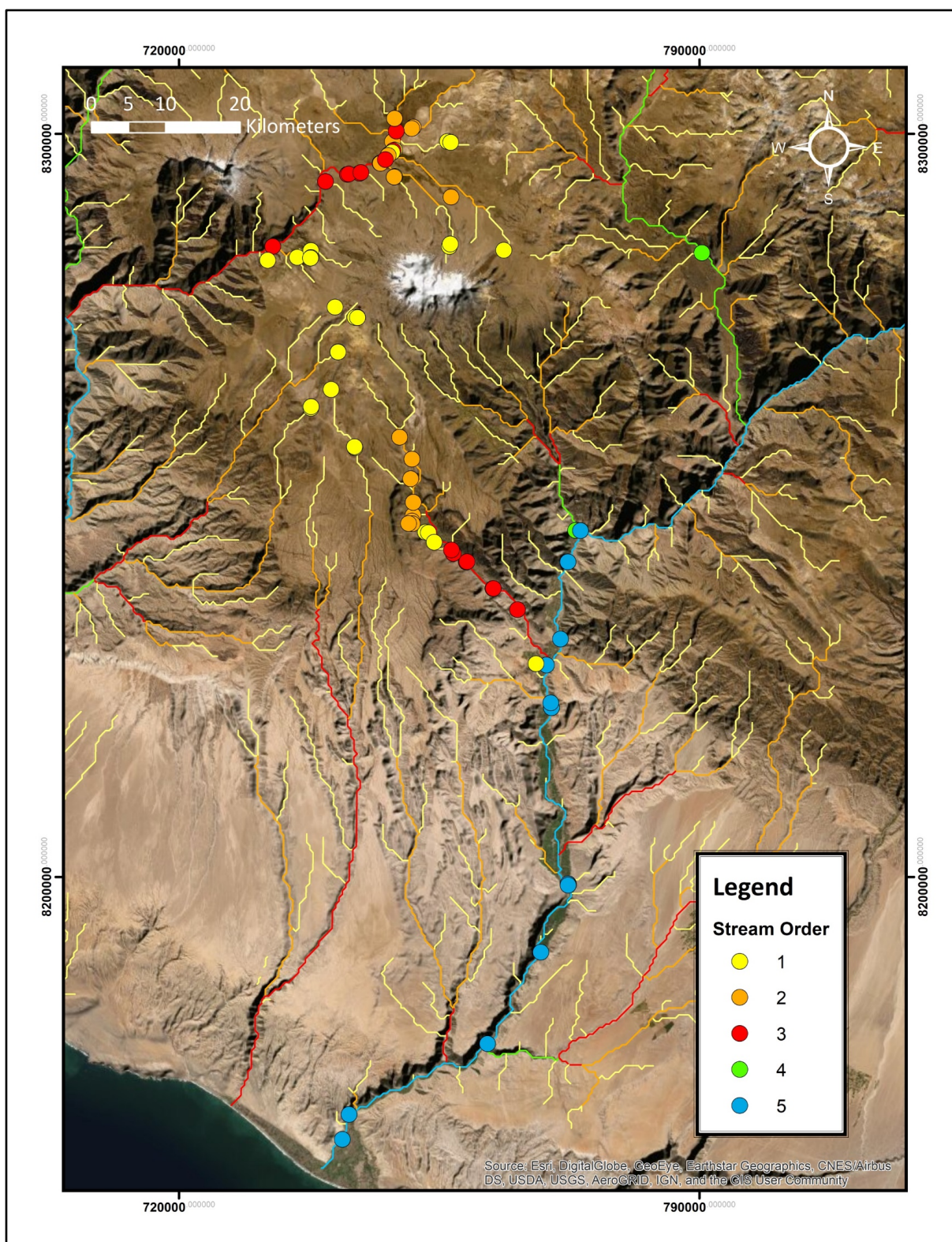


Figure 41: Map showing stream order for sampling locations.

4.3.4.1 Jaguay Surface Waters

All samples from the Jaguay watershed reflect first order streams. First order streams in the Jaguay drainage basin are more depleted than first order streams in the Ocoña watershed.

4.3.4.2 Majes Surface Waters

Majes samples encompass all five stream orders. Between 2000 to 4000 meters, first- and second-degree stream orders indicate higher $\delta^{18}\text{O}$ values in surface waters as elevation decreases, supporting published expectations. Stream orders 3-5 represent all sampled locations below 2000 meters elevation. Contrasting the 2000-4000 elevation range, $\delta^{18}\text{O}$ values of surface waters below 2000 meters reverse direction and indicate more depleted values. The lowest $\delta^{18}\text{O}$ values in the Majes drainage occur below 1000 meters elevation. Almost all represent a fifth order stream, the Río Majes, or its associated canals. The single exception the Quebrada de Castillo Canal. I estimated the source waters of the canal based on its map location. It is possible Quebrada de Castillo represents a misclassification and carries waters diverted from the Majes.

Stream order data help explain the low value from the outlier WS1815 (-16.70‰). WS1815 was derived from the Río Andagua, a fourth-order stream that becomes a fifth-order stream at the Río Colca (-17.10‰) before turning into the Río Majes (-16.55‰). The trajectory of $\delta^{18}\text{O}$ values from the Andagua to the Majes demonstrate the transportation of highland waters and highland isotopic values from the interior Andes to the coast.

4.3.4.3 Ocoña Surface Waters

Waters in the Ocoña represent first to third order streams, and both natural and canal waters. The plot indicate that first order streams demonstrate the highest $\delta^{18}\text{O}$ values, $\delta^{18}\text{O}$ is lower in second order streams than first order streams, and third order streams are lowest overall. First and second order streams feed into the Río Arma (order =3). WS1962, the Río Arma at Salamanca (3221 masl; -17.11‰), is a third order stream below the plateau. The Río Arma carries perennial highland waters to the Río Ocoña before discharging to the Pacific Ocean. Like WS1815 in the Majes, this sample likely reflects the general composition of waters transported from high elevation zones to the coast.

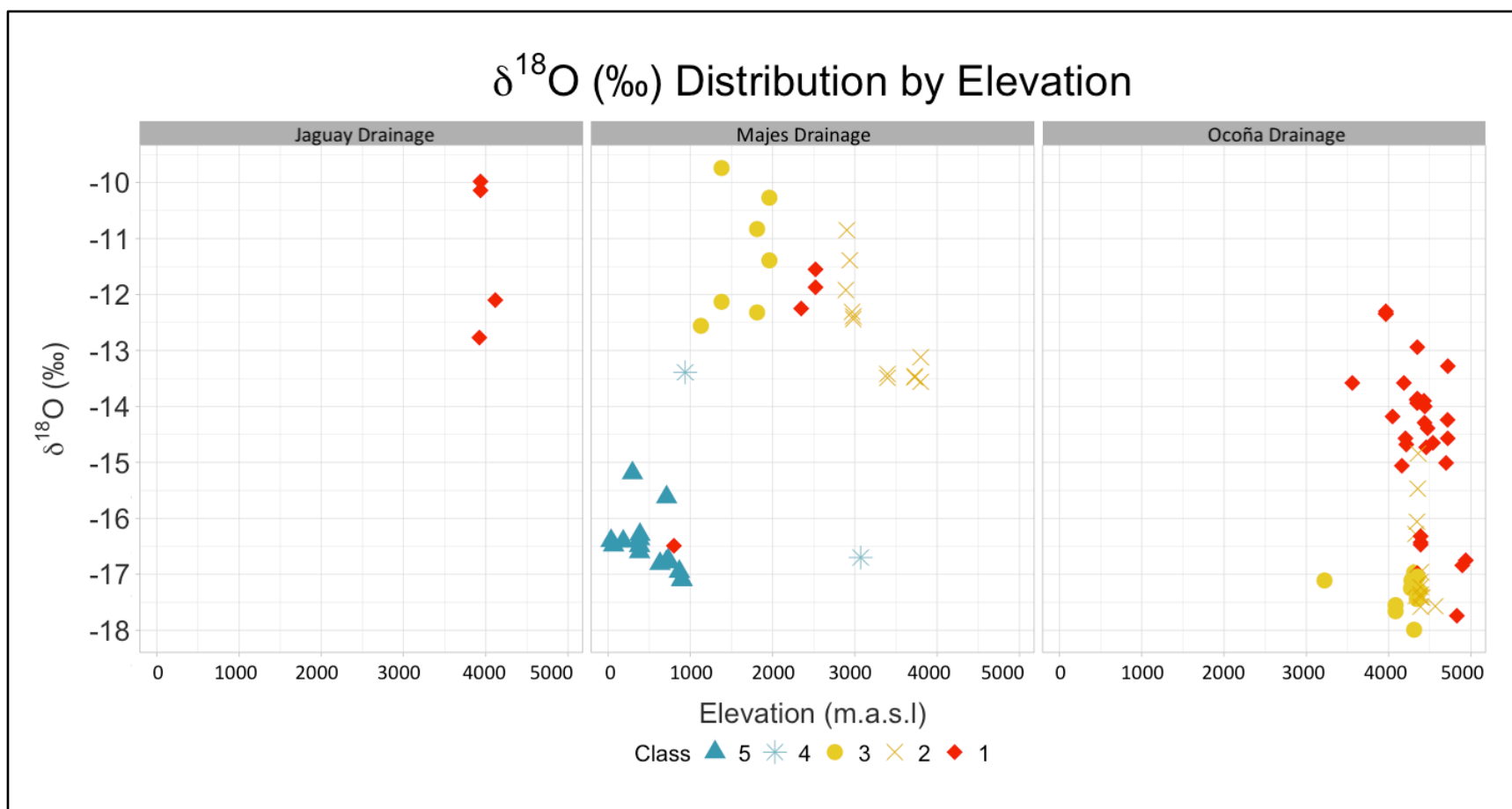


Figure 42: Stream order $\delta^{18}\text{O}$ values for the Jaguay, Majes and Ocoña watersheds.

4.3.5 Range of $\delta^{18}\text{O}$ Across Elevations Throughout the Central Andes

As drainages were not sampled equally across elevations, I compare these data to surface water samples (n=241) published for the Central Andean region by Bershaw et al. (2016). The $\delta^{18}\text{O}$ data collected by Bershaw et al. (2016) represent various latitudes between 13 to 20°S and elevations between 27 to 4762 masl (Figure 43). All samples were collected between May and June, dry season waters. At 15°S, my study area falls in the center of Bershaw et al.'s study area. Some sample locations were replicated between studies. I removed one value from Bershaw et al. (279511-05: value = 5.6‰) as an outlier to the dataset. This sample likely reflects very enriched waters from a sitting waterbody that is not representative of the surface waters considered in my own data. A summary of the retained data is presented in Table 14.

Table 14: Summary of Data from Bershaw et al. 2016.

Number of Samples (n=)	Minimum Elevation (masl)	Maximum Elevation (masl)	Minimum $\delta^{18}\text{O}$ (VSMOW)	Maximum $\delta^{18}\text{O}$ (VSMOW)	Mean $\delta^{18}\text{O}$ (VSMOW)
241	27	4762	-19.60	-2.90	-14.68

The surface waters sampled for this study are plotted with those from by Bershaw in a regression for $\delta^{18}\text{O}$ and δD with the Global Meteoric Water Line (Figure 44). The plot suggests the waters collected by Bershaw et al. include more evaporated waters than those presented in this thesis.

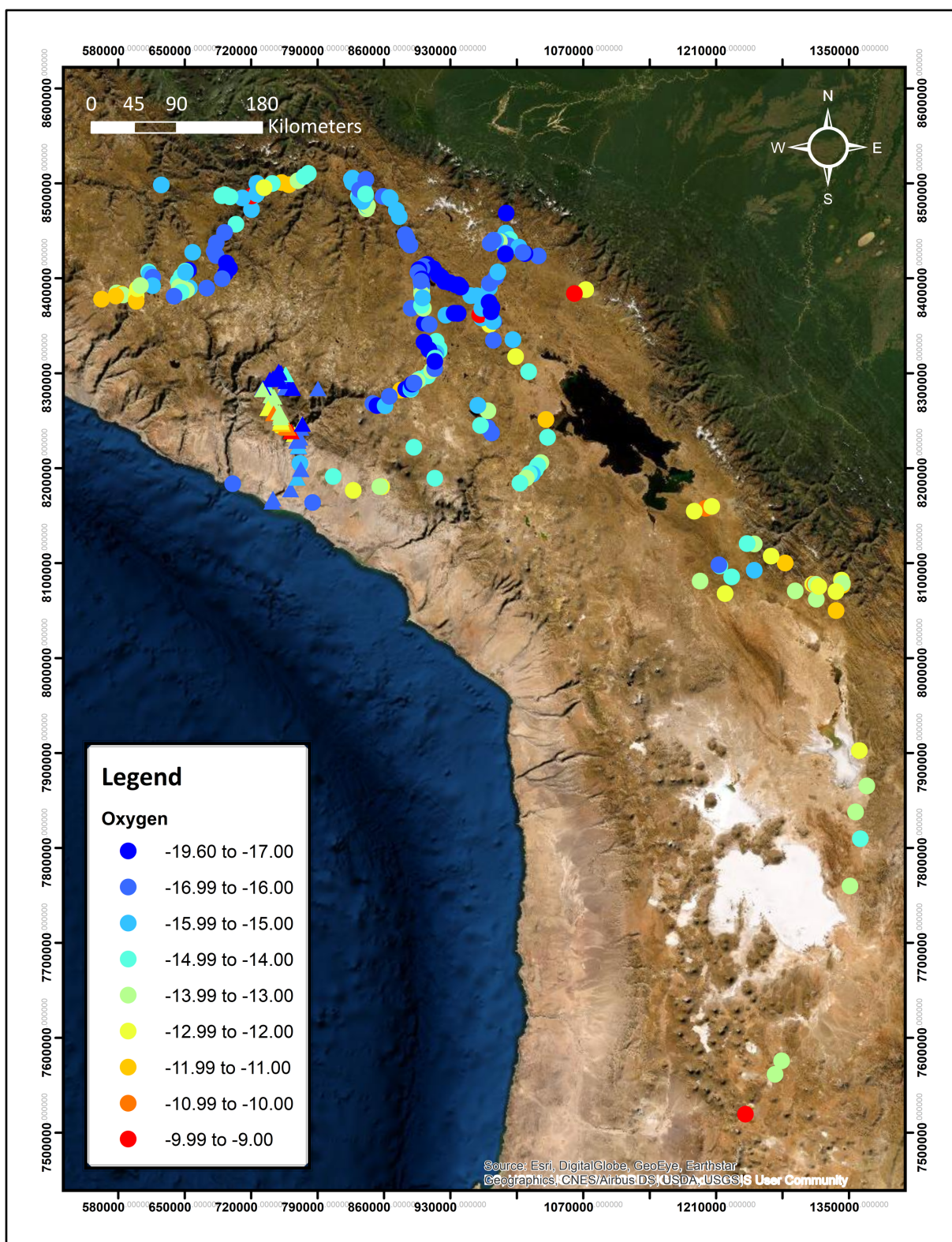


Figure 43: Map of Bershaw et al. 2016 (circles) and Milton 2018-2019 (triangles) water sample locations. $\delta^{18}\text{O}$ values scaled to be consistent across both datasets.

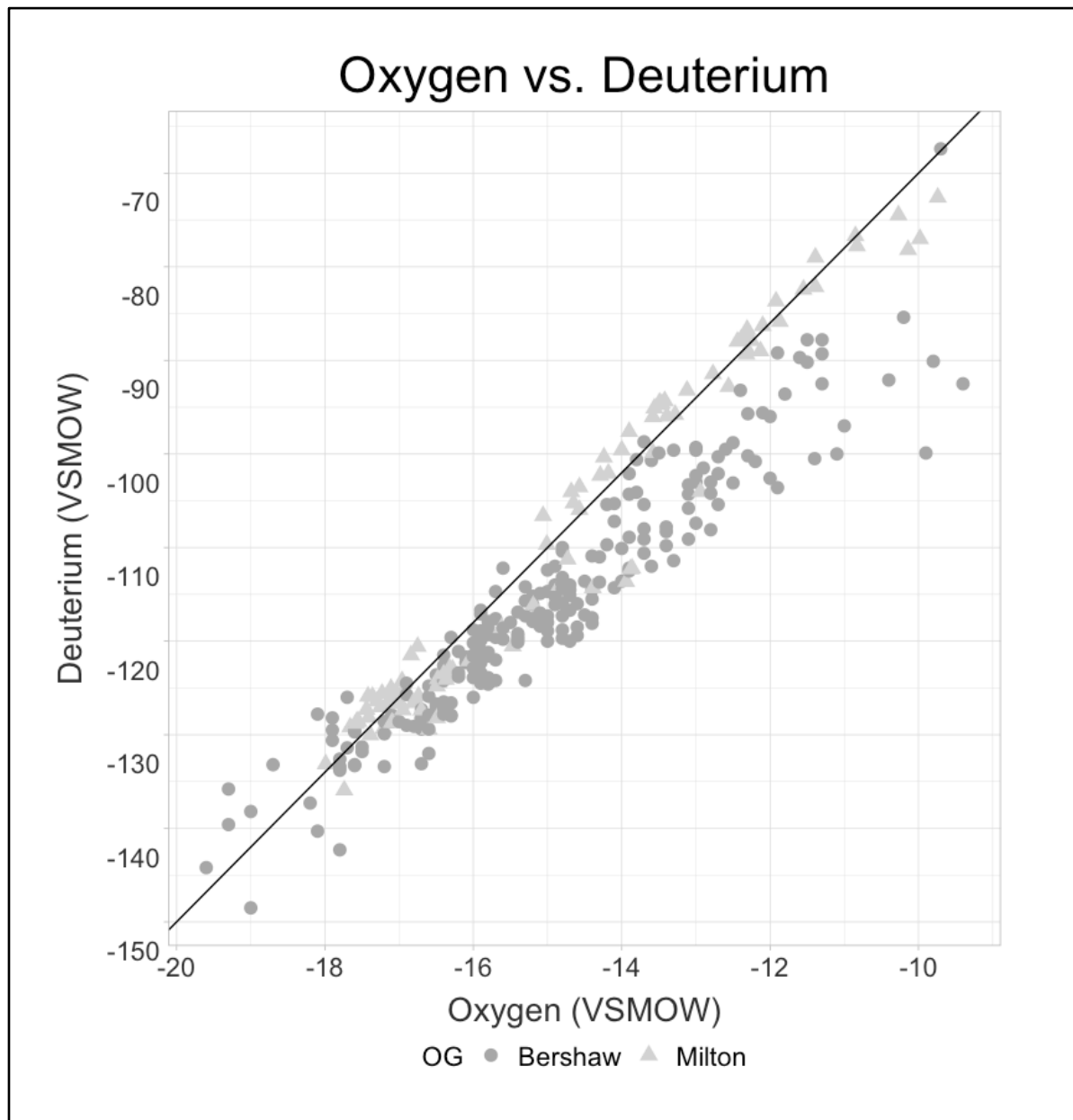


Figure 44: Bershaw et al. 2016 (dark grey circles) and Milton's 2018-2019 (light grey triangles) surface water samples plotted in a regression of $\delta^{18}\text{O}$ and δD . The solid black line is the Global Meteoric Water Line (GMWL) $\delta\text{D} = 8(\delta^{18}\text{O}) + 10\text{‰}$.

Figure 45 presents the distribution of $\delta^{18}\text{O}$ values across all sampled elevations for both datasets. The data from Bershaw et al. 2016 range from -2.90 to -19.60‰. The interquartile range of Q1 -16.30 to Q3 -13.60‰ overlaps with the interquartile range of the 98 surface water

samples presented here (-16.92 to -13.16‰). The range of stable oxygen in surface waters presented in this thesis is indistinguishable with surface water values from the surrounding Central Andes.

A sample collected by Bershaw et al. (2016) from the Ocoña river at 27 masl provides a low elevation value for the Ocoña watershed. The value is -16.40‰. Assuming stability in surface waters over multiple years (supported by Section 4.2), the Ocoña drainage shows less than a 1‰ increase in $\delta^{18}\text{O}$ between the 3221 masl sampled presented here (-17.11‰) and the coastal sample published by Bershaw et al. 2016. This example suggests that a “watershed effect” drives a lowland-highland overlap in $\delta^{18}\text{O}$ surface waters for large drainages in the western Central Andes.

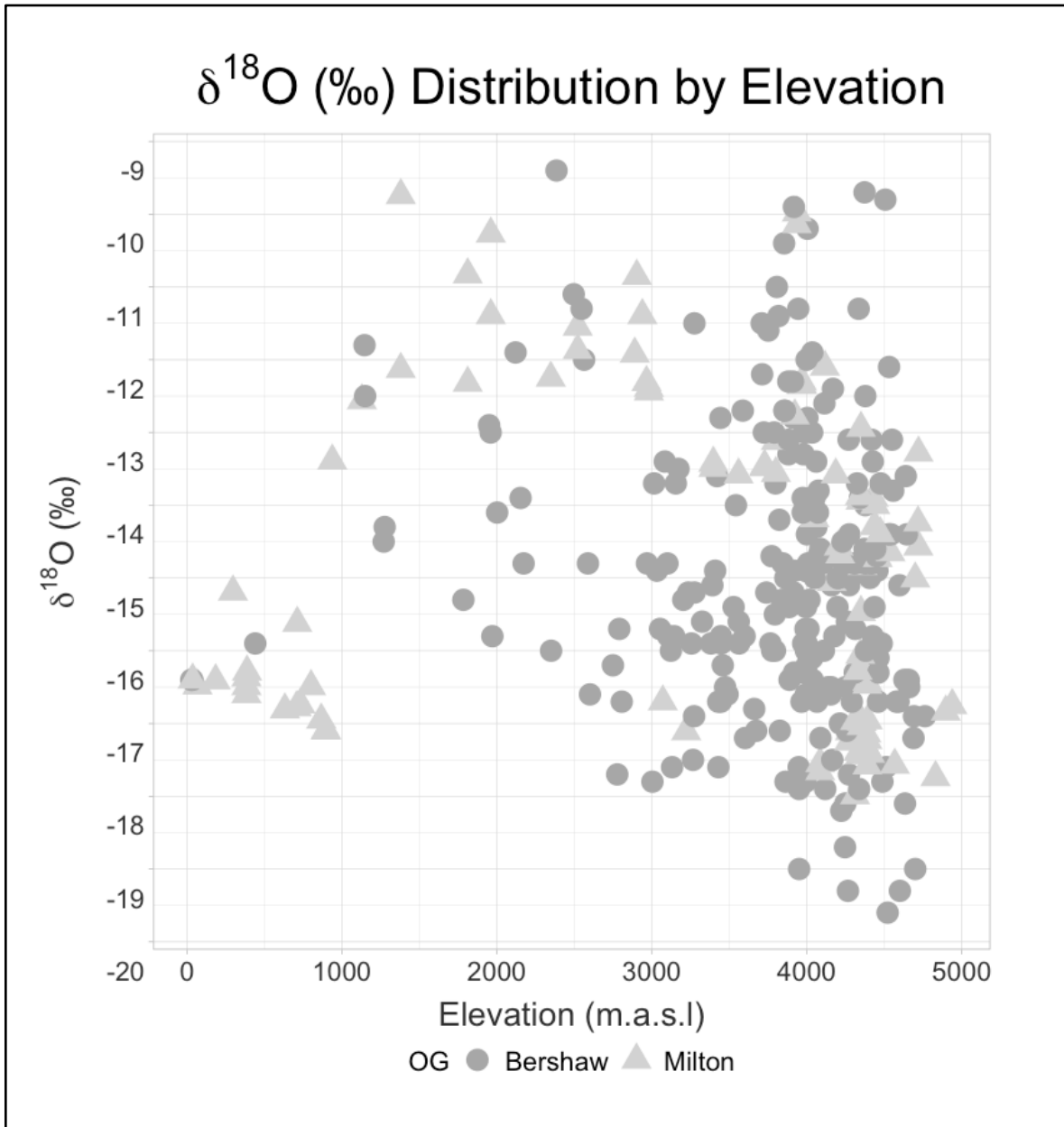


Figure 45: The elevation distribution of δ¹⁸O in surface waters for both Bershaw et al. 2016 (dark grey circles) and Milton 2018-2019 (light grey triangles) data.

4.4 δ¹⁸O for Archaeological Human Provenance Research

To situate the dataset within Andean archaeological literature of mobility research, the samples were divided into a series of “place” classifications. These trial explorations help determine whether oxygen isotopes are suited to identifying the migration history of an

individual based on the isotopic signals in their biological remains. I consider multiple geologic variables to identify underlying processes influencing the $\delta^{18}\text{O}$ in regional surface waters.

Second, I consider two arbitrarily defined “zones” of human residence. These zones refer to published archaeological studies: the Andean Plateau (Haas et al. 2017) and an abbreviated version of Pulgar Vidal’s (1987) ecological zones originally proposed by Knudson (2009) and later revised by Scaffidi and Knudson (2020); Scaffidi et al. (2020).

4.4.1 Waters On and Off the Plateau

For the first model, the study area was divided into plateau/non-plateau values. Because the Andean Plateau occurs at high-to extreme elevations, any tenured stay above the plateau rim reflects efficient acclimatization, or developmental or genetic adaptation. Samples were inspected in the GIS and coded to reflect whether they fell on or below the plateau. Results of the on/off plateau test were plotted using a dot plot to demonstrate the total range of observed $\delta^{18}\text{O}$ values (Figure 46). Plateau waters (3727-4938 masl; n=60) range from -17.99 to -9.98‰. The mean is -15.25‰. Off plateau waters (36-3559; n=38) range from -17.11 to -9.70‰. The mean is -14.15‰. Surface water $\delta^{18}\text{O}$ values are only slightly lower on the plateau than off the plateau (<0.5‰ difference). If the Quebrada de Rata samples are not considered, all plateau waters are less than -12‰, which would suggest up to a ~2.5‰ difference between plateau and non-plateau waters.

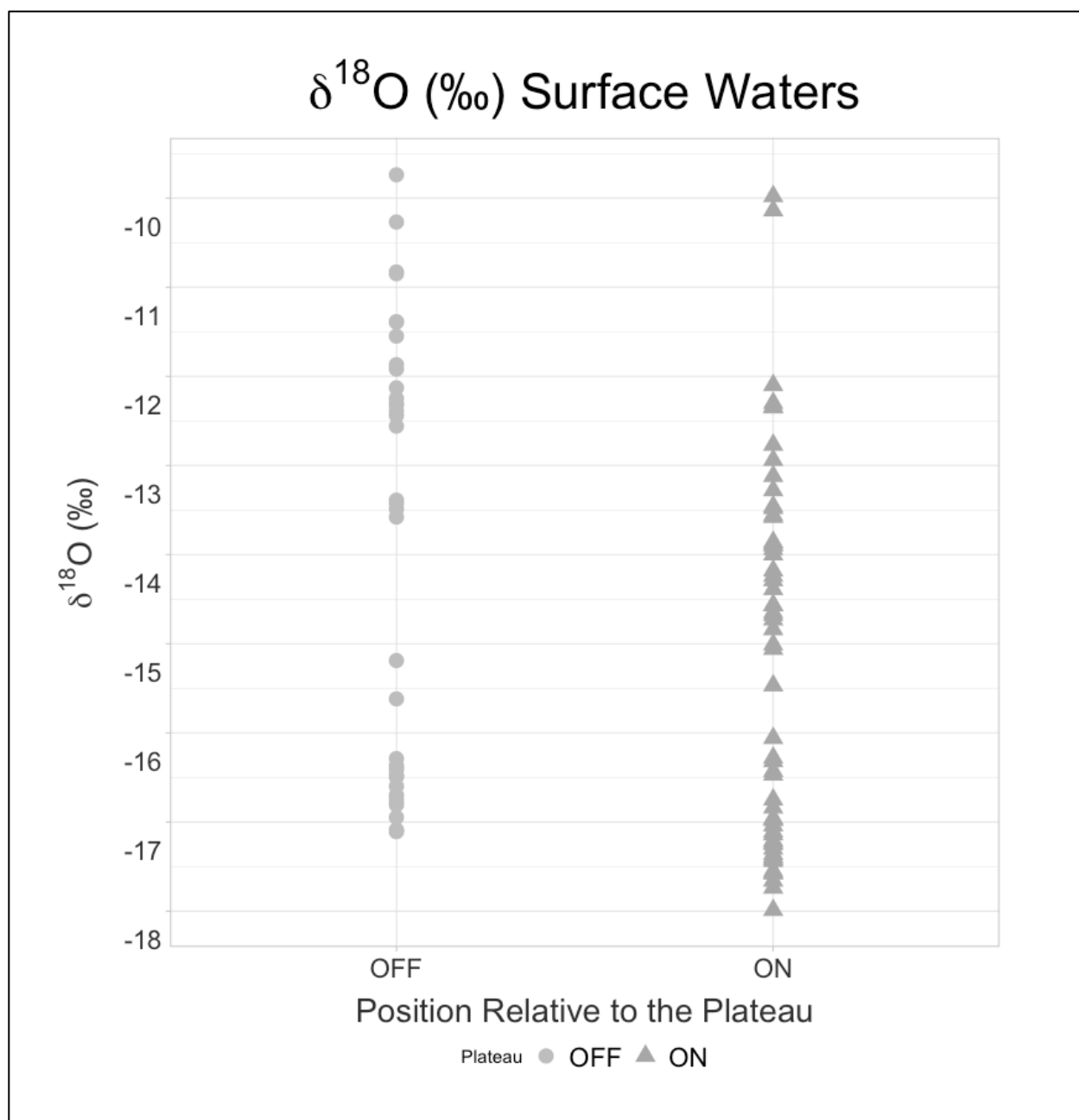


Figure 46: Plot comparing the spread of possible $\delta^{18}\text{O}$ values off (light grey circles) and on (dark grey triangles) the Andean Plateau.

4.4.2 Abbreviated Vidal Ecozones

Data were divided into an abbreviated version of Vidal's (1981) ecological zones following Scaffidi and Knudson (2020) and Scaffidi et al. (2020). The designation serves to situate these results within the broader literature of stable isotopic migration research in the

Andes, which frequently focus on the movement of humans between elevations. The three zones include a coastal zone (<500 masl), a mid-elevation terrestrial *Yunga* zone (500-2300 masl), and a high-elevation, *Highland* zone (2300+ masl). Coastal zones were expected to demonstrate the highest $\delta^{18}\text{O}$ values, and Highland waters the lowest $\delta^{18}\text{O}$ values (Knudson 2009) .

Observed $\delta^{18}\text{O}$ of surface waters do not demonstrate the predicted distributions when plotted by zones (Figure 47). The coastal zone (n=8) exhibits the most depleted $\delta^{18}\text{O}$ values. The mean coastal $\delta^{18}\text{O}$ value is -16.28‰ and the range -16.60 to -15.19 ‰. The *Yunga* zone (n=16) ranges from -17.10 to -9.74 ‰, the mean is -14.14‰. The highland zone (n=74) ranges from -17.99 to -9.98 ‰, the mean is -14.82‰ (n=74).

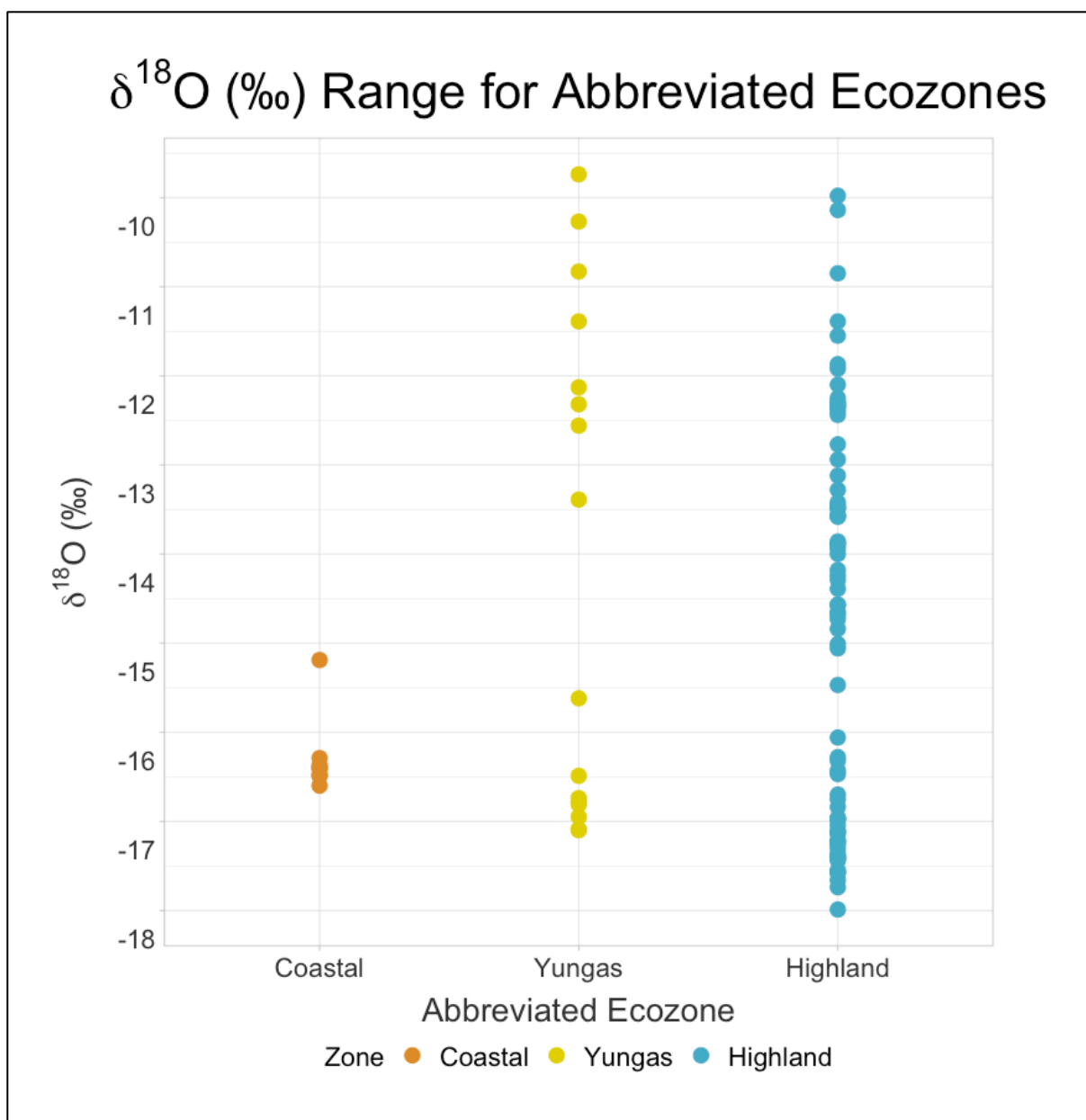


Figure 47: Dot plot of the spread of $\delta^{18}\text{O}$ values observed in the surface waters across three Central Andean ecozones. Coastal (<500 masl), Yungas (500-2500 masl), and Highland (>2500 masl).

While the coastal zone is distinct, it is completely encompassed by the range of values in both the *Yunga* and highland zones. The only distinct values from the *Yunga* zone are waters with $\delta^{18}\text{O}$ values > - 10‰. In the highlands, distinct waters include those > -17.10‰.

4.4.3 The Humans of Cuncaicha

The drinking water (DW) $\delta^{18}\text{O}$ values for the humans of Cuncaicha are presented in Table 155. The measured $\delta^{18}\text{O}_{\text{DW}}$ from the teeth of each individual is plotted against the study area surface water $\delta^{18}\text{O}$ data in Figure 48 and against the Bershaw et al. comparative $\delta^{18}\text{O}$ data in Figure 49.

Table 15: $\delta^{18}\text{O}_{\text{DW}}$, $^{87}\text{Sr}/^{86}\text{Sr}$, and $\delta^{13}\text{C}_{\text{VPDB}}$ values from the humans of Cuncaicha.

Individual AS #	Age 14C BP	Age Cal BP	Tübingen Lab Specimen ID	Period	$\delta^{18}\text{O}_{\text{DW}}$ (VSMOW)	$^{87}\text{Sr}/^{86}\text{Sr}$	$\delta^{13}\text{C}$ (VPDB)
15-04	3107±20	3361-3182	CUND 16	Late Holocene	-16.40	0.706607	-14.45
15-03	3836±21	4287-4085	CUND 19	Late Holocene	-15.54	NA	-12.17
15-06	7689±22	8536-8386	CUND 20	Early Holocene	-13.51	0.706433	-13.00
15-05	7999±31	8986-8691	CUND 17	Early Holocene	-14.04	0.706437	-12.60
15-07	8136±32	9133-8788	CUND 18	Early Holocene	-15.25	0.706427	-12.44

Figure 48, which plots samples collected from the study area, suggests the $\delta^{18}\text{O}_{\text{dw}}$ derived from the enamel carbonates of individuals 15-03, 15-04, 15-06, and 15-07 overlaps $\delta^{18}\text{O}_{\text{sw}}$ values observed below 1000 masl and above 4000 masl. 15-05 only intersects values observed above 4000 masl from this dataset. The $\delta^{18}\text{O}_{\text{DW}}$ value from individual 15-04 (-16.40‰) also crosses the Río Andagua sample from 3070 masl.

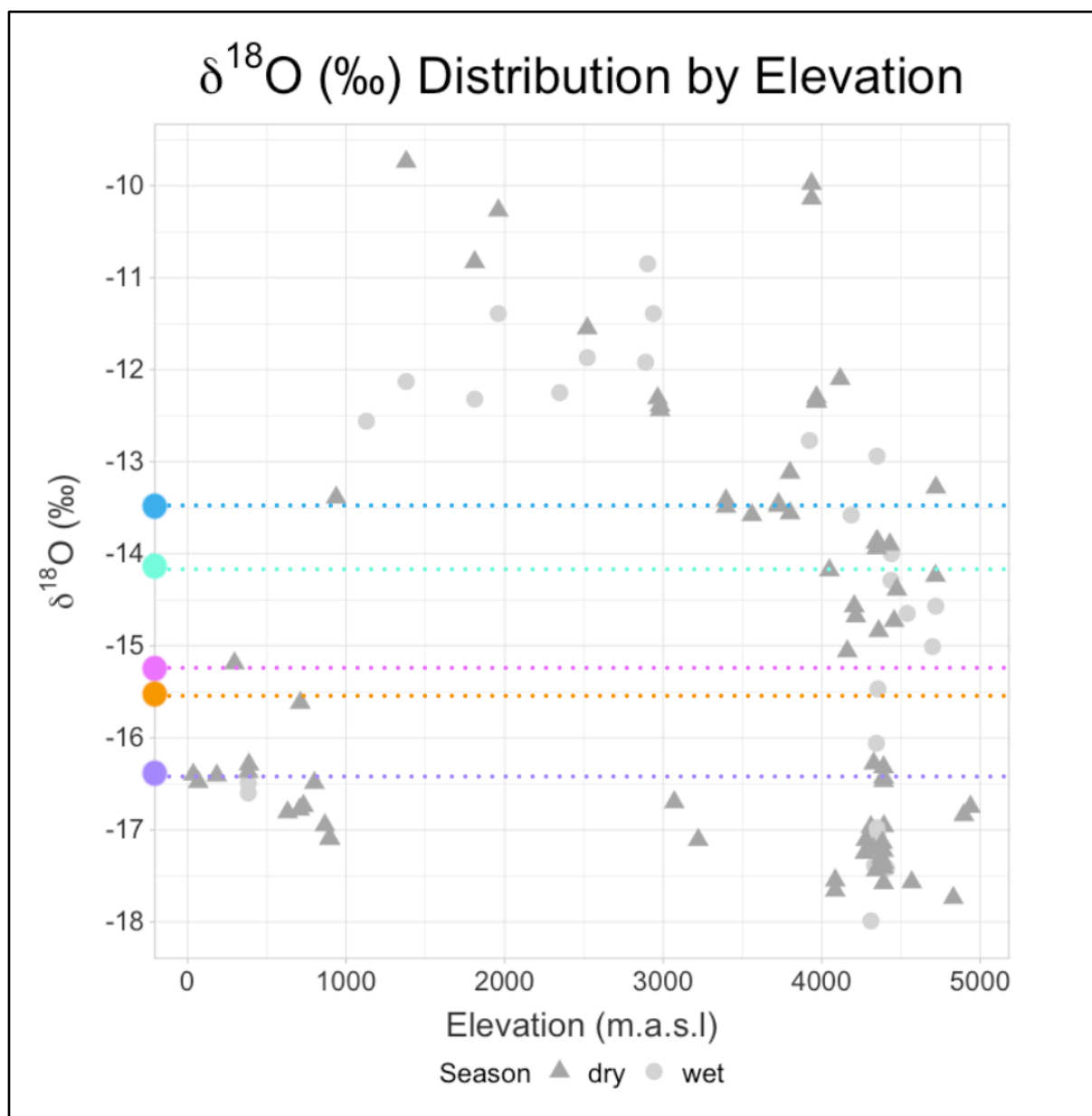


Figure 48: $\delta^{18}\text{O}_{\text{DW}}$ values for the five humans of Cuncaicha plotted against surface water values from the study area.

Figure 49, which includes Bershaw's et al.'s samples, demonstrates that all Cuncaicha individuals' $\delta^{18}\text{O}_{\text{DW}}$ values may be consistent with lower elevation $\delta^{18}\text{O}$ surface water values observed throughout the Central Andes region. Individuals 15-03, 15-04, and 15-07 have $\delta^{18}\text{O}_{\text{DW}}$ values that are found within the entire 5000 masl range. The $\delta^{18}\text{O}_{\text{DW}}$ from individuals

15-05 and 15-06 are consistent with surface water $\delta^{18}\text{O}$ values observed at elevations between 1000 to 5000 masl.

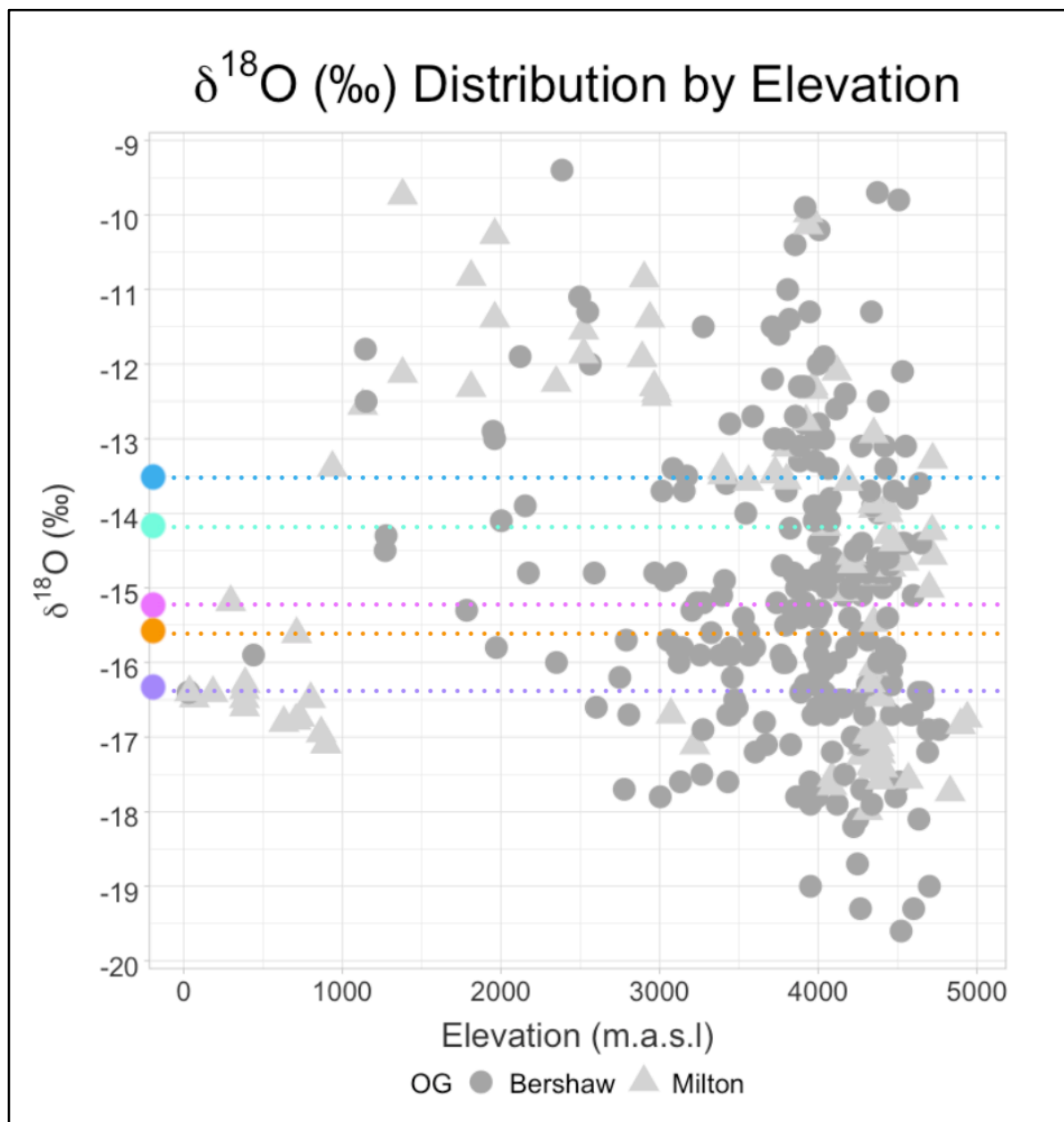


Figure 49: The $\delta^{18}\text{O}_{\text{DW}}$ for the humans of Cuncaicha plotted against the $\delta^{18}\text{O}$ values in surface waters from the Central Andes.

CHAPTER 5: DISCUSSION AND CONCLUSIONS

The goal of this work was to develop a surface water $\delta^{18}\text{O}$ baseline for the study area between three archaeological sites, Pampa Colorada 343, Quebrada Jaguay 280, and Cuncaicha rock shelter. I asked the questions: (1) does the $\delta^{18}\text{O}$ composition of surface waters in the Pucuncho Basin change seasonally? And (2) Do the surface waters between the three sites demonstrate distinct $\delta^{18}\text{O}$ values at different elevations? I discuss my results and synthesize the implications for the research objectives identified in Chapter 1. I conclude with some broader insights I encountered through this research.

5.1 General Comments

The instrumental precision for all measurements was good, so all 98 samples were retained for the analysis. The local surface water lines for both the wet and dry season in the sampling area are consistent with both the regional meteoric water line as well as the global meteoric water line, indicating that the $\delta^{18}\text{O}$ composition of surface waters in the Andes follow predicted isotopic behavior of other regions (Figure 21). The data collected for this study represent the first seasonal dataset measuring the degree of $\delta^{18}\text{O}$ change for surface waters in the study area. These data also represent the first set of inter-annual data published for the area. Without a decadal record it is not possible to determine whether there are long-term trends or shifts in the surface water values in the study area.

5.2 Seasonal $\delta^{18}\text{O}$ Variation in Regional Surface Waters

In the research area, the greatest degree of temporal variation for $\delta^{18}\text{O}$ was observed for seasonal samples (mean change: 1.21 per mil). The next greatest change was observed at

the annual scale (mean change: 0.22 per mil). Daily surface water change provided the smallest difference between samples (mean change: 0.10 per mil).

Seasonal change varied among water bodies in the study area. The sample size was too small to determine the underlying processes contributing to this variation. However, it is likely that groundwater contributes an important factor. Streams primarily fed by groundwater may be less sensitive to, or attenuate, $\delta^{18}\text{O}$ arriving through seasonal precipitation. Comparisons for daily, seasonal, and annual change at a single location suggest that the volume of the water body (stream order) may also be an important driver of temporal change in $\delta^{18}\text{O}$ at an isolated water source. If this is the case, it is likely because lower volume streams, or shallower water bodies, are more sensitive to evaporative processes and therefore reflect atmospheric seasonality more readily.

It is important to note that some water bodies do not reliably record a degree of seasonal change that is greater than the observed daily or annual change. For example, the Río Majes demonstrated a 0.23‰ shift between the 2019 wet and dry seasons but recorded a 0.34‰ change between the dry seasons of 2015 and 2019. It is fair to note that neither the seasonal nor annual change registered in the Río Majes are considered significant; further as a low-elevation river, the Río Majes would not inform on a seasonal highland proxy.

Figure 28 and Figure 32 show that two locations, the Río Majes at 383 masl (SEAS-01/Pair 9) and the Río Colunga at 4333 masl (SEAS-08/Pair 16), demonstrate less change between seasons than the baseline for daily change observed regionally. The Majes is a 5th order stream and Río Colunga a 2nd order, suggesting stream order may not be the underlying control for seasonal shift in surface water $\delta^{18}\text{O}$.

Three more seasonal pairs, Iray canal at 2521 masl (SEAS-05/Pair 13), Quebrada Japuchaca at 4435 masl (SEAS-10/Pair 18), and Quebrada Pucunchitoyocc at 4717 masl (SEAS-11/Pair 19), demonstrate less change between seasons than that observed interannually. All three are first order streams, which might suggest that smaller order streams are less sensitive to seasonal precipitation; however, the greatest magnitude of seasonal change is also observed in first order streams. For example, Quebrada de Rata (SEAS-06/Pair 14) provided the largest difference in $\delta^{18}\text{O}$ values between seasons. The Quebrada de Rata represents the only surface water location sampled seasonally in the Jaguay watershed. The Jaguay drainage does not extend into the central plateau but is perched at the western edge of the Andes. For this study, it is the watershed farthest from the incoming precipitation source. A tentative explanation may be that the Jaguay watershed has a smaller catchment that receives less seasonal precipitation and is therefore more sensitive to evaporative processes during the dry season, as reflected by the degree of seasonal change captured by the Quebrada de Rata. Catchment size and groundwater availability will constitute an important variable to consider in future studies.

The data provided here do not help predict which water bodies should demonstrate seasonal change, beyond the conclusion that higher order streams may be less sensitive than smaller order streams. Further testing should provide greater insight into regional seasonal change.

5.2.1 Prospectus for a Seasonal Proxy

A seasonal proxy utilizing $\delta^{18}\text{O}$ will face a number of challenges for the following reasons:

1. While seasonal variation does appear to be measurable in regional surface waters, the magnitude of $\delta^{18}\text{O}$ change is not consistent throughout the area. Not all surface waters

demonstrate a seasonal change that is greater than routine temporal (daily/annual) change.

2. Considering all locations sampled in the Pucuncho Basin, the total range of natural variability in $\delta^{18}\text{O}$ of surface waters encompasses the seasonal change observed in $\delta^{18}\text{O}$. For example, values between -16.98 and -13.94‰ $\delta^{18}\text{O}$ were observed for the Río Cuncaicha between the wet and dry seasons of 2019 (a 3.04‰ shift); other water bodies throughout the Pucuncho Basin annually (wet and dry season considered together) demonstrate a range in $\delta^{18}\text{O}$ values between -17.74 to -9.74‰. The 8‰ difference observed between water bodies across the plateau may obscure seasonal variation observed within a single water body in the high-elevation study area. Considering that vicuñas migrate (where a shell or speleothem does not), any further proxy development will also need to contend with the variation observed across a range of multiple water bodies.

It may be possible to control for the drinking source using another isotope and careful observational studies of animal behavior. Incremental strontium may provide an approach to translate these findings to archaeological material. For now, I recommend a second isotope, $\delta^{13}\text{C}$, to help isolate a seasonal signal in the Pucuncho Basin.

5.3 Spatial $\delta^{18}\text{O}$ Variation in the Central Andes

The elevation plots in Section 4.3 indicate that the $\delta^{18}\text{O}$ values of surface waters in the study area record limited change between low and high elevations (Figure 36, Figure 37, Figure 39, and Figure 42). Results indicate the primary predictors for $\delta^{18}\text{O}$ in surface waters include the positioning and size of a targeted watershed, and the stream order transporting water. The

overlapping highland and lowland $\delta^{18}\text{O}$ values are a genuine phenomenon driven by hydrogeological processes. WS1815 (Río Andagua, 3070 masl) and WS 1962 (Río Arma, 3221 masl), as well as the Río Ocoña value derived from Bershaw et al. (2016), suggest that the overlapping $\delta^{18}\text{O}$ values in highland and lowland values is likely a consistent phenomenon among higher order streams in the western Andes. Higher volumes of water likely move through elevation zones between the highlands and the coast more rapidly, providing little time for evaporative processes to affect the composition of surface waters. This creates a “watershed effect” where coastal values reflect $\delta^{18}\text{O}$ values of interior waters. This finding supports the hypothesis that high-volume lowland waterways preserve highland isotopic signatures, as originally proposed by Knudson (2009). Smaller bodies of water appear to express a greater range of variation than larger bodies of water within this dataset. The mean $\delta^{18}\text{O}$ of surface waters decreases with increasing stream order.

In summary higher order streams carry more depleted waters, likely reflecting rapid transport of depleted highland waters from the east; this, in turn, leads to overlapping $\delta^{18}\text{O}$ for surface waters at different elevations and latitudes in the western Andes. It remains unknown whether $\delta^{18}\text{O}$ in surface waters demonstrate a similar signal throughout all latitudes and longitudes of the Central Andes. However, it is highly likely that all rivers on the western (rain shadow) side follow this pattern, due to the homogeneity of the topography on the west-central edge of the continent. The data from Bershaw et al. 2016 suggests this to be so. More intensive sampling to the north and south of the research area should reveal the degree of overlap in $\delta^{18}\text{O}$ of surface waters in the area.

5.3.1 Reconciling the Watershed Effect and Archaeological Aims

In the course of my writing, Scaffidi (and Knudson 2020a; et al. 2020b) published two extensive radiogenic strontium isoscapes using archaeological materials and modern surface water samples. They conclude that while strontium isoscapes appear promising, they are complicated by the lack of distinct bedrock geology in the Central Andes. The results presented within this study suggest a similar story for oxygen isotopes: the patterning of $\delta^{18}\text{O}$ in surface waters between the highlands and the coast, or even between drainages, is difficult to resolve. Knudson (2009) discussed the challenges of $\delta^{18}\text{O}$ for Andean archaeological sites, in terms of archaeological $\delta^{18}\text{O}$ data. She states:

In conclusion, oxygen isotope data from archaeological enamel and bone hydroxyapatite carbonate demonstrate that the variability within each site, even among individuals identified as local based on strontium isotope signatures, is greater than the variability between sites located in different environmental zones. While some regional trends are apparent, it would be inappropriate to attempt to identify the environmental zone in which an individual lived based on her or his oxygen isotope signature alone. However, continuing to explore and better understand the complexities of oxygen isotope analyses in the Andes, and beyond, through detailed studies of drinking water sources and their isotopic signatures will better enable scholars to use oxygen isotope data to identify archaeological residential mobility. (185)

In this thesis I have provided evidence to suggest that the complexities of $\delta^{18}\text{O}$ extend to drinking water sources. This leads me to suggest reinterpretations of previous studies that have employed $\delta^{18}\text{O}$ to support arguments of residential mobility or provenance in the Andes. In Sections 1.2.1 and 4.4 I presented three examples of how stable isotopes have been used for archaeological research. Haas et al. (2017) and Haas et al. (2020) used the $\delta^{18}\text{O}$ of bone apatite from multiple Early to Middle Holocene humans to argue for permanent occupation of the Andean Plateau by 9,000 to 7,000 years ago. Similarly, Chala-Aldana et al. (2018) have stated

that the $\delta^{18}\text{O}_{\text{DW}}$ values derived from the tooth enamel of the Cuncaicha humans are consistent with high-elevation waters. The data presented herein suggest that while lower $\delta^{18}\text{O}$ values are observed in the highlands, they are also observable at intermediate and low elevations, including the coast. The data I collected overlap a study area first established by Chala-Aldana (2017). Therefore, I offer a reevaluation of the Cuncaicha human $\delta^{18}\text{O}_{\text{DW}}$ data. All five individuals provided $\delta^{18}\text{O}_{\text{DW}}$ values consistent with high elevation—*and low elevation*—waters. $\delta^{18}\text{O}$ cannot independently resolve whether the individuals from Cuncaicha lived at the coast or in the Andes. The same is likely true for Haas et al. 2017 and Haas et al. 2020, and all other migration studies employing $\delta^{18}\text{O}$ in the Central Andes. It would be worthwhile to test the local waters surrounding these sites directly.

The locality of faunal and lithic materials found with the humans of Cuncaicha, in concert with their final interment location, makes it reasonable that all five individuals did indeed spend time at high elevations. However, such a conclusion is not, at this time, justifiable on the basis of $\delta^{18}\text{O}_{\text{DW}}$ values alone. Archaeological analyses and refined local isotopic baselines promise a valuable, interdisciplinary means of resolving this question. For Cuncaicha, five other isotopic measurements may provide the answer. The dietary isotopes of $\delta^{13}\text{C}$, $\delta^{15}\text{N}$, $\delta^{34}\text{S}$ measured on bone collagen provided results that are consistent with expected high-elevation data (Haller von Hallerstein 2018). By testing these isotopes in the environment, we may show that a strong elevation signal occurs with these isotopes. For example, sulfur and strontium isotopes potentially demonstrate “sea spray effects,” that result in distinct lowland isotopic signatures (Nehlich 2015). The absence of such a signal in the Cuncaicha human collagen could

support the statement that any or all of these individuals remained above the Pacific fog or *garúa* zone (~0-1000 masl).

There are two more productive lines of inquiry. First, it will be worthwhile to reexamine the existing $^{87}\text{Sr}/^{86}\text{Sr}$ measurements from the Cuncaicha human enamel considering the larger datasets recently developed by Scaffidi (and Knudson 2020a; et al. 2020b).

Second, while already published, the $\delta^{13}\text{C}_{\text{VPDB}}$ from the Cuncaicha human enamel carbonates have not been formally considered. Dufour et al. (2014) provide data to suggest that $\delta^{13}\text{C}$ may be a secure indicator of high elevation use. Haas et al. (2017) and Haas et al. (2020) provided the $\delta^{13}\text{C}$ values of bone apatite as a secondary measure of highland occupation; though they note that preservation of their burials is challenging and apatite is susceptible to chemical alterations distinct from collagen (Bocherens et al. 2011; Lee-Thorp and van der Merwe 1991; Lee-Thorp and Sponheimer 2003). In the case of all concerned studies, Szpak et al. (2013) have recommended that $\delta^{13}\text{C}$ should be measured locally for Andean environments. The next phase of archaeological inquiry into high-elevation residence should attempt to develop multi-isotopic and multi-source (environmental and archaeological) baseline. I consider this further through the next section.

5.4 Isotopic Methods

5.4.1 The Baseline: Isotopes Through Time, Across Space

The results presented in this work renew attention for the assumptions underpinning archaeological applications of isotopic methods. In the last few years, a number of *isoscapes* have been established for archaeological research (Bataille et al. 2018; Bowen 2010; Scaffidi

and Knudson 2020; Scaffidi et al. 2020; Widga et al. 2010). The general idea behind the isoscape is to interpolate isotopic values across a landscape to create a map containing distinct isotopic zones (Bowen 2010). I acknowledge that the term *isoscape* has a particular connotation in isotopic research. While all isoscapes can serve as baselines, not all isotopic baselines make an isoscape. The benefits of applying the isoscape are apparent: they provide a clear map for “sourcing” humans or objects based on their isotopic values.

The data provided in this thesis reveal an important question for stable isotopic baselines: does averaging isotopic values across space tell us more than working with individual values? The baseline I have presented shows the exact $\delta^{18}\text{O}$ value of surface waters in the study area, as they were observed in 2015, 2018, and 2019. These data provide an important insight for baselines: local variation in $\delta^{18}\text{O}$ parallels and perhaps even exceeds regional variation.

Humans and their animal companions may spend days, months, or years within a single “interpolated area” of an isoscape, contacting multiple water sources and ingesting any range of values from the landscape. The actual water sources utilized cannot be known; therefore, it is safe to assume that any average possible, given the total range of values is an area, could be revealed when sampling a human’s biological tissue. This is to say: archaeological research considering pedestrian migration (pre horse, car, plane, or boat) must consider the spatial resolution of all *possible* values in a given landscape. It is all values within the *range* of observed variation on a landscape that matters, not the *mean*. I would revise this statement in the case of an isotope that does show distinct values between elevation zones—should that be shown convincingly.

I would submit that anthropological research concerning Andean populations, pre-dating motorized transport, should use caution when applying overly simplified or interpolated models. Rather, true variation baselines, that map the total range of variation within a region, will provide the most realistic data for understanding the explicit limitations or potentials of a given isotope for archaeology.

5.4.2 Consider the Dentist: Microdrills and Teeth

Tailing the isoscape, I briefly discuss the methods used to sample $\delta^{18}\text{O}$ from preserved tissue. To my knowledge, all three provenance studies cited within utilized a 'bulk' sampling approach, where a single sample of the tissue substrate was collected using a micro mill. Such approaches produce a single value, and in the process average months to years of time. Research questions seeking to identify mobility and seasonality must consider the temporal resolution of the values derived from the target record (tooth or bone). Much like an isoscape, microdrilling potentially masks important variation over time and across space. High resolution methods, such as Laser Ablation and SIMS, may provide a means to resolve where humans were going at the actual temporal scale being investigated (Blumenthal et al. 2016). At present, these methods require significant developments, such as accurate standards that reflect biological materials (Dr. John Valley, personal communication).

5.5 Next Steps

5.5.1 Seasonality Research

This research confirmed the presence of a seasonally driven signal in the $\delta^{18}\text{O}$ of Andean surface waters. The next phase of investigation requires controlling for the water body that

provides the signal. Seasonal stable oxygen research necessitates broader spatial and ecological considerations. Tests should target a wide range of waters to reflect a more diverse set of stream orders and watersheds. I was not able to use a few of my temporal samples in this dataset, due to poor spatial resolution during post-processing. In some locations I sampled too close to another water body, which generated confusion as I went to review the exact location in the GIS. I removed these locations from the temporal dataset to minimize the potential for error. If possible, seasonal sampling locations should be discretely marked and tagged, much like site datums. This would ensure the researcher could accurately identify and replicate specific water bodies, which will be necessary to capturing the total range of complexity for seasonality in surface waters of the Andes.

Strontium isotopes may provide the high-resolution provenance marker required to isolate movement between individual water bodies in the archaeological record but as discussed in Section 5.4.2, it is essential that the isotopic sampling method does not mask distinct movements of the organism across a landscape. High resolution strontium sampling may be possible with NanoSIMS (personal communication with directors of the Arizona State University National Science Foundation SIMS Workshop, 2019).

It is important to consider that the seasonal $\delta^{18}\text{O}$ change in surface waters could be highly variable across latitudes. Multiple sites across the Andes are potential candidates for a seasonal analysis using vicuña teeth; therefore, I intend to sample more areas for surface water seasonality. For example, the Junín region (three degrees to the north) has a longer wet season than the Pucuncho Basin. The extended duration of precipitation may completely attenuate a seasonal signal in surface waters, paralleling the effect observed in higher order streams. In

contrast, sites in southern areas of Peru (Haas et al. 2017), Bolivia (Capriles et al. 2016), and northern Chile (Osorio et al. 2011), receive less precipitation and may reflect greater amplitudes in surface water seasonality, mirroring the Jaguay Watershed. Like the studies presented in this thesis, both predictions may be thrown into question through local testing, due to regional differences in hydrology.

As an interim consideration, other isotopes could (and should) be explored. Enamel carbonates comprise oxygen and carbon, therefore the latter seems a reasonable course of investigation. Serial sampling of modern camelid incisors supports this as promising route for further study (Author's personal data 2018 & 2019). Demonstrating that the $\delta^{13}\text{C}$ values in teeth reflects seasonal change (and not a separate behavioral or environmental variable) will require the same baseline work as $\delta^{18}\text{O}$. A carbon baseline should test the seasonal and spatial variation of $\delta^{13}\text{C}$ in the preferred forage of camelids. A baseline modeled after the work of Blumenthal et al. (2016) and Samec et al. (2018), would provide the necessary data to interpret the $\delta^{13}\text{C}$ captured by camelid tooth enamel.

5.5.2 Mobility Research

Human mobility research in the study area, and perhaps the Central Andes as a region, should transition to isotopes other than $\delta^{18}\text{O}$. The collection of rainwater and drink-preparation strategies by humans add to the complexity of interpreting $\delta^{18}\text{O}$ values derived from teeth, as discussed thoroughly by Knudson (2009). Past climates may also complicate the use of $\delta^{18}\text{O}$ for archaeological research as even a ~1-2 per mil shift could push the location of a surface water into a different "zone". For example, Buffen (2008) measured the $\delta^{18}\text{O}_{\text{ICE}}$ of the Coropuna ice cap and identified Terminal Pleistocene values 8-10‰ lower than present day.

These considerations, in combination with the data presented in this thesis, leads me to recommend that oxygen isotopes not be considered further for archaeological studies of human mobility and migration in this region. I instead recommend the use of targeted isotopes, such as carbon, strontium, and sulfur. As discussed, sulfur and strontium have “sea spray” signals that may be useful in determining whether humans lived near the coast or in terrestrial zones.

In all cases of provenance: more stable isotopic sampling of the environment is needed. This research demonstrates the importance of both local and regional data. Sampling strategies concerned with imbibed materials should consider any and all possible drinking/eating sources within an area and generated spatial baselines to reflect the full degree of regional variability.

As the final consideration for mobility research, I emphasize a final time: the resolution of the method matters. Archaeology has revealed again and again the highly mobile nature of the South American people over the last 13,000 years. It is important that our methods capture the time frame we are interested in.

5.6 For Posterity

As of 2020, stable isotopic research in archaeology constitutes a destructive analytical method. Destroyed materials are not preserved materials and cannot be studied by future generations, or by ourselves as better methods become available. Archaeologists must invest in constructing adequate baselines for their methods before applying destructive techniques to invaluable archaeological materials. Such an approach will ensure adequate material for the future.

5.7 Summary of Conclusions

The data presented in this thesis offer only preliminary insights into the seasonal and altitudinal patterning of stable oxygen of surface waters in the Jaguay, Majes, and Ocoña drainages; it is evident we need further testing to define the spatial and temporal constraints of isotopes in the Central Andes. I summarize the most direct take-aways from my four results sections, then discuss my final considerations.

- 1.) First, measurements of $\delta^{18}\text{O}$ in the surface waters of the study area are consistent with global meteoric waters and regional water compositions throughout the western Central Andes.
- 2.) Second, individual water bodies in the study area demonstrate higher $\delta^{18}\text{O}$ values during the dry season and lower $\delta^{18}\text{O}$ values in the wet season. Seasonal change in the study area may be unappreciable when considered at the system-scale. Determining whether stable oxygen is suited to a developing a new archaeological record of seasonality will require more systematic and widespread sampling, and probably a second isotope to isolate the signals from individual water bodies. A second isotope, such as $\delta^{13}\text{C}$, may be the most direct route of deriving a seasonal signal from an animal record. As the next phase of research for the Pucuncho Basin, I suggest incremental sampling of modern camelid teeth and a seasonal isotopic analysis of vicuña forage.
- 3.) Third, plateau and lowland surface waters both show an appreciable and overlapping range of $\delta^{18}\text{O}$. It does not appear possible to predict the $\delta^{18}\text{O}$ values of surface waters based on elevation. Rather, surface water $\delta^{18}\text{O}$ appears to reflect stream order,

catchment size, and the geographic position of a waterbody within the watershed.

Differentiating low and high elevation landscapes will require another isotope.

The data presented within do not support $\delta^{18}\text{O}$ as an efficient or effective isotope for assessing residential mobility in human remains in the Central Andes; they do, however, suggest that other information, such as paleoseasonality, may be gained from $\delta^{18}\text{O}$ analyses of faunal teeth. Carefully planned field seasons could resolve outstanding questions about landscape patterning in short time.

5.8 A Case for Interdisciplinary Science

Throughout this research I frequently found myself saying, “uh oh”. Few of my results matched my expectations or predictions. By working closely with committee members from multiple fields, I had the good fortune to encounter perspectives on isotopes not considered in most archaeological literature. Both the establishment of environmental baselines and the selection of laboratory methods merits closer attention in future stable isotopic studies conducted in the Central Andes. Accurate future assessments of migration will require multiple isotopes to resolve lateral and vertical questions of movement. I caution that any isotopic suitor in the race for a migration proxy be studied with care across a broad transect that encompasses multiple ecological and geological areas. The people of South America are known for geographically extensive social and trade networks that transect diverse and sometimes harsh environments. Researchers must be prepared to untangle the complexities of both human and natural systems in the Andes.

The material and post-processing that goes into making archaeological baselines matters. Based on my results, I advocate for archaeologists to invest in developing extensive

baselines constructed from extant materials and forgo archaeological sampling until they are sufficiently confident their approach is justified. Ancient human remains and incremental structures, like those found in vicuña teeth, are rare—and therefore invaluable. Environmental baselines offer an unprecedented opportunity for archaeologists collaborate on interdisciplinary teams and with local communities to bring about high-impact, transdisciplinary science. Water samples especially may provide data for environmental monitoring, activism, and justice. The waters collected for this study will be available to other researchers for use in other research areas. Interdisciplinary collaborations serve as a radical approach to ensuring the posterity of archaeological curation practices and the longevity and relevance of our discipline; and, based on personal experience, prevent an “uh oh” from becoming “oh no.” Something we might all applaud.

REFERENCES

REFERENCES

- Abbott, Mark B., Brent B. Wolfe, Alexander P. Wolfe, Geoffrey O. Seltzer, Ramon Aravena, Brian G. Mark, Pratigya J. Polissar, Donald T. Rodbell, Harry D. Rowe, and Mathias Vuille
2003 Holocene paleohydrology and glacial history of the central Andes using multiproxy lake sediment studies. *Palaeogeography, Palaeoclimatology, Palaeoecology* 194(1-3):123-138.
- Aldenderfer, Mark
2006 Modelling plateau peoples: the early human use of the world's high plateaux. *World Archaeology* 38(3):357-370.

2011 Peopling the Tibetan Plateau: Insights from Archaeology. *High Altitude Medicine & Biology* 12(2):141-147.
- Aldenderfer, Mark S.
1998 *Montane Foragers Asana and the South-Central Andean Archaic*. University of Iowa Press, Iowa City.
- Balasse, Marie, Stanley H. Ambrose, Andrew B. Smith, and T. Douglas Price
2002 The Seasonal Mobility Model for Prehistoric Herders in the South-western Cape of South Africa Assessed by Isotopic Analysis of Sheep Tooth Enamel. *Journal of Archaeological Science* 29(9):917-932.
- Balasse, Marie, Andrew B. Smith, Stanley H. Ambrose, and Steven R. Leigh
2003 Determining Sheep Birth Seasonality by Analysis of Tooth Enamel Oxygen Isotope Ratios: The Late Stone Age Site of Kasteelberg (South Africa). *Journal of Archaeological Science* 30(2):205-215.
- Bataille, Clement P., Isabella von Holstein, C. C., Jason E. Laffoon, Malte Willmes, Xiao-Ming Liu, and Gareth R. Davies
2018 A bioavailable strontium isoscape for Western Europe: A machine learning approach. *PLoS One* 13(5):e0197386.
- Bershaw, John, Carmala N. Garziona, Pennilyn Higgins, Bruce J. MacFadden, Frederico Anaya, and Herculano Alvarenga
2010 Spatial-temporal changes in Andean plateau climate and elevation from stable isotopes of mammal teeth. *Earth and Planetary Science Letters* 289(3-4):530-538.
- Bershaw, John, Joel E. Saylor, Carmala N. Garziona, Andrew Leier, and Kurt E. Sundell
2016 Stable isotope variations ($\delta^{18}\text{O}$ and δD) in modern waters across the Andean Plateau. *Geochimica et Cosmochimica Acta* 194:310-324.

- Blard, P. H., Florence Sylvestre, Aradhna Tripathi, Christelle Claude, C. Causse, Anne Coudrain, Thomas Condom, Jean L. Seidel, Françoise Vimeux, C. Moreau, J. P. Dumoulin, and Jérôme Lavé
2011 Lake highstands on the Altiplano (Tropical Andes) contemporaneous with Heinrich 1 and the Younger Dryas: new insights from ^{14}C , U–Th dating and $\delta^{18}\text{O}$ of carbonates. *Quaternary Science Reviews* 30(27-28):3973-3989.
- Blumenthal, Scott A., Jessica M. Rothman, Kendra L. Chritz, and Thure E. Cerling
2016 Stable isotopic variation in tropical forest plants for applications in primatology: Kibale Plant Isotopes. *American Journal of Primatology* 78(10):1041-1054.
- Bocherens, Hervé, Dorothée G. Drucker, Miriam N. Haidle, Hansjürgen Müller-Beck, Susanne C. Münzel, and Yuichi I. Naito
2016 Isotopic evidence (C, N, S) for a high aquatic dietary contribution for a Pre-Dorset muskox hunter from Umingmak (Banks Island, Canada). *Journal of Archaeological Science: Reports* 6:700-708.
- Bocherens, Herve, Gilles Pacaud, Petr A. Lazarev, and Andre Mariotti
1996 Stable isotope abundances (^{13}C , ^{15}N) in collagen and soft tissues from Pleistocene mammals from Yakutia: Implications for the palaeobiology of the Mammoth Steppe. *Palaeogeography, Palaeoclimatology, Palaeoecology* 126(1-2):31-44.
- Bocherens, Hervé, Oliver Sandrock, Ottmar Kullmer, and Friedemann Schrenk
2011 Hominin palaeoecology in Late Pliocene Malawi: First insights from isotopes (^{13}C , ^{18}O) in mammal teeth. *South African Journal of Science* 107(3/4).
- Bowen, Gabriel J.
2010 Isoscapes: Spatial Pattern in Isotopic Biogeochemistry. *Annual Review of Earth and Planetary Sciences* 38(1):161-187.

2017 The Online Isotopes in Precipitation Calculator <http://www.waterisotopes.org>, accessed.
- Bowen, Gabriel J., and Justin Revenaugh
2003 Interpolating the isotopic composition of modern meteoric precipitation: ISOTOPIC COMPOSITION OF MODERN PRECIPITATION. *Water Resources Research* 39(10).
- Bowen, Gabriel J., Leonard I. Wassenaar, and Keith A. Hobson
2005 Global application of stable hydrogen and oxygen isotopes to wildlife forensics. *Oecologia* 143(3):337-348.
- Bowen, Gabriel J., and Bruce Wilkinson
2002 Spatial distribution of d^{18}O in meteoric precipitation.

- Braje, Todd J., Jon M. Erlandson, Torben C. Rick, Loren Davis, Tom Dillehay, Daryl W. Fedje, Duane Froese, Amy Gusick, Quentin Mackie, Duncan McLaren, Bonnie Pitblado, Jennifer Raff, Leslie Reeder-Myers, and Michael R. Waters
2019 Fladmark + 40: What Have We Learned about a Potential Pacific Coast Peopling of the Americas? *American Antiquity* 85(1):1-21.
- Bromley, Gordon
2010 A Glacial-Geologic Approach to Studying Late Quaternary Climate and Ice Fluctuation in the Southern Hemisphere:164.
- Bromley, Gordon R. M., Brenda L. Hall, Kurt M. Rademaker, Claire E. Todd, and Adina E. Racovteanu
2011 Late Pleistocene snowline fluctuations at Nevado Coropuna (15°S), southern Peruvian Andes. *Journal of Quaternary Science* 26(3):305-317.
- Bromley, Gordon R. M., Brenda L. Hall, Joerg M. Schaefer, Gisela Winckler, Claire E. Todd, and Kurt M. Rademaker
2011 Glacier fluctuations in the southern Peruvian Andes during the late-glacial period, constrained with cosmogenic ³He. *Journal of Quaternary Science* 26(1):37-43.
- Bromley, Gordon R. M., Joerg M. Schaefer, Gisela Winckler, Brenda L. Hall, Claire E. Todd, and Kurt M. Rademaker
2009 Relative timing of last glacial maximum and late-glacial events in the central tropical Andes. *Quaternary Science Reviews* 28(23-24):2514-2526.
- Buffen, Aron
2008 Abrupt Holocene Climate Change: Evidence from a New Suit of Ice Cores from Nevado Coropuna, Southwestern Peru and Recently Exposed Vegetation from the Quelccaya Ice Cap, Southern Peru Master's, Ohio State University.
- Capriles, José M., Juan Albarracin-Jordan, Douglas W. Bird, Steven T. Goldstein, Gabriela M. Jarpa, Sergio Calla Maldonado, and Calogero M. Santoro
2018 Mobility, subsistence, and technological strategies of early Holocene hunter-gatherers in the Bolivian Altiplano. *Quaternary International* 473:190-205.
- Capriles, José M., Juan Albarracin-Jordan, Umberto Lombardo, Daniela Osorio, Blaine Maley, Steven T. Goldstein, Katherine A. Herrera, Michael D. Glascock, Alejandra I. Domic, Heinz Veit, and Calogero M. Santoro
2016 High-altitude adaptation and late Pleistocene foraging in the Bolivian Andes. *Journal of Archaeological Science: Reports* 6:463-474.
- Cerling, Thure E., Samuel A. Andanje, Scott A. Blumenthal, Francis H. Brown, Kendra L. Chritz, John M. Harris, John A. Hart, Francis M. Kirera, Prince Kaleme, Louise N. Leakey, Meave G. Leakey, Naomi E. Levin, Fredrick Kyalo Manthi, Benjamin H. Passey, and Kevin T. Uno

- 2015 Dietary changes of large herbivores in the Turkana Basin, Kenya from 4 to 1 Ma. *Proceedings of the National Academy of Sciences* 112(37):11467-11472.
- Cerling, Thure E., and John M. Harris
1999 Carbon Isotope Fractionation between Diet and Bioapatite in Ungulate Mammals and Implications for Ecological and Paleoecological Studies. *International Association for Ecology* 120(3):347-363.
- Cerling, Thure E., and Zachary D. Sharp
1996 Stable carbon and oxygen isotope analysis of fossil tooth enamel using laser ablation. *Palaeogeography Palaeoclimatology Palaeoecology* 126:173-186.
- Chala-Aldana, Döbereiner
2017 Assessment of Mobility and Highland Occupation Strategies during the Early Holocene at the Cuncaicha Rock Shelter through Strontium and Oxygen Isotopes Master's, University of Tübingen.
- Chala-Aldana, Döbereiner, Hervé Bocherens, Christopher Miller, Katherine Moore, Gregory Hodgins, and Kurt Rademaker
2018 Investigating mobility and highland occupation strategies during the Early Holocene at the Cuncaicha rock shelter through strontium and oxygen isotopes. *Journal of Archaeological Science: Reports* 19:811-827.
- Craig, Harmon
1961a Isotopic Variation in Meteoric Waters. *Science* 133(3465):1702-1703.

1961b Standard for Reporting Concentrations of Deuterium and Oxygen-18 in Natural Waters. *Science* 133(3467):1833-1834.
- Dansgaard, Willi
1954 The O18-abundance in fresh water. *Geochimica et Cosmochimica Acta* 6:241-260.

1964 Stable Isotopes in Precipitation. *Tellus* XVI.
- Daux, Valérie, Christophe Lecuyer, Marie-Anne Heran, Romain Amiot, Laurent Simon, François Fourel, François Martineau, Niels Lynnerup, Hervé Reyhler, and Gilles Escarguel
2008 Oxygen isotope fractionation between human phosphate and water revisited. *J Hum Evol* 55(6):1138-1147.
- DeNiro, M.J.
1985 Postmortem preservation and alteration of *in vivo* bone collagen isotope ratios in relation to palaeodietary reconstruction. *Nature* 317:806-809.

- DeNiro, M.J., and S. Epstein
1978 Influence of Diet on the Distribution of Carbon Isotopes in Animals. *Geochimica et Cosmochimica Acta* 42:495-506.
- Díaz-Zorita Bonilla, Marta, Dorothée G. Drucker, Pascale Richardin, Verónica Silva-Pinto, Marcela Sepúlveda, and Hervé Bocherens
2016 Marine food consumption in coastal northern Chilean (Atacama Desert) populations during the Formative Period: Implications of isotopic evidence (C, N, S) for the Neolithic process in south central Andes. *Journal of Archaeological Science: Reports* 6:768-776.
- Dillehay, Tom D., C. Ramírez, M. Pino, M. B. Collins, J. Rossen, and J. D. Pino Navarro
2008 Monte Verde: Seaweed, Food, Medicine, and the Peopling of South America. *Science, New Series* 320(5877):784-786.
- Dornbusch, Uwe
1998 Current Large-Scale Climatic Conditions in Southern Peru and Their Influence on Snowline Altitudes (Gegenwärtige großräumige klimatische Bedingungen in Südperu und ihr Einfluß auf die Höhenlage der Schneegrenze):41-54.
- Drucker, Dorothée G., and Hervé Bocherens
2004 Carbon and nitrogen stable isotopes as tracers of change in diet breadth during Middle and Upper Palaeolithic in Europe. *International Journal of Osteoarchaeology* 14(3-4):162-177.
- Drucker, Dorothée G., Anne Bridault, Keith A. Hobson, Elwira Szuma, and Hervé Bocherens
2008 Can carbon-13 in large herbivores reflect the canopy effect in temperate and boreal ecosystems? Evidence from modern and ancient ungulates. *Palaeogeography Palaeoclimatology Palaeoecology* 266(1-2):69-82.
- Dufour, Elise, Nicolas Goepfert, Belkys Gutiérrez León, Claude Chauchat, Régulo Franco Jordán, and Segundo Vásquez Sánchez
2014 Pastoralism in Northern Peru during Pre-Hispanic Times: Insights from the Mochica Period (100–800 AD) Based on Stable Isotopic Analysis of Domestic Camelids. *PLoS ONE* 9(1):e87559.
- Eerkens, Jelmer W., Alex DeGeorgey, Howard J. Spero, and Christophe Descantes
2014 Seasonality of Late Prehistoric Clamming on San Francisco Bay: Oxygen Isotope Analyses of *Macoma nasuta* Shells from a Stege Mound, CA-CCO-297. *California Archaeology* 6(1):23-46.
- Erlandson, Jon M.
2001 The Archaeology of Aquatic Adaptations: Paradigms for a New Millennium. *Journal of Archaeological Research* 9:287-350.

- Erlandson, Jon M., Torben C. Rick, Todd J. Braje, Molly Casperson, Brendan Culleton, Brian Fulfroost, Tracy Garcia, Daniel A. Guthrie, Nicholas Jew, Douglas J. Kennett, Madonna L. Moss, Leslie Reeder, Craig Skinner, Jack Watts, and Lauren Willis
2011 Paleoindian Seafaring, Maritime Technologies, and Coastal Foraging on California's Channel Islands. *Science* 331(6021):1181-1185.
- Fonkén, M. S. Maldonado
2014 An introduction to the bofedales of the Peruvian High Andes:13.
- Francken, Michael, Judith Beier, Hugo Reyes-Centeno, Katerina Harvati, and Kurt Rademaker
2018 The human skeletal remains from the Cuncaicha rockshelter, Peru. In *New Perspectives on the Peopling of the Americas*, edited by Katerina Harvati, Hugo Reyes-Centeno, and Jaeger Gerhard, Tuebingen, Germany.
- Franklin, William
1983 Contrasting socioecologies of South America's wild camelids: the vicuña and the guanaco. In *Advances in the Study of Mammalian Behavior*, edited by John F. Eisenberg, and Devra G. Kleiman.
- Fry, Brian
1991 Stable isotope diagrams of freshwater food webs. *Ecology* 72(6):2293-2297.
- Furlotte, Brett A
2018 *Macrobotanical Report for the Cuncaicha-1 Rock Shelter Site, Department of Arequipa, Peru: Terminal Pleistocene and Early Holocene Occupation Components*.
- Galaś, Andrzej
2011 The extent and volcanic structures of the Quaternary Andahua Group, Andes, southern Peru. *Annales Societatis Geologorum Poloniae* 81:1-19.
- Garreaud, René D., Mathias Vuille, Rosa Compagnucci, and José Marengo
2009 Present-day South American climate. *Palaeogeography, Palaeoclimatology, Palaeoecology* 281(3-4):180-195.
- Garreaud, René, Mathias Vuille, and Amy C. Clement
2003 The climate of the Altiplano: observed current conditions and mechanisms of past changes. *Palaeogeography, Palaeoclimatology, Palaeoecology* 194(1-3):5-22.
- Gat, Joel R.
1996 Oxygen and Hydrogen Isotopes in the Hydrologic Cycle. *Annual Review of Earth and Planetary Sciences* 24(225-62).

2000 Atmospheric water balance—the isotopic perspective. *Hydrological Processes* 14:1357-1369.

- Green, Daniel R., Tanya M. Smith, Gregory M. Green, Felicitas B. Bidlack, Paul Tafforeau, and Albert S. Colman
2018 Quantitative reconstruction of seasonality from stable isotopes in teeth. *Geochimica et Cosmochimica Acta* 235:483-504.
- Gruver, Stephanie Melissa
2018 Occupational Seasonality and Paleoenvironmental Reconstruction at Quebrada Jaguay 280 Master's, Northern Illinois University.
- Haas, Randall, Ioana C. Stefanescu, Alexander Garcia-Putnam, Mark S. Aldenderfer, Mark T. Clementz, Melissa S. Murphy, Carlos Viviano Llave, and James T. Watson
2017 Humans permanently occupied the Andean highlands by at least 7 ka. *Royal Society Open Science* 4(6):170331.
- Haas, Randall, James T. Watson, Tammy Buonasera, John R. Southon, Jennifer C. Chen, Sarah Noe, Kevin Smith, Carlos Viviano Llave, Jelmer Eerkens, and Glendon Parker
2020 Female hunters of the early Americas. *Sci Adv* 6(45).
- Haller von Hallerstein, Sophia
2018 Multi-isotopic paleo-diet reconstruction of hunter-gatherer in the Peruvian Puna. MSc, Institut für Naturwissenschaftliche Archäologie, Eberhard-Karls-Universität Tübingen.
- Herreros, J., Isabel Moreno, Jean D. Taupin, Patrick Ginot, Nicolas Patris, M. De Angelis, Marie-Pierre Ledru, F. Delachaux, and Ulrich Schotterer
2009 Environmental records from temperate glacier ice on Nevado Coropuna saddle, southern Peru. *Advances in Geosciences* 22:27-34.
- Hillson, Simon
2005 *Teeth*. 2nd ed ed. Cambridge manuals in archaeology. Cambridge University Press, New York.
- Iacumin, P., H. Bocherens, A. Mariotti, and A. Longinelli
1996 Oxygen isotope analyses of co-existing carbonate and phosphate in biogenic apatite: a way to monitor diagenetic alteration of bone phosphate? *Earth and Planetary Science Letters* 142:1-6.
- Iacumin, Paola, V. G. Nikolaev, and Michele Ramigni
2000 C and N stable isotope measurements on Eurasian fossil mammals, 40 000 to 10 000 years BP: Herbivore physiologies and palaeoenvironmental reconstruction. *Palaeogeography, Palaeoclimatology, Palaeoecology* 163(1-2):33-47.
- Introduction to Water Sampling and Analysis for Isotope Hydrology* . International Atomic Energy Agency, Vienna.

- Jones, Kevin B., Gregory W. L. Hodgins, and Daniel H. Sandweiss
2017 Radiocarbon Chronometry of Site QJ-280, Quebrada Jaguay, a Terminal Pleistocene to Early Holocene Fishing Site in Southern Peru. *The Journal of Island and Coastal Archaeology*:1-19.
- Kendall, Carol, and Eric A. Caldwell
1998 Fundamentals of Isotope Geochemistry. In *Isotope Tracers in Catchment Hydrology*, edited by C. Kendall and J.J. McDonnell, pp. 51-86. Elsevier Science,, Amsterdam.
- Kennedy, Casey D., Gabriel J. Bowen, and James R. Ehleringer
2011 Temporal variation of oxygen isotope ratios ($\delta^{18}\text{O}$) in drinking water: implications for specifying location of origin with human scalp hair. *Forensic Sci Int* 208(1-3):156-166.
- Knudson, Kelly J.
2009 Oxygen isotope analysis in a land of environmental extremes: the complexities of isotopic work in the Andes. *International Journal of Osteoarchaeology* 19(2):171-191.
- Knudson, Kelly J., Arthur E. Aufderheide, and Jane E. Buikstra
2007 Seasonality and paleodiet in the Chiribaya polity of southern Peru. *Journal of Archaeological Science* 34(3):451-462.
- Knudson, Kelly J., Christina Torres-Rouff, and Christopher M. Stojanowski
2015 Investigating human responses to political and environmental change through paleodiet and paleomobility: HUMAN RESPONSES TO POLITICAL AND ENVIRONMENTAL CHANGE. *American Journal of Physical Anthropology* 157(2):179-201.
- Knudson, Kelly J., Hope M. Williams, Jane E. Buikstra, Paula D. Tomczak, Gwyneth W. Gordon, and Ariel D. Anbar
2010 Introducing $\delta^{88}/^{86}\text{Sr}$ analysis in archaeology: a demonstration of the utility of strontium isotope fractionation in paleodietary studies. *Journal of Archaeological Science* 37(9):2352-2364.
- Knudson, Kelly J., Sloan R. Williams, Rebecca Osborn, Kathleen Forgey, and Patrick Ryan Williams
2009 The geographic origins of Nasca trophy heads using strontium, oxygen, and carbon isotope data. *Journal of Anthropological Archaeology* 28(2):244-257.
- Koch, Paul L., Daniel C. Fisher, and David Dettman
1989 Oxygen isotope variation in the tusks of extinct proboscideans: A measure of season of death and seasonality. *Geology* 17:515-519.

- Koch, Paul L., Kathryn A. Hoppe, and S. David Webb
1998 The isotopic ecology of late Pleistocene mammals in North America - Part 1. Florida. *Chemical Geology* 152(1-2):119-138.
- Lee-Thorp, Julia A.
2002 Two decades of progress towards understanding fossilization processes and isotopic signals in calcified tissue minerals. *Archaeometry* 44:435-446.
- Lee-Thorp, Julia A., Matt Sponheimer, and N. H. Van der Merwe
2003 What do stable isotopes tell us about hominid dietary and ecological niches in the Pliocene? *International Journal of Osteoarchaeology* 13(1-2):104-113.
- Lee-Thorp, Julia A., and Nikolaas J. van der Merwe
1991 Aspects of the Chemistry of Modern and Fossil Biological Apatites. *Journal of Archaeological Science* 18:343-354.
- Lee-Thorp, Julia, and Matt Sponheimer
2003 Three case studies used to reassess the reliability of fossil bone and enamel isotope signals for paleodietary studies. *Journal of Anthropological Archaeology* 22(3):208-216.
- Longinelli, Antonio
1984 Oxygen isotopes in mammal bone phosphate: A new tool for paleohydrological and paleoclimatological research? *Geochimica et Cosmochimica Acta* 48:385-390.
- Luz, Boaz, Eugeni Barkan, Ruth Yam, and Aldo Shemesh
2009 Fractionation of oxygen and hydrogen isotopes in evaporating water. *Geochimica et Cosmochimica Acta* 73(22):6697-6703.
- Luz, Boaz, Yehoshua Kolodny, and Michal Horowitz
1984 Fractionation of oxygen isotopes between mammalian bone-phosphate and environmental drinking water. *Geochimica et Cosmochimica Acta* 48(8):1689-1693.
- Marín, Juan C., C. S. Casey, M. Kadwell, Kaltouma Yaya, D. Hoces, Juan Olazabal, Raul Rosadio, J. Rodriguez, Angel Spotorno, Michael W. Bruford, and Jane C. Wheeler
2007 Mitochondrial phylogeography and demographic history of the Vicuña: implications for conservation. *Heredity* 99(1):70-80.
- Marín, Juan C., K. Romero, R. Rivera, Warren E. Johnson, and Benito A. González
2017 Y-chromosome and mtDNA variation confirms independent domestications and directional hybridization in South American camelids. *Animal Genetics* 48(5):591-595.

- Mark, Bryan G., and Jeffrey M. McKenzie
 2007 Tracing Increasing Tropical Andean Glacier Melt with Stable Isotopes in Water. *Environmental Science & Technology* 41(20):6955-6960.
- McInnis, Heather
 2006 Middle Holocene Culture and Climate on the South Coast of Peru: Archaeological Investigation of the Pampa Colorada. Doctor of Philosophy, Anthropology, University of Oregon.
- Michener, Robert, and Kate Lajtha
 2007 *Stable Isotopes in Ecology and Environmental Science*. Second ed. Ecological Methods and Concepts Series. Blackwell Publishing Malden, MA.
- Moore, Katherine
 2013 *Large Mammal Zooarchaeology at Cuncaicha: Exploration of Research Potential*.

 2016a Early Domesticated Camelids in the Andes. In *The Archaeology of Andean Pastoralism*, edited by Jose M. Capriles, and Nicholas Tripcevich.

 2016b Report on the 2015 Season of Excavation and Cuncaicha and the 2015 and 2016 Study Seasons of the Zooarchaeological Samples from the Site. .
- Moore, Katherine M.
 1998 Measures of Mobility and Occupational Intensity in Highland Peru. In *Seasonality and Sedentism: Archaeological Perspectives from Old and New World Sites*, edited by Thomas R. Rocek and Ofer Bar-Yosef, pp. 181-197. Peabody Museum of Archaeology and Ethnology, Cambridge, Massachusetts.
- Moore, Lorna G.
 1979 Biology of High-Altitude Peoples - Baker, Pt. *American Anthropologist* 81(3):708-710.

 2017 Human Genetic Adaptation to High Altitudes: Current Status and Future Prospects. *Quat Int* 461:4-13.
- Nehlich, Olaf
 2015 The application of sulphur isotope analyses in archaeological research: A review. *Earth-Science Reviews* 142:1-17.
- Osorio, Daniela, Donald Jackson, Paula C. Ugalde, Claudio Latorre, Ricardo De Pol-Holz, and Calogero M. Santoro
 2011 Hakenasa Cave its relevance for peopling of the southern Andean Altiplano. *Antiquity* 85:1194-1208.

- Osorio, Daniela, James Steele, Marcela Sepúlveda, Eugenia M. Gayo, José M. Capriles, Katherine A. Herrera, Paula C. Ugalde, Ricardo De Pol-Holz, Claudio Latorre, and Calogero M. Santoro
2017 The Dry Puna as an ecological megapatch and the peopling of South America: Technology, mobility, and the development of a late Pleistocene/early Holocene Andean hunter-gatherer tradition in northern Chile. *Quaternary International* 461:41-53.
- Passey, Benjamin H., Todd F. Robinson, Linda K. Ayliffe, Thure E. Cerling, Matt Sponheimer, M. Denise Dearing, Beverly L. Roeder, and James R. Ehleringer
2005 Carbon isotope fractionation between diet, breath CO₂, and bioapatite in different mammals. *Journal of Archaeological Science* 32(10):1459-1470.
- Price, T. Douglas, James H. Burton, and Robert A. Bentley
2002 The characterization of biologically available strontium isotope ratios for the study of prehistoric migration. *Archaeometry* 44:117-135.
- Rademaker, Kurt
2006 Geoarchaeological investigations of the Wayñuna site and Alca obsidian source, Peru. MSc, Quaternary and Climate Studies, University of Maine, Orono, Main.

2017 Chronology, seasonality, and inter-zonal connections in a Terminal Pleistocene-Early Holocene settlement system, southern Peru. NSF, Peru.
- Rademaker, Kurt, Gordon R. M. Bromley, and Daniel H. Sandweiss
2013 Peru archaeological radiocarbon database, 13,000–7000 14C B.P. *Quaternary International* 301:34-45.
- Rademaker, Kurt, Michael D. Glascock, Bruce Kaiser, David Gibson, Daniel R. Lux, and Martin G. Yates
2013 Multi-technique geochemical characterization of the Alca obsidian source, Peruvian Andes. *Geology* 41(7):779-782.
- Rademaker, Kurt, and Stephanie Melissa Gruver
2018 Chronology and seasonality at Quebrada Jaguay: Implications for the early settlement of South America. Chicago, IL.
- Rademaker, Kurt, and Gregory Hodgins
2018 Exploring the chronology of occupations and burials at Cuncaicha rockshelter, Peru. In *New Perspectives on the Peopling of the Americas*, edited by Katerina Harvati, Hugo Reyes-Centeno, and Gerhard Jaeger, Tuebingen, Germany.
- Rademaker, Kurt, Gregory Hodgins, Katherine Moore, Sonia Zarrillo, Christopher Miller, Gordon R. M. Bromley, Peter Leach, David A. Reid, Willy Yépez Álvarez, and Daniel H. Sandweiss

- 2014 Paleoindian settlement of the high-altitude Peruvian Andes. *Science* 346(6208):466-469.
- 2016 Cuncaicha Rockshelter, a Key Site for Understanding Colonization of the High Andes. *Current Anthropology* 57(1):101-103.
- Rademaker, Kurt M.
2012 Early Human Settlement of the High-Altitude Pucuncho Basin, Peruvian Andes Dissertation, University of Maine, Orono.
- Rademaker, Kurt, and Katherine Moore
2018 Variation in Occupation Intensity of Early Forager Sites of the Andean Puna: Implications for Settlement and Adaptation:44.
- Rutllant, Jose, and Pablo Ulriksen
1979 Boundary-layer dynamics of the extremely arid northern part of Chile. *Boundary-Layer Meteorology* 17(1):41-55.
- Samec, Celeste T., Hugo D. Yacobaccio, and Héctor O. Panarello
2018 Stable isotope compositions of South American camelids in the Dry Puna of Argentina: A frame of reference for the study of prehistoric herding and hunting strategies. *Journal of Archaeological Science: Reports* 18:628-636.
- Sandweiss, Daniel H., Heather McInnis, Richard L. Burger, Asunción Cano, Bernardino Ojeda, Rolando Paredes, María del Carmen Sandweiss, and Michael D. Glascock
1998 Quebrada Jaguay: Early South American Maritime Adaptations. *Science* 281:4.
- Santana-Sagredo, Francisca, Julia Lee-Thorp, Rick Schulting, and Mauricio Uribe
2018 Mobility in the Atacama Desert, northern Chile, in the Late Intermediate Period (AD 900–1450): A re-evaluation using stable isotope analysis. *Quaternary International*.
- Scaffidi, Beth K., and Kelly J. Knudson
2020 An archaeological strontium isoscape for the prehistoric Andes: Understanding population mobility through a geostatistical meta-analysis of archaeological $^{87}\text{Sr}/^{86}\text{Sr}$ values from humans, animals, and artifacts. *Journal of Archaeological Science* 117.
- Scaffidi, Beth K., Tiffany A. Tung, Gwyneth Gordon, Aleksa K. Alaica, Luis Manuel González La Rosa, Sara J. Marsteller, Allisen Dahlstedt, Emily Schach, and Kelly J. Knudson
2020 Drinking Locally: A Water $^{87}\text{Sr}/^{86}\text{Sr}$ Isoscape for Geolocation of Archeological Samples in the Peruvian Andes. *Frontiers in Ecology and Evolution* 8.
- Schoeninger, Margaret, K. Hallin, H. Reeser, J. W. Valley, and J. Fournelle
2003 Isotopic alteration of mammalian tooth enamel. *International Journal of Osteoarchaeology* 13(1-2):11-19.

- Schoeninger, Margaret J.
1995 Stable isotope studies in human evolution. *Evolutionary Anthropology* 4:83-98.
- Schoeninger, Margaret J., and K. Moore
1992 Bone Stable Isotope Studies in Archaeology. *Journal of World Prehistory* 6:247-296.
- Schwarcz, Henry P., and Margaret J. Schoeninger
1991 Stable Isotope Analyses in Human Nutritional Ecology. *Yearbook of Physical Anthropology* 34:283-321.
- Sharp, Zachary D., and Thure E. Cerling
1998 Fossil isotope records of seasonal climate and ecology: Straight from the horse's mouth. *Geology* 26(3):219.
- Silverio, Walter, and Jean-Michel Jaquet
2012 Multi-temporal and multi-source cartography of the glacial cover of Nevado Coropuna (Arequipa, Peru) between 1955 and 2003. *International Journal of Remote Sensing* 33(18):5876-5888.
- Sitzia, Luca, Eugenia M. Gayo, Marcela Sepulveda, Juan S. González, Lucia Ibañez, Alain Queffelec, and Ricardo De Pol-Holz
2019 A perched, high-elevation wetland complex in the Atacama Desert (northern Chile) and its implications for past human settlement. *Quaternary Research* 92(1):33-52.
- Smith, Tanya M., Christine Austin, Daniel R. Green, Renaud Joannes-Boyau, Shara Bailey, Dani Dumitriu, Stewart Fallon, Rainer Grün, Hannah F. James, Marie-Hélène Moncel, Ian S. Williams, Rachel Wood, and Manish Arora
2018 Wintertime stress, nursing, and lead exposure in Neanderthal children. *Science Advances* (4):eaau9483.
- Somerville, A. D., P. S. Goldstein, S. I. Baitzel, K. L. Bruwelheide, A. C. Dahlstedt, L. Yzurdiaga, S. Raubenheimer, K. J. Knudson, and M. J. Schoeninger
2015 Diet and gender in the Tiwanaku colonies: Stable isotope analysis of human bone collagen and apatite from Moquegua, Peru. *Am J Phys Anthropol* 158(3):408-422.
- Sponheimer, Matt, and Thure E. Cerling
2014 Investigating Ancient Diets Using Stable Isotopes in Bioapatites. In *Treatise on Geochemistry*, pp. 341-355. Elsevier.
- Szpak, Paul, Christine D. White, Fred J. Longstaffe, Jean-François Millaire, and Víctor F. Vasquez Sanchez
2013 Carbon and nitrogen isotopic survey of northern peruvian plants: baselines for paleodietary and paleoecological studies. *PLoS One* 8(1):e53763.

- Tanner, Benjamin R.
2001 Lithic Analysis of Chipped Stone Artifacts Recovered From Quebrada Jaguay, Peru Master's, University of Maine, Orono.
- Tanz, Nicole, and Hanns-Ludwig Schmidt
2010 $\delta(34)\text{S}$ -value measurements in food origin assignments and sulfur isotope fractionations in plants and animals. *J Agric Food Chem* 58(5):3139-3146.
- Thompson, Lonnie G., Ellen Mosley-Thompson, and Keith A. Henderson
2000 Ice-core palaeoclimate records in tropical South America since the Last Glacial Maximum. *Journal of Quaternary Science* 15(4):377-394.
- Tomka, Steve A.
1992 Vicuñas and Llamas: Parallels in Behavioral Ecology and Implications for the Domestication of Andean Camelids. *Human Ecology* 20(4):407-433.
- Troll, Carl
1968 *The Cordilleras of the tropical Americas: aspects of climatic, phytogeographical and agrarian ecology*. . Carl Troll. Colloquium Geographicum 9., Bonn, Germany.
- Tung, Tiffany A., and Kelly J. Knudson
2018 Stable isotope analysis of a pre-Hispanic Andean community: Reconstructing pre-Wari and Wari era diets in the hinterland of the Wari empire, Peru. *American Journal of Physical Anthropology* 165(1):149-172.
- van Klinken, Gert J.
1999 Bone Collagen Quality Indicators for Paleodietary and Radiocarbon Measurements. *Journal of Archaeological Science* 26:687-695.
- Venturelli, G., M. Fragipane, M. Weibel, and D. Antiga
1978 Trace Element Distribution in the Cainozoic Lavas of Nevado Coropuna and Andagua Valley, Central Andes of Southern Peru. *Bulletin Volcanologique* 41:213-228.
- Vidal, Pulgar J.
1981 *Geografía del Perú: Las Ocho Regiones Naturales del Perú*, Lima.
- Vimeux, Françoise, Patrick Ginot, Margit Schwikowski, Mathias Vuille, Georg Hoffmann, Lonnie G. Thompson, and Ulrich Schotterer
2009 Climate variability during the last 1000 years inferred from Andean ice cores: A review of methodology and recent results. *Palaeogeography, Palaeoclimatology, Palaeoecology* 281(3-4):229-241.

- Vuille, Mathias, and Raymond S. Bradley
2000 Mean annual temperature trends and their vertical structure in the tropical Andes. *Geophysical Research Letters* 27(23):3885-3888.
- Vuille, Mathias, Stephen J. Burns, B. L. Taylor, Francisco W. Cruz, Broxton W. Bird, Mark B. Abbott, L. C. Kanner, Hai Cheng, and Valdir F. Novello
2012 A review of the South American monsoon history as recorded in stable isotopic proxies over the past two millennia. *Climate of the Past* 8(4):1309-1321.
- Widga, Christopher C., J. Douglas Walker, and Lisa D. Stockli
2010 Middle Holocene Bison diet and mobility in the eastern Great Plains (USA) based on $\delta^{13}\text{C}$, $\delta^{18}\text{O}$, and $^{87}\text{Sr}/^{86}\text{Sr}$ analyses of tooth enamel carbonate. *Quaternary Research* 73(3):449-463.
- Yann, Lindsey T., Larisa R. G. DeSantis, Paul L. Koch, and Ernest L. Lundelius
2016 Dietary ecology of Pleistocene camelids: Influences of climate, environment, and sympatric taxa. *Palaeogeography, Palaeoclimatology, Palaeoecology* 461:389-400.
- Zazzo, Antoine, Marie Balasse, and William P. Patterson
2006 The reconstruction of mammal individual history: refining high-resolution isotope record in bovine tooth dentine. *Journal of Archaeological Science* 33(8):1177-1187.
- Zazzo, Antoine, Mattieu Lebon, Laurent Chiotti, Clothilde Comby, Emmanuelle Delque-Kolic, Roland Nespoulet, and Ina Reiche
2013 Can We Use Calcined Bones for C-14 Dating the Paleolithic? *Radiocarbon* 55(2-3):1409-1421.